# ANTIBACTERIAL ACTION OF GRAPHENE OXIDE TOWARDS BACTERIA AND ITS TOXICOLOGICAL EFFECTS ON HUMAN EPIDERMAL KERATINOCYTES

THIRUCHELVI PULINGAM

INSTITUTE FOR ADVANCED STUDIES
UNIVERSITY OF MALAYA
KUALA LUMPUR

2020

# ANTIBACTERIAL ACTION OF GRAPHENE OXIDE TOWARDS BACTERIA AND ITS TOXICOLOGICAL EFFECTS ON HUMAN EPIDERMAL KERATINOCYTES

**THIRUCHELVI PULINGAM**

**THESIS SUBMITTED IN FULFILMENT OF THE REQUIREMENTS FOR THE DEGREE OF DOCTOR OF PHILOSOPHY**

**INSTITUTE FOR ADVANCED STUDIES**
**UNIVERSITY OF MALAYA**
**KUALA LUMPUR**

**2020**

**UNIVERSITY OF MALAYA**

**ORIGINAL LITERARY WORK DECLARATION**

Name of Candidate: **Thiruchelvi Pulingam**

Matric No: **17005743/1**

Name of Degree: **Doctor of Philosophy**

Title of Project Paper/Research Report/Dissertation/Thesis ("this Work"):

**Antibacterial Action of Graphene Oxide towards Bacteria and Its Toxicological Effects on Human Epidermal Keratinocytes**

Field of Study: **Biology and Biochemistry**

I do solemnly and sincerely declare that:

(1) I am the sole author/writer of this Work;
(2) This Work is original;
(3) Any use of any work in which copyright exists was done by way of fair dealing and for permitted purposes and any excerpt or extract from, or reference to or reproduction of any copyright work has been disclosed expressly and sufficiently and the title of the Work and its authorship have been acknowledged in this Work;
(4) I do not have any actual knowledge nor do I ought reasonably to know that the making of this work constitutes an infringement of any copyright work;
(5) I hereby assign all and every rights in the copyright to this Work to the University of Malaya ("UM"), who henceforth shall be owner of the copyright in this Work and that any reproduction or use in any form or by any means whatsoever is prohibited without the written consent of UM having been first had and obtained;
(6) I am fully aware that if in the course of making this Work I have infringed any copyright whether intentionally or otherwise, I may be subject to legal action or any other action as may be determined by UM.

Candidate's Signature Date: 30/10/2020

Subscribed and solemnly declared before,

Witness's Signature Date: 30/10/2020

Name:

Designation:

**ANTIBACTERIAL ACTION OF GRAPHENE OXIDE TOWARDS BACTERIA AND ITS TOXICOLOGICAL EFFECTS OF HUMAN EPIDERMAL KERATINOCYTES**

## ABSTRACT

The antibacterial nature of graphene oxide (GO) has stimulated wide interest in the medical field. Although the antibacterial activity of GO towards bacteria has been well studied, a deeper understanding of the mechanism of action of GO is still lacking. The objectives of the study were to characterize the physicochemical properties of GO, to determine the antibacterial and antibiofilm activity and the mechanistic action of GO against Gram-positive *Staphylococcus aureus* and *Enterococcus faecalis* and Gram-negative *Escherichia coli* and *Pseudomonas aeruginosa*, to determine the synergistic behaviour of GO with selected antibiotics against bacterial cells in suspension and biofilm and to determine the *in vitro* toxicological effects of GO against human epidermal keratinocytes (HaCaT). GO was characterized using Ultraviolet-visible (UV-VIS), Raman and Attenuated Total Reflectance-Fourier-transform infrared (ATR-FTIR) spectroscopy techniques, Field Emission Scanning Electron Microscopy (FESEM), Transmission Electron Microscopy (TEM) and X-Ray Diffraction analysis (XRD) techniques. Viability, time-kill and Lactose Dehydrogenase (LDH) release assays were carried out to determine the antibacterial activity of GO towards bacterial cells in suspension and biofilm while FESEM and TEM analysis were conducted for GO treated bacterial cells in suspension. Interactions at molecular level between GO and antibiotics were analyzed using ATR-FTIR and UV-Vis techniques. Increase in the activity of antibiotics through the addition of GO was investigated using selected antibiotics such as ampicillin, chloramphenicol and tetracycline. Additionally, toxicity of GO towards HaCaT cells were examined through 3-(4,5-Dimethyl-2-thiazolyl)-2,5-diphenyl-2H-tetrazolium bromide (MTT) viability, reactive oxygen species (ROS)

detection and LDH release assays while surface morphology of GO treated HaCaT cells were analyzed using FESEM. Characterization techniques confirmed the presence and morphology of GO in sheet-like formation. Antibacterial activity of GO was concentration and time-dependent for the bacterial cells in suspension. Optimal GO concentration with more than 60% of bacterial cell death was at 10 μg/mL. In contrast, GO enhanced the viability of the biofilm cells when treated with higher concentrations and for longer exposure period. Loss of membrane integrity among bacteria in suspension was enhanced with increasing GO concentrations and this corresponded to the elevated release of LDH in the reaction medium. Bacterial cell morphology of GO treated bacterial culture showed apparent differences in the mechanism of action of GO towards Gram-positive and Gram-negative bacteria. ATR-FTIR characterizations of the GO treated bacterial cells showed changes in the fatty acids, amide I and amide II of proteins, peptides and amino acid regions compared to untreated bacterial cells. The ATR-FTIR and UV-Vis characterizations of GO and antibiotics showed adsorption of tested antibiotics onto GO through molecular interactions. The combinatorial antibacterial activity of GO and antibiotics towards bacteria in suspension was found to be increased when compared to GO or antibiotic alone but no changes were observed with the biofilm cells. Cytotoxicity of GO was found to be dose dependent towards HaCaT cell line and hence it is suggested to impose only low toxic effects against the epidermal keratinocytes. Therefore, this study reaffirms that GO has strong antibacterial potentials and could act as an adjuvant to enhance the antimicrobial activity of antibiotics.

**Keywords**: antibacterial activity; graphene oxide; antibiotics; membrane damage; keratinocytes

**TINDAKAN ANTIBAKTERIA GRAPHENE OKSIDA TERHADAP BAKTERIA DAN KESAN TOKSIKOLOGINYA TERHADAP KERATINOSIT EPIDERMIS MANUSIA**

## ABSTRAK

Sifat antibakteria graphene oxida (GO) telah merangsang minat yang luas dalam bidang perubatan. Walaupun aktiviti antibakteria GO terhadap bakteria telah dipelajari dengan baik, pemahaman yang lebih mendalam tentang mekanisma tindakan GO masih kurang. Objektif kajian ini adalah untuk mengenalpasti sifat fizikokimia GO untuk menentukan aktiviti antibakteria dan antibiofilm dan tindakan mekanisma GO terhadap bakteria Gram-positif (*Staphylococcus aureus* dan *Enterococcus faecalis*) dan Gram-negatif (*Escherichia coli* dan *Pseudomonas aeruginosa*), untuk menentukan tingkah laku sinergistik GO dengan antibiotik terpilih terhadap sel-sel bakteria dalam suspensi dan biofilm dan untuk menentukan kesan toksikologi *in vitro* GO terhadap sel keratinosit epidermis manusia (HaCaT). GO telah dicirikan menggunakan teknik spektroskopi inframerah (UV-Vis), Total Reflectance-Fourier-transform inframerah (ATR-FTIR), Mikroskopi Pengimbasan Pelepasan Medan (FESEM), Mikroskopi Elektron Transmisi (TEM) dan melalui teknik X-Ray analisis penyebaran (XRD). Pemeriksaan daya hidup, tempoh pendedahan dan pembebasan enzim Lactose Dehydrogenase (LDH) telah dijalankan untuk menentukan aktiviti antibakteria GO terhadap sel-sel bakteria dalam suspensi dan biofilm sementara analisis FESEM, TEM dan ATR-FTIR telah dijalankan untuk sel-sel bakteria dalam suspensi yang telah dirawat dengan GO. Interaksi pada tahap molekul antara GO dan antibiotik dianalisis menggunakan teknik ATR-FTIR dan UV-Vis. Peningkatan aktiviti antibakteria antibiotik terhadap bakteria melalui penambahan GO disiasat menggunakan antibiotik terpilih seperti ampicillin, chloramphenicol dan tetracycline. Selain itu, toksisiti GO terhadap sel-sel HaCaT diperiksa melalui kaedah daya tahan 3-(4,5-Dimethyl-2-thiazolyl)-2,5-diphenyl-2H-tetrazolium bromida (MTT),

pengesanan spesies oksigen reaktif (ROS) dan pembebasan enzim LDH sementara morfologi permukaan sel-sel HaCaT yang dirawat GO diperhatikan melalui kaedah FESEM. Kaedah pencirian mengesahkan kehadiran GO manakala analisis FESEM dan TEM menunjukkan morfologi GO dalam bentuk lembaran. Aktiviti antibakteria GO adalah bergantung kepada konsentrasi dan masa untuk sel-sel bakteria dalam suspensi. Konsentrasi GO optimum dengan lebih daripada 60% kematian sel bakteria adalah pada 10 µg/mL. Sebaliknya, GO meningkatkan daya tahan sel biofilm apabila dirawat dengan konsentrasi GO yang lebih tinggi walaupun untuk tempoh pendedahan yang lebih lama. Kehilangan integriti membran dalam bakteria dipertingkatkan dengan peningkatan konsentrasi GO dan ini berpadanan dengan pembebasan enzim LDH dalam media reaksi. Morfologi sel bakteria yang dirawat GO menunjukkan perbezaan nyata dalam mekanisma tindakan GO terhadap bakteria Gram-positif dan Gram-negatif. Pencirian ATR-FTIR sel bakteria yang dirawat GO menunjukkan perubahan dalam asid lemak, amide I dan amide II protein, peptida dan kawasan asid amino berbanding sel bakteria yang tidak dirawat. Pencirian GO dan antibiotik melalui kaedah ATR-FTIR dan UV-Vis menunjukkan penyerapan antibiotik teruji terhadap GO adalah menerusi interaksi molekul. Kombinasi aktiviti antibakteria GO dan antibiotik terhadap sel-sel bakteria dalam suspensi didapati meningkat apabila dibandingkan dengan GO atau antibiotik sahaja tetapi tiada perubahan yang dapat diperhati dengan sel biofilm bakteria. Toksisiti GO terhadap sel-sel HaCaT didapati bergantung kepada konsentrasi GO dan oleh itu dicadangkan untuk menyebabkan kesan toksik yang rendah terhadap sel keratinosit epidermis. Oleh itu, kajian ini menunjukkan bahawa GO mempunyai potensi antibakteria yang kuat dan boleh bertindak sebagai pembantu untuk meningkatkan aktiviti antimikrob antibiotik.

**Kata kunci**: aktiviti antibakteria; graphene oksida; antibiotik; kerosakan membran; keratinosit

## ACKNOWLEDGEMENTS

I would like to take this opportunity to sincerely thank my supervisors Dr. Leo Bey Fen and Ir. Dr. Lai Chin Wei for their continuous support, motivation and encouragement throughout my research. Their limitless guidance has helped me tremendously in removing countless obstacles that came in my way during this research period. I am also ever grateful for their assistance and supervision during my years as a postgraduate student.

Another most important person I would like to express my gratitude is my supervisor, Prof. Dr. Thong Kwai Lin. Her continuous support and guidance in correcting me in every aspect of this study have shaped me to be a better researcher. I would also like to thank her for granting me a space in her laboratory to conduct my research and also for her kind contribution of bacterial strains used in this study.

I would like to thank my parents for always supporting me and their continuous encouragement to complete this study successfully. I am also grateful to Dr. Jimmy Nelson, my husband, and Harenthiran, my brother, for their ultimate support and assurance for making this thesis a reality.

Not forgetting my cheerful friends Mariyammal, Soh Chee Hoong, Sharmin Quazi Bonny, Shalini Muniandy and Ignatius Julian Dinshaw for always coming up with ideas to help with difficulties that I faced in the laboratory. My sincere thanks to all staff at Electron Microscopy Unit, Faculty of Medicine, UM for their full guidance in helping me to generate beautiful images for my thesis. Lastly, I would like to express my gratitude to all staff from Nanotechnology and Catalysis Research Center (NANOCAT) and Institute for Advanced Studies (IAS) for their guidance and support throughout my candidature.

## TABLE OF CONTENTS

## LIST OF FIGURES

## LIST OF TABLES

## LIST OF SYMBOLS AND ABBREVIATIONS

| | | |
|---|---|---|
| °C | : | Celsius |
| µg/mL | : | microgram per millilitre |
| µL | : | microlitre |
| $\lambda_{max}$ | : | lambda maximum |
| AFM | : | atomic force microscopy |
| AMP | : | ampicillin |
| AMP-GO | : | ampicillin-graphene oxide |
| ATR-FTIR | : | attenuated total reflectance-Fourier-transform infrared |
| Bcl-2 | : | B-cell lymphoma-2 |
| BSA | : | bovine serum albumin |
| CDDP | : | chemotherapy drug cisplatin |
| cfu | : | colony forming unit |
| cfu/mL | : | colony forming unit per millilitre |
| CHL | : | chloramphenicol |
| CHL-GO | : | chloramphenicol-graphene oxide |
| DMEM | : | Dulbecco's modified eagle medium |
| DMSO | : | dimethyl sulfoxide |
| DNA | : | deoxyribonucleic acid |
| EPS | : | extracellular polymeric substances |
| FBS | : | fetal bovine serum |
| FESEM | : | field emission scanning electron microscopy |
| GLA | : | glutaraldehyde |
| GO | : | graphene oxide |
| Gt | : | graphite |

| | | |
|---|---|---|
| GtO | : | graphite oxide |
| HaCaT | : | human epidermal keratinocytes |
| HLF | : | human lung fibroblasts |
| $IC_{50}$ | : | inhibitory concentration |
| k | : | kilo |
| kV | : | kilovolt |
| LA-PEG | : | lactobionic acid-polyethylene glycol |
| LB | : | Langmuir-Blodgett |
| LC3 | : | light chain 3 |
| LDH | : | lactose dehydrogenase |
| LPS | : | lipopolysaccharide |
| MAPK | : | mitogen-activated protein kinase |
| mm | : | milimetre |
| MRSA | : | methicillin-resistant *S. aureus* |
| MTT | : | 3-(4,5-dimethylthiazol-2-yl)-2,5-diphenyl tetrazolium bromide |
| NAC | : | N-acetylcysteine |
| NF-κB | : | Necrosis factor kappa B |
| NIR | : | intrinsic near infrared |
| NM | : | nano material |
| nm | : | nanometre |
| PBS | : | phosphate buffered saline |
| PEG | : | polyethylene glycol |
| PEI | : | polyethylenimine |
| RFU | : | relative frequency unit |
| rGO | : | reduced graphene oxide |
| ROS | : | reactive oxygen species |

| | | |
|---|---|---|
| rpm | : | rotation per minute |
| RT | : | room temperature |
| TEM | : | transmission electron microscopy |
| TET | : | tetracycline |
| TET-GO | : | tetracycline-graphene oxide |
| TGF-β | : | transforming growth factor beta |
| TLR | : | toll-like receptor |
| TNF-α : | | tumor necrosis factor |
| TNF-R | : | tumor necrosis factor receptor |
| TSA | : | tryptic soy agar |
| TSB | : | tryptic soy broth |
| U/mL | : | unit per milimetre |
| UV-VIS | : | ultraviolet-visible |
| WHO | : | World Health Organization |
| XRD | : | X-Ray diffraction analysis |

## LIST OF APPENDICES

# CHAPTER 1: INTRODUCTION

## 1.1 Background of study

Antibiotic resistance due to the improper use of antibiotics has become one the most pressing problems of the medical sector (Syed, 2019). Nearly 700, 000 deaths are recorded each year and if it continues in this direction, World Health Organization (WHO) has estimated that 10 million deaths and a loss of 100 trillion USD could occur by year 2050 due to antimicrobial resistance (O'neill, 2014). Although the discovery of new antibiotics may help to overcome antibiotic resistance, however, the impact of a new antibiotic would not last long if current practice of non-judicial use of antibiotic continues (Molnar, 2019). There are several obstacles that currently hinder changes in improper use of antibiotics and these include; problems regarding increasing antibiotic resistance and knowledge on proper use of antibiotics are poorly conveyed to the public; the public considers that this matter is of no importance and a solution will soon be found (Molnar, 2019; O'Connor, O'Doherty, O'Regan, & Dunne, 2018).

Consequently, excessive use and abuse of antibiotics have led to the selection of resistant bacteria where bacterial infections caused by antibiotic-resistant bacteria contributed to increased mortality rate, extended hospital stay and higher treatment cost which burdens the economy (Wang, Kodiyanplakkal, & Calfee, 2019). As a result, the current treatment for infectious diseases are no longer effective and may risk currently existing prevention and infection treatment plans (Ouwehand, Forssten, Hibberd, Lyra, & Stahl, 2016). Moreover, the emergence of clinical strains of *Acinetobacter* spp. and *Klebsiella pneumoniae* that are resistant to all available antibiotics has led researchers to claim that we are presently in the 'post-antibiotic' era (Resistance, 2016). Hence, this prediction corresponds with WHO's estimation that antibiotic resistance will become the most common cause of death by year 2050 (WHO, 2014).

Antibacterial effects of antibiotics are exerted through various mechanistic pathways and similarly resistance to the antibiotic displayed by the bacteria is not limited to one but several modes of action (Blair, Webber, Baylay, Ogbolu, & Piddock, 2015). Although the resistance mechanisms differ according to the drug used, they typically include the following general mechanisms, for instance, modification of the antibiotic target site, modification/destruction of the antibiotic and prevention of the antibiotic from reaching its target through elimination/seclusion method (Pham, Loupias, Dassonville-Klimpt, & Sonnet, 2019). Resistance gene or determinant too can be acquired by bacteria from another bacterium through three main routes including transformation (uptake of new genetic material from the environment), transduction (use of viral vector for transferring bacterial DNA) and bacterial conjugation (transfer of genetic material between bacteria) (Admassie, 2018). Additionally, it is also noteworthy to include that bacteria may have more than one resistance mechanism towards a single antibiotic (Wang et al., 2019).

Although, antibiotics have saved millions of lives for the past 70 years, it is clear now that the accomplishment of this wonder drug may not last long and it is crucial that a different approach is needed to address the ever-increasing antibiotic resistance (Medina Cruz, Mi, & Webster, 2018). Various alternatives to antibiotics have been proposed, however, it is commonly accepted that the first generation of antibiotic alternatives would be an adjunctive or preventive therapy that works along with currently existing antibiotics (Czaplewski et al., 2016). Alternatives to antibiotics are generally characterised as products that display non-compound methods which includes targeting of the bacteria itself. This is different from antibiotics which are known to mainly target key bacterial processes (Waldetoft & Brown, 2017). Moreover, these alternatives have been suggested for use in combination with conventional antibiotics too (Czaplewski et al., 2016).

As the need for antimicrobial agents that are difficult for bacteria to generate resistance escalates, advances in the field of nanotechnology have paved way for the discovery of nanomaterials with antibacterial activity (Hemeg, 2017). It was in 2010 that GO made the headlines for having antibacterial properties and these articles have found that inactivation of bacterial cells mainly occurs through cell membrane damage (Akhavan & Ghaderi, 2010; Hu et al., 2010). Other mechanisms of action have been reported as well which includes oxidative stress, cell deposition onto the GO, wrapping of bacterial cell by the GO sheets and phospholipid extraction (Liu et al., 2011; Perreault, de Faria, Nejati, & Elimelech, 2015; Sodhi, 2016; Tu et al., 2013; Zou, Zhang, Wang, & Luo, 2016).

GO wields its toxic nature mainly through physicochemical attributes including size and length, surface properties and aggregation factor (Pang, Dai, Bi, Guo, & Fan, 2017). These aspects influence the order of death which is initiated by deposition of bacterial cell onto the nanomaterials, membrane disruption upon contact with sharp edges of GO, cell content leakage into the environment and eventual cell death (Liu et al., 2011). An additional reaction of mechanism has been described where GO sheet completely wraps the bacterial cell and prevents nutrient uptake from the media and indirectly inhibits the cell proliferation (Liu et al., 2012).

Difference in the cell wall components between the Gram-positive and Gram-negative bacteria also contributes to the better antibacterial potential of GO towards *S. aureus*. This is mainly due to the absence of outer membrane protein that is only found in the Gram-negative bacteria (Akhavan & Ghaderi, 2010; Deokar, Lin, Chang, & Ling, 2013). The antibacterial activity of GO is increasingly reported however, the detailed mechanism of reaction is not prioritized and most of the time poorly understood and less described (Wang, Hu, & Shao, 2017).

Besides the apparent difference of bacterial membrane playing a role in defining the antibacterial activity of GO, bacterial growth state too may contribute to the bactericidal activity of GO. Biofilm is the common mode of bacterial growth typically found in the nature, although bacterial cells in suspension is often used for antibacterial investigations in laboratories (Hernández-Jiménez et al., 2013). Bacterial biofilm is a complex microbial community that is reversibly attached to a surface and protected by an extracellular polymeric substances (EPS) layer. Biofilm formation involves attachment of bacteria to a surface, subsequent formation of a microcolony and production of the EPS layer around the biofilm (Olsen, 2015). Major differences between biofilm bacteria compared to bacterial cells in suspension are that biofilm have reduced metabolic activity, higher regulation of genes needed for anaerobic growth and the biofilm cells are located closely together (Crabbé, Jensen, Bjarnsholt, & Coenye, 2019).

Moreover, the established biofilm can release bacterial cells from its structure for colonization of new habitat for formation of new biofilm structure and this accounts for the spread of bacterial infection in medical devices or even in human tissues (Admassie, 2018). These characteristics causes biofilm to be generally resistant to harsh environmental condition and displays increased resistance and tolerance to antibiotics (Flemming et al., 2016). Therefore, occurrence of biofilm in clinical infections often leads to complications in available treatment options due to its chronic nature and its ability to resist antibiotics (Hanke & Kielian, 2012). Currently, studies on antibacterial actions of GO towards biofilm are limited in the literature and also reports contradicting results (Fallatah et al., 2019; Mokkapati et al., 2018). A study by He *et al.* (2017) has shown that GO was able to inhibit the biofilm only in the early stage of growth whereas a study conducted by Guo *et al.* (2017) reported that GO enhanced the growth of biofilm formation even when exposed to 500 mg/L of GO (Guo et al., 2017; He et al., 2017).

Combinatorial therapy of nanoparticles and antibiotics have been lately suggested to enhance the antibacterial activity of antibiotics with reduced cytotoxicity of both the nanoparticle and antibiotic component (Allahverdiyev, Kon, Abamor, Bagirova, & Rafailovich, 2011). Interest in the studies on using nanoparticles for the delivery of antibiotics has escalated as nanoparticles improve antibiotic's efficacy by increasing the concentration of antibiotics at the target site and also helps in binding of antibiotic to the bacteria (Kalita et al., 2016; Panáček et al., 2016).

The use of nanomaterial as antibiotic adjuvants has been proposed and investigated mainly using metal-based nanoparticles. Metal/metal oxide nanoparticles such as silver, titanium dioxide, zinc and gold nanoparticles as antibiotic adjuvants has been vastly reported in the literature for their synergistic antibacterial effects with antibiotics (Allahverdiyev et al., 2011; Bellio et al., 2018; Hwang, Hwang, Choi, Kim, & Lee, 2012). Unique qualities of nanoparticles including its small size (<100nm) and high surface area have come in aid of antibiotics in gaining better bactericidal activity (Lam et al., 2016). This is mainly achieved by improving the chances of antibiotic penetration due to the small size of nanoparticles and an increase in the volume of antibiotic at target site through higher loading capacity of the nanoparticles (Yang et al., 2019).

Despite high number of articles reporting the antibacterial activity of GO, studies on the role of GO in increasing the efficacy of antibiotics is still lacking (He et al., 2015; Liu et al., 2018). A study conducted by Gao *et al.* (2017) has shown that GO affects the antibacterial activity of conventional antibiotics including lincomycin hydrochloride and gentamycin sulfate by acting as an antibiotic carrier (Gao et al., 2017). Besides that, studies on the antibacterial activity of GO working along with antibiotics to inhibit bacterial biofilm is also limited.

Rapid advancement in nanotechnology has created a wide range of health-related purposes for nanomaterials. Although, nanomaterials have been suggested for various medical uses, human safety remains a major concern that need to be addressed urgently (Liang et al., 2017b). Similarly, as the discovery of nanomaterials as antibacterial agents escalate, biosafety of these materials for human use has become a priority to be further investigated before approved clinical use (Schütz, Juillerat-Jeanneret, Mueller, Lynch, & Riediker, 2013). Potential health risks may occur in human body if these nanomaterials were to accumulate upon use in humans, interact with chemical components of major biochemical processes or induce physical damage to the internal organs which may induce internal bleeding and ultimately cause death (Su et al., 2018). Similarly, the nanosafety aspects of GO should be researched further for human exposure as the use of this nanomaterial increased in several medical sectors such as bioimaging, drug loading, cancer therapy and antibacterial (Pang et al., 2017).

Therefore, higher production rates of GO would undeniably expose humans to GO through multiple modes of entry which include cutaneous contact, inhalation and gastrointestinal pathways. Ma *et al.* (2015) reported that GO induced inflammatory effects through adsorption onto the plasma membrane which stimulated production of pro-inflammatory cytokines (Ma et al., 2015). Xu *et al.* (2016) claimed that GO sheets were able to enwrap the cell, get inserted into the lipid bilayer or interact with cells to enter the cytoplasm (Xu et al., 2016). Additionally, exposure to prolonged or high concentrations of GO were shown to induce physical damage to the cell membrane which affects the cytoskeleton of the cell and ultimately causes cell death (Li et al., 2013).

## 1.2 Problem statement

Antibacterial activity of GO is increasingly reported however, the detailed mechanism of action is still lacking and poorly understood (Wang et al., 2017). Although, GO has been reported to have better antibacterial activity towards Gram-positive bacteria than Gram-negative bacteria, the difference in the mechanism of action of GO between these types of bacteria was also not dealt with (Akhavan & Ghaderi, 2010; Hou, Lee, Chou, & Wang, 2017; Hui et al., 2014; Nanda, Yi, & Kim, 2016; Zou et al., 2017). Moreover, bactericidal applications of GO that are reported in the literature often described for bacterial cells in suspension only. However, bacteria are known to exist mostly in the biofilm mode of life in nature or even in clinical settings (Żur, Wojcieszyńska, & Guzik, 2016). Yet, research on the antibacterial activity of GO towards mature biofilm are still lacking and often reports conflicting results. Furthermore, there are also limited studies comparing the activity of GO against biofilm of Gram-positive and Gram-negative bacteria.

Increasing bacterial resistance to antibiotics has encouraged researchers to investigate alternatives such as combinatorial therapies with nanomaterials (Wang et al., 2017). Although metal-based nanoparticles have been continuously studied for the enhancement of antibiotic activity, studies on the role of GO in increasing the efficacy of antibiotics are inadequate although GO has been proven to act as an antibacterial agent (He et al., 2015; Liu et al., 2018). Similar to the antibiofilm studies of GO, synergistic activity of GO and antibiotics against mature biofilm are also under reported.

Data on the nanosafety of GO are increasingly reported against a wide variety of *in vitro* cell lines including macrophages, lung epithelial, neural stem, human breast cancer, human fibroblast, cervical cancer and colorectal carcinoma cells (Ou et al., 2016). However, cutaneous contact of GO towards human posed a higher risk compared to other route of administration. Since the skin is the first part of human body to come in contact with foreign particles, it is pertinent to study the cytotoxicity aspects of GO towards skin keratinocytes as other carbon-based materials such as carbon nanotubes and graphite have previously been linked to skin-related diseases (Pelin et al., 2017). However, studies on the toxic effects of GO towards skin keratinocytes are still insufficient.

## 1.3 Research objectives

(a) To characterize the physicochemical properties of graphene oxide (GO) as received.

(b) To determine the antibacterial and antibiofilm activity and the mechanistic action of GO against Gram-positive and Gram-negative bacteria.

(c) To determine the synergistic behaviour of GO with selected antibiotics against bacterial cells in suspension and biofilm of Gram-positive and Gram-negative bacteria.

(d) To determine the *in vitro* toxicological effects of GO against human epidermal keratinocytes.

## 1.4 Thesis organization

This thesis consists of five chapters which include an introduction, literature review, materials and method, results, discussions and conclusion along with future recommendations.

The contents of each chapter are summarized:

**Chapter 1: Introduction**

This chapter explains the overall background of the study, problem statement and the involved research objectives. The rational for this study is also explained.

**Chapter 2: Literature Review**

This chapter reviews the importance of antibiotics and the need for an alternate solution to address emerging antibiotic resistance. Previous findings regarding the antibacterial activity of GO are described in this section. Additionally, the toxicology aspects of the use of GO in cell lines have been explained in this part.

**Chapter 3: Materials and Methods**

Materials used for the experiments described in this study have been listed in this section. The detailed procedure of each methodology carried out in this work are also included in this chapter.

**Chapter 4: Results**

The experimental results are fully described in this chapter. They include characterization results of as received GO, antibacterial activity of GO against bacteria in suspension and in biofilm state, combinatorial therapy of GO and conventional antibiotics and cytotoxicity studies of GO against HaCaT cells.

**Chapter 5: Discussions**

The interpretation and explanation of experimental results and observation are elaborated and discussed in this chapter.

**Chapter 6: Conclusion and Recommendation for Future Works**

Overall findings of this work are briefly described in this section and suggestions for future works have been included in this section as well.

# CHAPTER 2: LITERATURE REVIEW

## 2.1 Antibiotic resistance

### 2.1.1 Discovery of antibiotics

The term 'antibiotic' originally refers to natural substances that are produced by microorganisms which render bacteriostatic or bactericidal effects on other bacteria (Clardy, Fischbach, & Currie, 2009). In recent times, this term has evolved to include even synthetic chemical products along with natural compounds that exhibit antibacterial activities (Brown & Wright, 2016). The origins of antibiotics are usually traced back to the discovery of penicillin by Sir Alexander Fleming in 1929 when he found that a substance secreted by *Penicillium chrysogenum* mould was able to inhibit the growth of bacteria in a contaminated culture plate (Fleming, 1929). However, it was not until the 1940s that advances in the techniques of purification technology have made possible for penicillin to be produced in large quantity for medical use (Aminov, 2010).

After this breakthrough, the following 20 years were referred to as the 'Golden Age' as most of the classes of antibiotics present today were first discovered during this time period as shown in Figure 2.1 (Saga & Yamaguchi, 2009). The initial sources for the antibiotics were from other microorganisms where soil samples from various places on earth were searched for naturally occurring substances with antibacterial potential. This includes vancomycin, a glycopeptide antibiotic used for treating penicillin-resistant *S. aureus* which was isolated from a soil sample from Borneo in 1952 and this drug was made available for use in 1958 (Levine, 2006). By then, resistance to antibiotics began to emerge where penicillin became ineffective due to the presence of β-lactamase enzyme in bacteria that can hydrolyse the β-lactam ring found in the antibiotics (Gould, 2016).

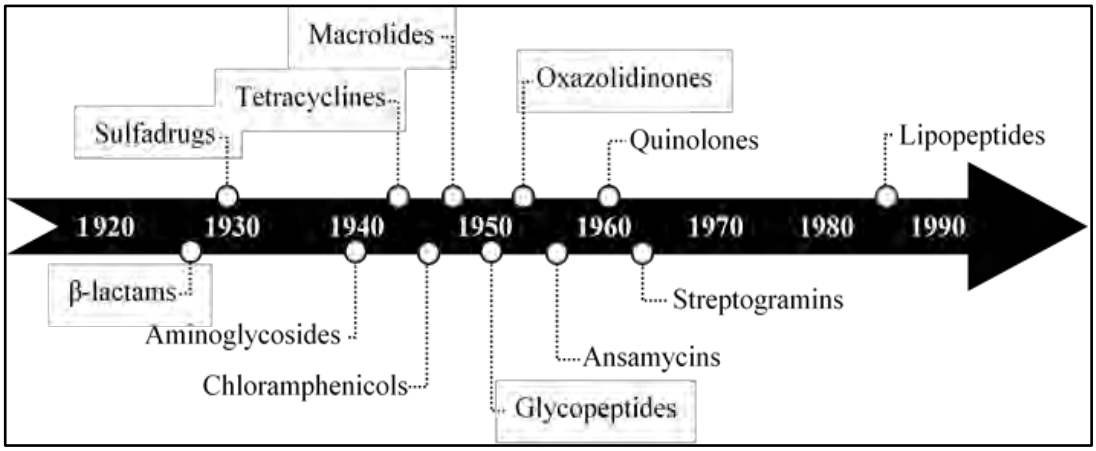


**Figure 2.1:** The timeline shows the discovery of antibiotics ever since penicillin was accidentally discovered by Sir Alexander Fleming. It is clearly illustrated that the discovery of new classes of antibiotic has almost come to an end during the 1990s. Adapted from Lewis *et al.* (2012) with permission from Springer Nature.

Methicillin was brought into clinical use as the first penicillinase-resistant antibiotic in 1959 and followed by the introduction of ampicillin in 1961, which had improved pharmacokinetics and antibacterial spectrum of penicillin (Kowalski, Berbari, & Osmon, 2005). Cephalosporins were approved for use in the 1960s for the treatment of skin and soft tissue infections and this class was divided into four generations categorized according to their antibacterial spectrum (Russell, 1975). Later in 1976, substances that inhibit the bacterial β-lactamase were discovered and this includes clavulanic acid. This compound was combined with amoxicillin to become the co-amoxiclav and thienamycin, the precursors for another class of antibiotics, carbapenems (Drawz & Bonomo, 2010).

Imipenem, a carbapenem antibiotic was made available for medical use in 1980s and later, meropenem, another member of the carbapenem class was available for use in 1995 with fewer side effects compared to imipenem. This class of antibiotic was commonly prescribed for treating multi-drug resistant bacterial infections (Papp-Wallace, Endimiani, Taracila, & Bonomo, 2011).

Nalidixic acid, a synthetic quinolone antibiotic was introduced in 1967 for treating urinary tract infections and later the more successful fluoroquinolones which were available in oral form were developed for the treatment of both Gram-positive and Gram-negative bacterial infections (Emmerson & Jones, 2003).

Emergence of antibiotic-resistant strains of *S. aureus* or methicillin-resistant *S. aureus* (MRSA) and enterococci such as *E. faecalis* and *Enterococcus faecium* has led to the shift in the focus of antibiotic discovery mainly to treat bacterial infections caused by these microorganisms (Gould, 2016). Although vancomycin was still in use for the treatment of these bacterial infections, this drug was only available in the intravenous form. Newer glycopeptide antibiotic such as teicoplanin was made available for use in the 1990s and still widely used (Greenwood, 1988). Cycloserine, an oxazolidinone, was used for treating TB infections in 1956. Linezolid, another member of this class of antibiotic was considered to be an alternative to glycopeptides for the treatment of Gram-positive bacterial infections as this drug had better oral availability and displayed antibacterial activity against glycopeptide-resistant enterococci and even drug-resistant mycobacteria (Gould, 2011).

### 2.1.2 Emergence of antibiotic resistance

Increasing use of antibiotics in the medical field and in non-therapeutic animal use has become the stepping stone for the development of antibiotic resistant bacteria (Banin, Hughes, & Kuipers, 2017). As the total number of antibiotics that have been produced since the golden age of antibiotics in 1950s will definitely be a considerable amount, it is likely that this amount is significantly higher than the quantity that naturally occurs in the soil environment (Davies, 2006). While approximately 50% of the total antibiotic production has been devoted to human use, the remainder has been applied to the agriculture, aquaculture and animal husbandry sectors.

The overflow of antibiotics from human use into the natural ecosystem greatly affected the microbial environment. Therefore, the bacterial population in the soil responded to the selective pressure using natural genetic modifications and horizontal gene transfers for their survival. Hence, bacteria with high levels of resistance to antibiotics prevail in the ecosystem (Lerner, Matthias, & Aminov, 2017).

Bacterial resistance to a particular antibiotic has always been claimed to appear shortly after its approval for use (Saha et al., 2018). The two main important reasons for the problem of antibiotic resistance are: use of antibiotic actively inhibits susceptible bacteria and selects the resistant bacteria to thrive; and activation of resistance mechanism that previously exist in the bacteria due to the antibiotic pressure. Resistance to antimicrobial drug often appears when these two phenomena occur together in a biological setting contributing to a difficult clinical situation (Levy & Marshall, 2004). The selected bacteria with resistant genes continue to spread and proliferate under continuous antibiotic pressure and this often extends to different human hosts and even other geographical sites. Substantial amount of antibiotics (millions of kilograms) are produced and consumed each year for medical treatments and prophylactic treatment of animals and agricultural sectors globally which contributes to the endless drive of antibiotic-resistant bacteria selection and elimination of the susceptible strains (Li & Webster, 2018).

Widespread multidrug resistance has been suggested to occur due to bacteria acquiring resistance genes and amplification of these genes through selection process for survival (Sandoval-Motta & Aldana, 2016). The ability of the bacteria to capture, accumulate and spread of these resistance genes are contributory to mobile genetic elements.

These elements are responsible for the movement of intracellular DNA which is inclusive of DNA mobility from the chromosome to a plasmid or even between plasmids and the movement of intercellular DNA between different cells (Brown-Jaque, Calero-Cáceres, & Muniesa, 2015). Intracellular DNA movement of resistance genes within a single cell are usually aided by insertion sequences, transposons and integrons to move to a new location often within the same or a different DNA molecule (Partridge, Kwong, Firth, & Jensen, 2018). Comparatively, intercellular DNA movement of resistance genes between different cells are accommodated by three main methods; conjugation (transfer of genetic elements between bacterial cells aided by plasmid and integrative conjugative elements), transduction (introduction of resistance gene to a bacterium through viral vector or bacteriophage) and transformation (uptake and incorporation of extracellular DNA) (von Wintersdorff et al., 2016).

Acquisition of resistance gene gives rise to a subgroup of bacteria that are able to withstand the activity of the antibiotic. Although the antibiotic was able to fully eliminate the susceptible population of bacteria, the resistant bacteria remain and continue to predominate the site of infection (Trastoy et al., 2018). However, the maintenance of resistance genes burdens the bacterial fitness and therefore these genes are only maintained in the presence of the antibiotic itself (Melnyk, Wong, & Kassen, 2015). Although various bacterial resistance mechanisms have been described previously as shown in Figure 2.2, the mechanisms of resistance can be categorized into three pathways. Typically, the three major pathways bacteria exert resistance to antibiotics includes: (1) the alteration of the antibiotic compound where enzymes such as β-lactamases inactivate penicillins and cephalosporins; (2) active efflux of the antibiotic; and (3) intracellular modification of the antibiotic binding target (Levy, 1992; Munita & Arias, 2016; Nikaido, 1996).

Antibiotic resistance usually develops when a single antibiotic was used for longer than necessary. The extended usage will favour the growth of bacteria that is resistant to the specific antibiotic and additionally the normal flora of the human organ will be wiped out and replaced by colonization of the resistant bacteria (Langdon, Crook, & Dantas, 2016). Usually, long term use of antibiotics too selects for the bacteria that is resistant not only to that same antibiotic, but also towards other antibiotics from the same class as well. This occurrence has been linked to the existence of different resistant genes which originates from a single plasmid or transposon (Garneau-Tsodikova & Labby, 2016).

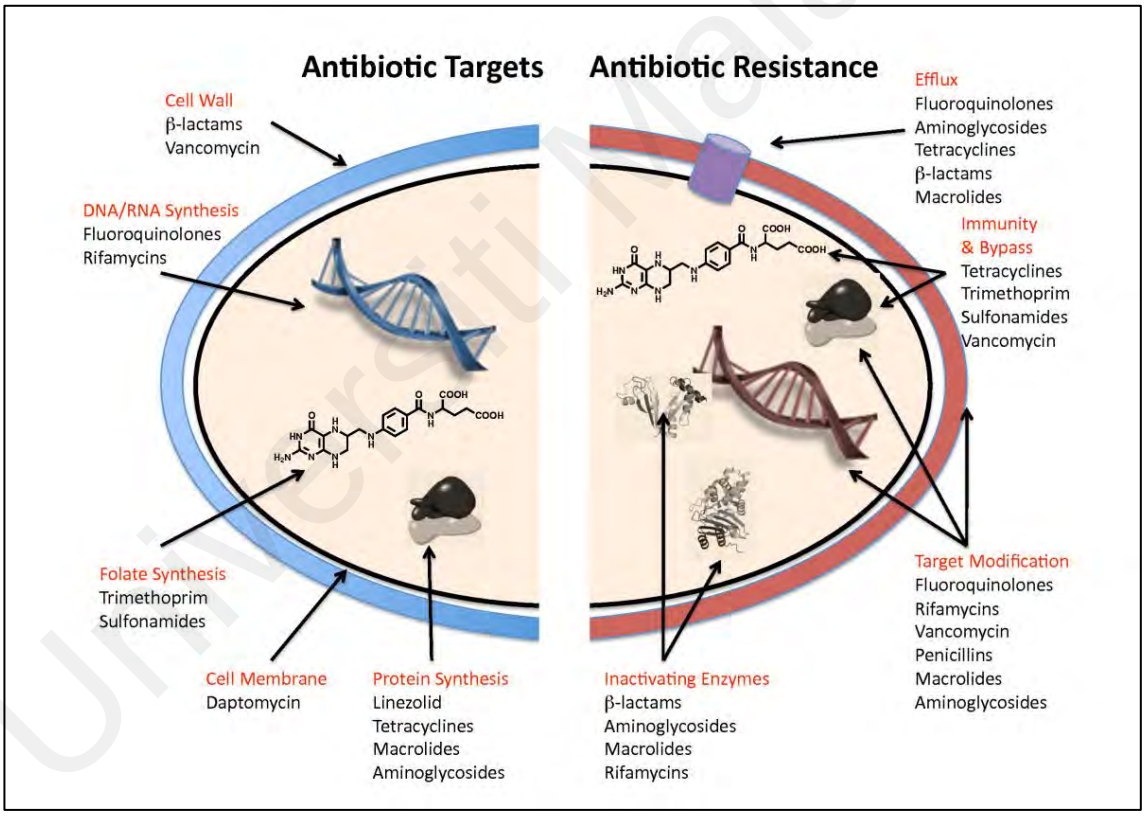


**Figure 2.2:** Common antibiotic resistance mechanisms. The antibiotic can be prevented from reaching its target through antibiotic inactivation, modification of cell wall protein, bypass of pathway targeted by the antibiotic, active efflux of antibiotic out of the bacterial cell membrane or alteration at the antibiotic binding site. Adapted from Wright *et al.* (2010).

It was initially assumed that acquisition of resistance genes causes additional energy use for bacterial survival and thus these multidrug resistant bacteria were considered to be unstable at laboratory conditions (Davies & Davies, 2010). However, currently available literature suggests that these group of bacteria are able to survive and evolve successfully even in culture media (Händel, Schuurmans, Brul, & ter Kuile, 2013; Melnyk et al., 2015).

### 2.1.3 Antibiotic resistance through biofilm mode of life

Bacteria can become resistant to antibiotics when they form biofilm. Biofilm are currently considered to be the contributing factor in many chronic infections caused by resistant bacterial pathogens (Koo, Allan, Howlin, Stoodley, & Hall-Stoodley, 2017). Formation of biofilm occurs after extended periods of clinical dormancy which reduces bacterial metabolic rate and causes the bacteria to develop tolerance to antibiotics (Flemming et al., 2016). They are irreversibly attached to a surface and protected by a layer of extracellular polymeric substance (EPS).

The main features that distinguish biofilm cells from non-adherent bacterial cells are that biofilm cells constantly experience a decrease in available nutrients and increase in the waste products which lead towards a stressful environment for its growth. Bacterial cells within a biofilm are often characterized by phenotype, metabolic activity, antibiotic tolerance and gene expression, respective to the localization of the bacteria in the biofilm (Flemming & Wingender, 2010). The trademark of biofilm cells is that they are inherently resistant to disinfectants, antibiotics and even immune modulators (Koo et al., 2017). Therefore, this makes biofilm to be comprised of physiologically heterogeneous bacterial subpopulations which makes removal of biofilm to be notoriously difficult (Olsen, 2015).

It is a known fact that bacterial cells of the biofilm are highly resistant to antibiotics compared to similar bacterial cells in suspension (Sharma, Misba, & Khan, 2019). Hence, our ability to ultimately reduce biofilm infections is nearly impossible even with the currently available antibiotics (Königs, Flemming, & Wingender, 2015). Interactions of biofilm cells with the environment are partly modulated by the self-produced EPS layer which protects the biofilm cells and this layer consists of protein, lipids, polysaccharides and extracellular DNA. The EPS layer has been occasionally ruled out as the cause of limited antibiotic penetration into the biofilm matrix (Flemming & Wingender, 2010). This layer is responsible for controlling the growth conditions of the bacteria within the biofilm and also for the stability of the biofilm structure. EPS layer too has been reported to entrap or inactivate antibiotic that comes into contact with this layer (Brown, Allison, & Gilbert, 1988; Pandey et al., 2019). This problem has led to the increase in biofilm-related infections to persist in chronic infections despite prolonged antibiotic therapy (Ciofu, Rojo-Molinero, Macià, & Oliver, 2017).

Besides the protective effects of the EPS matrix, the bacteria in the biofilm evade antimicrobials by reducing its growth rate which then leads to dormancy as depicted in Figure 2.3. As biofilm contain considerable number of bacteria in the stationary phase, antibiotic susceptibility reduces as antibiotics usually target metabolically active bacteria (Brown et al., 1988; Yang, Bening, & Collins, 2017). Although it has been reported that only 1% of biofilm bacteria in the stationary phase becomes antibiotic tolerant, this number increases over time (Amato et al., 2014; Maisonneuve & Gerdes, 2014). Certain antibiotics such as vancomycin were found to exhibit a reduced rate of killing as maturity of the biofilm increases (Monzón, Oteiza, Leiva, Lamata, & Amorena, 2002; Song, Duperthuy, & Wai, 2016). Additionally, horizontal gene transfer of resistance gene may occur in biofilm through conjugative plasmids (Król et al., 2013).

Cell to cell contact between bacteria in biofilm promotes the spread of resistance genes as the EPS layer acts as an excellent medium by offering a stable environment for contact between cells and also a rich source of environmental DNA (Stalder & Top, 2016). This process was found to be 7 to 700-fold more efficient in biofilm than in bacterial cells in suspension due to the close proximity of bacteria in the biofilm structure (Król et al., 2013; Madsen, Burmølle, Hansen, & Sørensen, 2012).

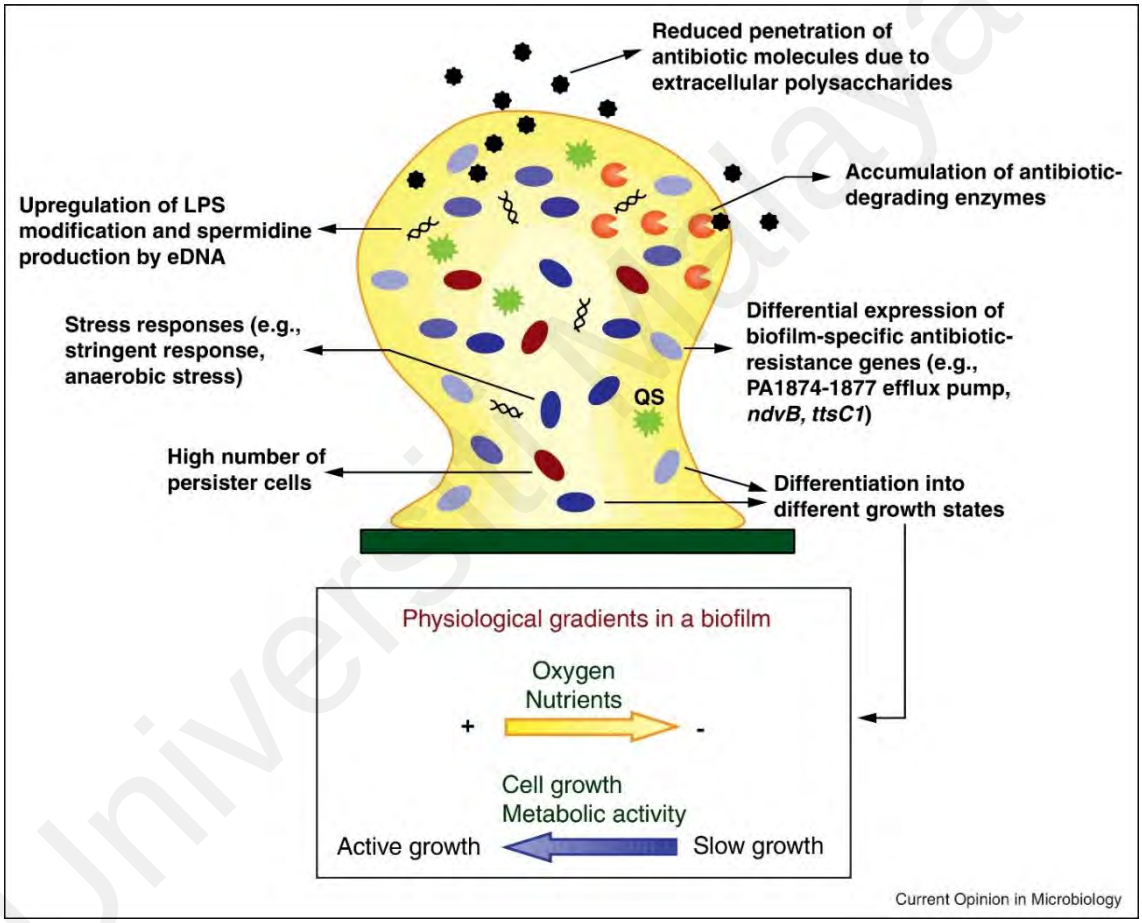


**Figure 2.3:** Graphic illustration of antibiotic resistance mechanisms among biofilm. Differentiation of biofilm cells into different stages of growth is influenced by the concentration gradients of oxygen and nutrients present in the biofilm structure as depicted in the box within the diagram. Abbreviations: QS for quorum-sensing signal; eDNA for extracellular DNA. Adapted from de la Fuente-Núñez, Reffuveille, Fernández, & Hancock (2013) with permission from Elsevier.

## 2.2 Alternate antimicrobial agents

Antimicrobial resistance is a major concern in the treatment of bacterial infections and the gap between the need for new antibiotics and the discovery of novel drugs to treat bacterial infections escalates (Fair & Tor, 2014). Therefore, it is essential to preserve the use of currently existing antibiotics and one of the important ways of achieving this is by using alternate antimicrobial agent, such as nanomaterials which have antibacterial action (Beyth, Houri-Haddad, Domb, Khan, & Hazan, 2015; Hemeg, 2017). The use of nanomaterials to fight bacterial infections is particularly interesting due to the existence of several mechanism of action of antibacterial activity. These are mainly due to the various physicochemical properties of the nanomaterial (Zhang, Pornpattananangkul, Hu, & Huang, 2010). The general mechanism of action of nanomaterials are bacterial membrane disruption and generation of ROS (Blecher, Nasir, & Friedman, 2011; Pelgrift & Friedman, 2013).

Disruption in bacterial membrane occurs when the nanomaterial binds to the cell wall of the bacteria through electrostatic binding. Contact between the nanomaterial and bacteria leads to membrane depolarization and subsequent changes in bacterial membrane potential (Bondarenko et al., 2018). Therefore, the loss of bacterial membrane integrity often interrupts physiological processes in bacteria such as respiration, imbalance of nutrient transport and loss of energy production (Pelgrift & Friedman, 2013). Ultimately, this leads to bacterial cell death. On the other hand, generation of ROS leads to oxidative stress, lipid peroxidation, DNA damage and mutations. Production of ROS in the bacteria is often due to the interruption of the bacterial respiratory process or generated from the nanomaterial itself (Nathan & Cunningham-Bussel, 2013).

Commonly studied nanomaterials for their antibacterial activity include metal-based nanomaterials such as silver (Ag), titanium dioxide ($TiO_2$), copper oxide (CuO), iron oxide ($Fe_3O_4$) and zinc oxide (ZnO). The bactericidal properties of metal-based nanomaterials are mostly through generation of ROS, physical damage and release of metal ions (Beyth et al., 2015). Silver (Ag) nanoparticles have been widely studied for their bactericidal properties against bacteria, virus and fungi isolates and their antibacterial activity has been acknowledged since ancient times. Ag nanoparticles have been reported to cause pits on the bacterial cell wall which increases membrane permeability and inactivation of the bacterial respiratory process as shown in Figure 2.4 (Slavin, Asnis, Häfeli, & Bach, 2017; Sondi & Salopek-Sondi, 2004).

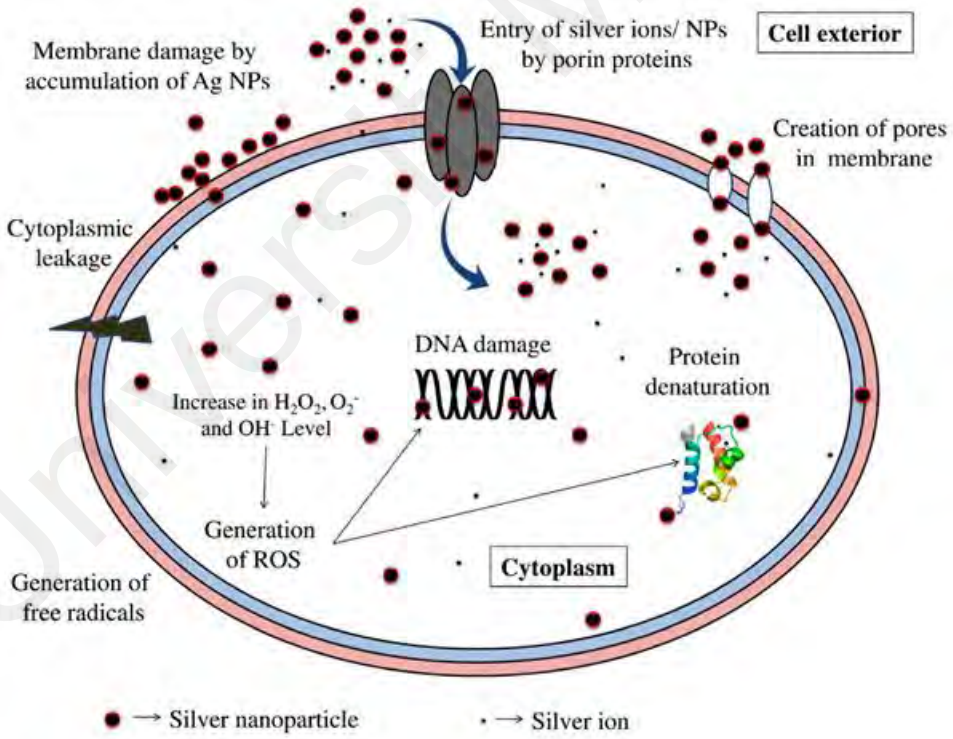


**Figure 2.4:** Antibacterial mechanism of Ag nanoparticles against bacteria. Generation of ROS species in the bacteria due to the exposure to Ag nanoparticles induces destructive pathways that lead to cell death. Adapted from Pareek, Gupta, & Panwar (2018) with permission from Elsevier.

Similarly, $TiO_2$ has antibacterial activity towards Gram-positive and Gram-negative bacteria as well. This nanoparticle has been shown to stimulate ROS burst which damages bacterial membrane, organelles and DNA (Blecher et al., 2011). ZnO-based nanoparticles too have a wide range of bactericidal activity depending on its dose and particle size. Additionally, these nanoparticles were previously reported to inhibit the growth of multidrug resistant pathogens such as MRSA and methicillin-resistant *Staphylococcus epidermidis* without being affected by these microorganism's drug resistant mechanisms (Ansari, Khan, Khan, Sultan, & Azam, 2012).

These metal/metal oxide nanomaterials have the potential to be used as an alternate bactericidal agent and have been used in the past decade as antibacterial materials to curb antibiotic resistance (Allahverdiyev et al., 2011). Although the antibacterial action of metal/metal oxide nanomaterials seems relevant in the past, these nanomaterials are not chemically inert (Trivedi, Patil, Shettigar, Bairwa, & Jana, 2015). This inadequacy may affect the stability and the antibacterial actions of metal/metal oxide nanomaterial, thus it is not recommended for long-term use especially in the clinical application (Gao et al., 2017).

## 2.3 Graphene oxide

Graphene oxide (GO) is one of the promising materials that has been reported to have excellent antibacterial properties due to the ease and low cost of preparation and ability to be produced in a large-scale (Papi et al., 2016; X. Wu et al., 2017; Zhou & Bongiorno, 2013). GO is the preferred nanomaterial in the biomedical field over other carbon allotropes because of its stability in colloidal form and the reliability of graphene's aqueous dispersibility when it is in a single or multi-layered state (Liu et al., 2010).

Ever since the first medical application of GO was demonstrated in the field of drug delivery in 2008, the research initiative in exploring other uses of graphene material in the biomedical field has been increasing exponentially (Liu, Robinson, Sun, & Dai, 2008; Sun et al., 2008; Yang, Feng, Shi, & Liu, 2013).

Graphene is a single atomic layered two-dimensional (2D) nanomaterial that has garnered remarkable attention for various applications such as conductors, transistors, energy storage, biosensing, gene delivery and mass spectrometry techniques in the recent years (Li et al., 2013). Graphene's high values of elastic modulus, breaking strength, specific surface area, thermal conductivity and its fascinating quantum Hall effect have given it a unique place in material science (Novoselov et al., 2007; Park & Ruoff, 2009). The single sheet of graphene was isolated and characterized only in 2004 (Boehm, Clauss, Fischer, & Hofmann, 1962; Boehm, Setton, & Stumpp, 1994; Novoselov et al., 2004). The carbon atoms in GO are oriented in a honeycomb-like structure where bonding between graphene sheet and several oxygen molecules in the form of carboxyl (COOH), epoxy (C-O-C), hydroxyl (C-OH) and carbonyl (C=O) groups as shown in Figure 2.5.

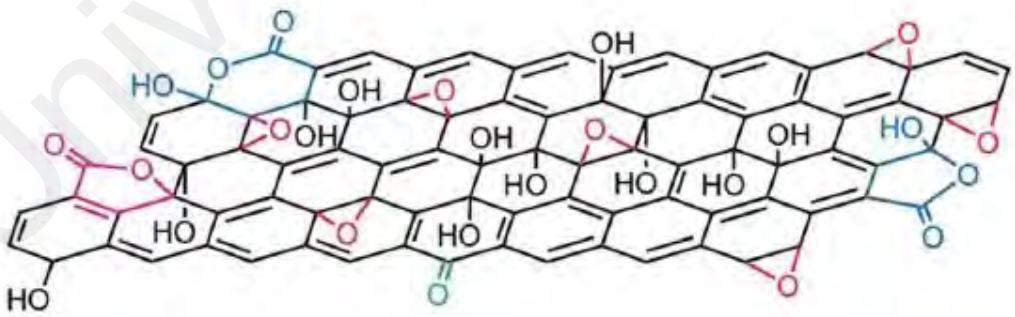


**Figure 2.5:** The structural model of GO. Functional groups that are found on GO are five- and six-membered lactol rings (blue), ester of tertiary alcohol (purple), hydroxyl (black), epoxy (red) and ketone (green) functionalities. Adapted from Gao, Alemany, Ci, & Ajayan (2009) with permission from Springer Nature.

The backbone of graphene is made up of strong σ bonds, and the π bonds are situated perpendicular to the plane that collectively have made up its electronic structure (Si, Sun, & Liu, 2016).

The emerging fields of nanotechnology are increasingly accommodating because of its nano-sized dimension that can easily penetrate cells, biocompatibility, capability of tunable surface functionalization with biological agents, possibility of drug carriage in the hollow lumen, high-tensile strength for use in scaffolding agent for bone generation, semiconducting properties that are suitable for biosensing of toxic agent (Amenta & Aschberger, 2015; He et al., 2013; Jain, 2012). Moreover, GO can be freely modified making it an excellent material for biosensor construction and drug loading in medical applications (Ostrikov, Neyts, & Meyyappan, 2013). Furthermore, GO has been utilized as a photothermal agent for the treatment of cancer cells because of its intrinsic near-infrared (NIR) absorbance values (Li, Yang, Ren, Qu, & Qu, 2012; Robinson et al., 2011; Yang, Asiri, Tang, Du, & Lin, 2013b). Additionally, enrichment and detection of aromatic molecules and single-stranded DNA can be done with graphene via the π-π stacking interactions (Tang et al., 2010).

### 2.3.1 Synthesis of GO

The common synthesis of graphene nanomaterial is through micromechanical cleavage of graphite, reduction of graphite oxide, graphite intercalation technique and chemical vapour deposition (Geng, Kong, Yang, & Jung, 2010; Hu, Lu, Chen, & Zhang, 2013; Kim et al., 2009). However, methods such as longitudinal unzipping of CNT has been used to produce graphene nanoribbons, chemical vapour deposition on nickel and copper films for large scale synthesis of graphene and also through hydrothermal synthesis and sonication (Choucair, Thordarson, & Stride, 2009; Hu et al., 2013; Kosynkin et al., 2009; Reina et al., 2008).

GO, a derivative of graphene sheet with oxygen-containing functional groups, are more hydrophilic in comparison to hydrophobic qualities of graphite and the hydrogen bonds between the water molecules and the polar functional groups provides a better dispersion rate under certain pH conditions (Bitounis, Ali-Boucetta, Hong, Min, & Kostarelos, 2013). Up to date, the most classical method of GO synthesis is by the Hummers method, initially introduced in 1958 and this procedure involves the oxidation of graphite through the use of potassium permanganate in a solution of concentrated sulphuric acid as illustrated in Figure 2.6 (Hummers Jr & Offeman, 1958; Soltani & Lee, 2017).

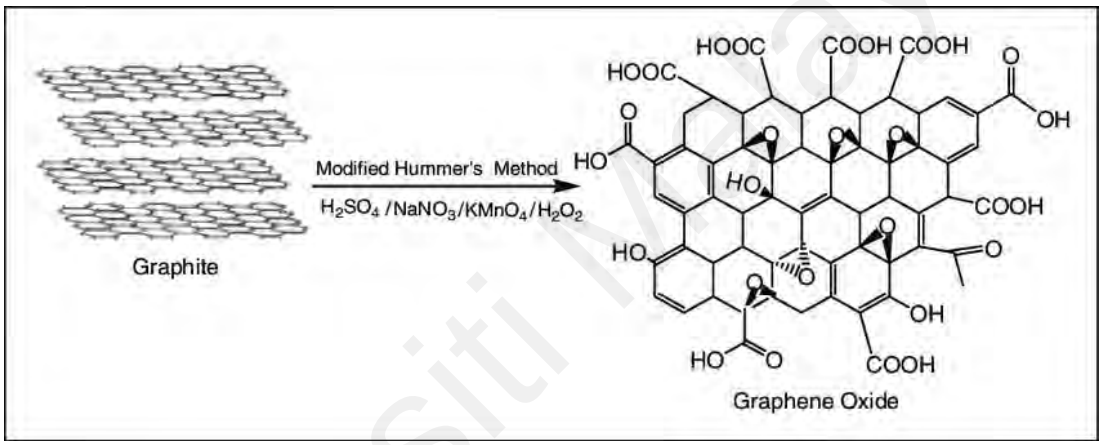


**Figure 2.6:** An illustrated preparation of graphene oxide through modified Hummer's method. Adapted from Ahmad, Kausar, & Muhammad (2016) with permission from Sage Publishing.

The use of graphene nanomaterial extends into various fields of applications which include but not limited to applications in polymer composites, mechanical resonators, energy-storage material and 'paper-like' materials (Acik & Chabal, 2011; Park & Ruoff, 2009). Besides industrial use, graphene nanomaterial may also be a suitable candidate for uses in the health-related field for its excellent physicochemical characteristics. Applications of graphene nanomaterial in the biomedical field can be categorized into different applications such as sensing, tissue engineering, delivery systems and bactericidal agents (Wu et al., 2017).

The intrinsic characteristics of graphene nanomaterial that are contributory to their beneficial effects include; high availability of surface area for drug loading, flexible surface coating that can be modified according to specific biological usage and high NIR absorbance rate that is convenient for photothermal therapy especially for cancer treatment (Papi et al., 2016).

### 2.3.2 Mechanistic actions of GO

The number of antibacterial studies involving the use of graphene nanomaterial has been on the rise, especially those exploring the differences in physicochemical properties that influence the antimicrobial potential of the nanomaterial itself (Zou et al., 2016). However, variance in the activity of graphene have led to many reports with contradictory results. Therefore, it is important to elucidate the bactericidal activity of graphene in accordance to the physicochemical attributes of graphene. Intrinsic properties of graphene differ from one to another as a result of the synthesis method used, leading to variations in lateral size, morphology, dispersibility and number of layers (Wang, Bai, & Shi, 2011; Zhang et al., 2009). Mechanical defects on the surfaces of graphene nanomaterial during the synthesis of the material are often responsible for the increasing number of active sites that can improve interaction with the bacterial cells and exert its antibacterial properties (Ameen, Akhtar, Seo, & Shin, 2013; Zhang, Zou, & Zhao, 2015b).

**a. Membrane disintegration**

The first report on the potentials of GO as an antibacterial nanomaterial was published in year 2010 (Akhavan & Ghaderi, 2010). Since then, three major types of mechanism have been reported for the antibacterial action of graphene towards bacterial models, particularly nano-knives or nano-darts, a name mainly derived due to the very sharp edges of the graphene sheets, ROS-dependent or ROS-independent oxidative stress and the masking of bacterial cells by graphene thin films.

These are the mechanisms that are reported most frequently in comparison to the lesser-known mechanisms including the lipid bilayer extraction and disruption of protein-protein interaction mechanisms (Szunerits & Boukherroub, 2016).

The key mechanism of graphene is through the sharp edges of the nanomaterial that acts like a blade upon contact with the bacterial cell and induces disruption on the membrane structure which causes leakage of intracellular compound and eventual cell death (Pumera, 2010). One of the earliest study on antibacterial potential of graphene, reported that sharp edges of GO nanowalls were found to inactivate *S. aureus* and *E. coli* through membrane damage (Akhavan & Ghaderi, 2010). Additionally, RNA efflux in the bacterial growth medium indicated a higher amount of membrane damage for *S. aureus* in comparison to *E. coli* and a greater toxicity rate was observed in the bacterial sample when GO reduced by hydrazine was utilized. It was suggested that improved charge transfer between the bacterial cell and the nanomaterial occurred in the reaction medium due to the reduced state of the GO (Akhavan & Ghaderi, 2010).

Antibacterial activity of graphite (Gt), graphite oxide (GtO), graphene oxide (GO) and reduced graphene oxide (rGO) were systemically tested against *E. coli* for comparison of their bactericidal ability. GO dispersion had the highest antibacterial activity followed by rGO, Gt and GtO. Liu *et al.* (2011) credited the sharp edges of GO for being responsible for its antibacterial activity as shown in Figure 2.7 (Liu et al., 2011). Moreover, difference in length of edge and angle of orientation of graphene were observed to influence the bactericidal efficiency of the graphene, where, a study specifically conducted to address this issue, reported that density of the edges of graphene was a critical factor in determining antibacterial behavior (Pham et al., 2015).

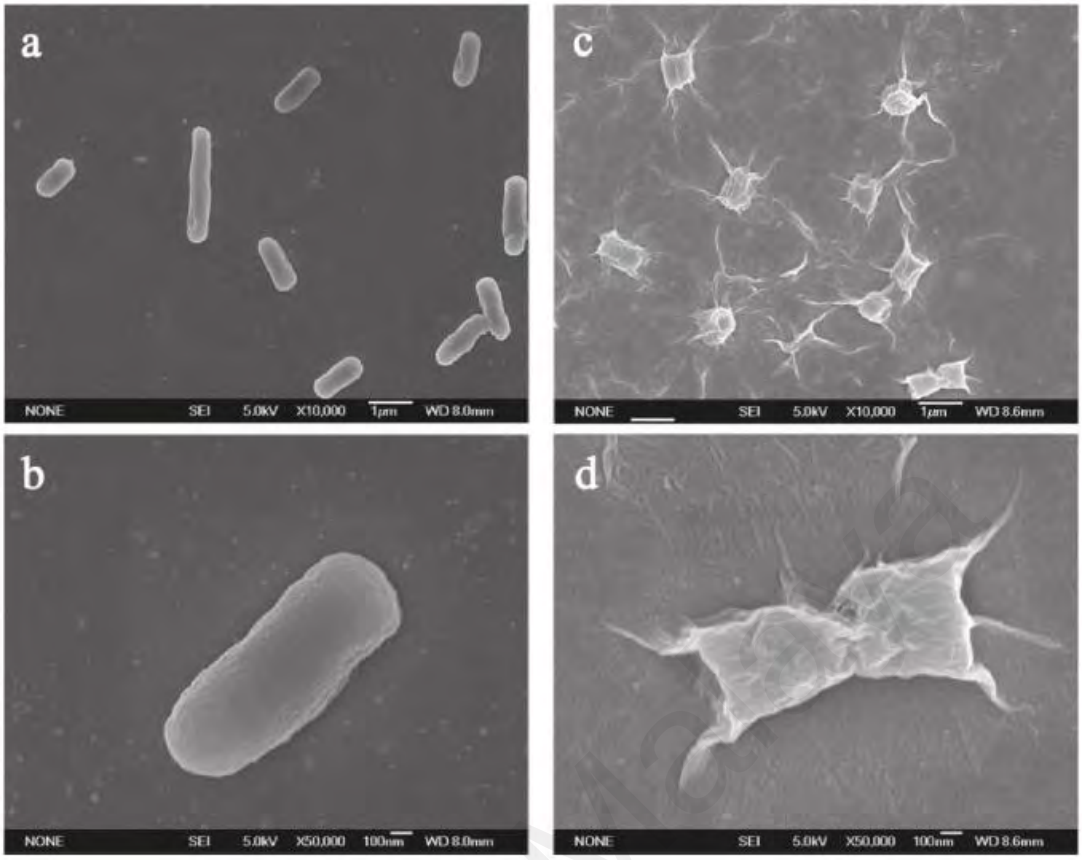


**Figure 2.7:** Electron microscopic images of *E. coli* before and after treatment with graphene oxide dispersion. A clear disruption of bacterial membrane was observed after the graphene oxide treatment. (a, b) Control *E. coli* cell after incubation in just saline solution for 2 h. (c, d) *E. coli* cell after treatment with 40 µg/mL of graphene oxide dispersion for 2 h. Adapted from Liu *et al.* (2011) with permission from American Chemical Society.

Nevertheless, a few studies indicated that sharp edges of graphene alone is not responsible for its antimicrobial potential but the adsorption on the basal planes of graphene plays a role in damaging the bacterial membrane (Li et al., 2014; Mangadlao et al., 2015; Pham et al., 2015). The Langmuir-Blodgett (LB) technique was used to immobilize GO sheets on a polyethylene terephthalate (PET) substrate to mask the edge from engaging in bacterial interaction, however, GO was still able to exert bactericidal effects on *E. coli*. Therefore, it is proposed that bacterial inactivation is likewise dependent on chemical functionalities that are available on the basal plane of the graphene nanomaterial (Mangadlao et al., 2015).

Similarly, when GO was exposed to saline supplemented with 10% of nutrient broth, the antibacterial activity of the GO sheets was inactivated completely. It was deduced that non-covalent adsorption of nutrients present in bacterial growth media onto the basal plane of GO, causes attenuation of GO's bacterial toxicity as the GO-bacterial cell interaction has been hindered through non-covalent adsorption (Hui et al., 2014).

Therefore, non-covalent adsorption on the basal planes of graphene hinders its antibacterial activity. Simulation studies have demonstrated that larger GO sheets may disrupt and contribute towards upturned phospholipids from the bacterial membrane through interaction with the membrane layer by partaking a parallel attachment on the top of the membrane layer (Wang, Yu, Gui, Jin, & Xia, 2016). Nevertheless, membrane disintegration of bacterial cells is one of the key mechanistic cytotoxic actions of GO towards bacterial cells.

**b. Oxidative stress**

Abundance of ROS in the intracellular component of bacterial cells induces oxidative stress in bacteria, which can interrupt important cellular functions that affects the mortality of the bacteria (Mani, Chen, & Lou, 2013). It has been indicated that graphene too induces oxidative stress in the bacterial model upon exposure. Additionally, the generation of ROS in bacterial cells exposed to GO was higher than any other graphene-based nanomaterials (Sodhi, 2016; X. Zou et al., 2016). Expression of higher ROS in the cells that have been exposed to GO nanosheets is contributory to the stability of the GO aggregation in the suspension-based reaction medium (Pumera, 2010). The existence of defect density on GO sheets mediates the adsorption of $O_2$ mainly on the defect sites and the edges of the nanomaterial while the presence of ROS causes the reduction of the reducing enzymes such as glutathione that are present in the cells (Koch et al., 2014).

Glutathione maintains a stable redox state in bacteria by the prevention of cellular damage due to the ROS and studies often conclude on generation of ROS within the bacterial cells through the ratio of glutathione to glutathione disulfide to determine the state of oxidative stress among the bacterial cells (McKenna, 2013).

Oxidation of glutathione is influenced by the size of GO nanosheets and smaller GO nanosheets were reported to induce increased oxidation of glutathione compared to larger GO sheets and the increase in oxidation rate also have been linked to the better antibacterial potential of the smaller GO sheets (Perreault et al., 2015). The oxidation of glutathione has been proposed to facilitate through two mechanisms where one of the methods is by direct oxidation of the reducing enzyme by the GO nanosheets and the other method is by adsorption of dissolved dioxygen at the edges and defect corners of GO. Adsorption of $O_2$ on to the defects of GO causes the formation of oxides on the surfaces of the GO. Then, glutathione enzyme, the intracellular redox mediator reduces these oxides through electron transfer which liberates ROS, which are in turn then reduced back by the glutathione enzyme (Koch et al., 2014).

Therefore, oxidative stress in bacterial cells are mediated through exposure to GO nanosheets which causes cell damage facilitated by ROS or through depletion of natural antioxidants that are present in the cells (Sanchez, Jachak, Hurt, & Kane, 2012). Another study demonstrated that the generation of ROS which causes GO-mediated cell death, was associated with incubation of the bacterial cells with an external addition of antioxidants such as glutathione or N-acetylcysteine (NAC).This reduced the ROS-mediated oxidative stress experienced by the bacteria model (Gurunathan et al., 2013; Sodhi, 2016).

Lipid peroxidation is yet another membrane disintegration process mediated by oxidative stress experienced by bacterial cells through interaction with graphene nanomaterial. This reactive mechanism is facilitated through ROS which initiates the oxidation of lipid molecules to form lipid peroxide radicals, which in turn propagates oxidative damage throughout the bacterial cell membrane by causing the formation of lesions and subsequent leakage of cellular content (Hanif, Ahmed, Shin, Kim, & Um, 2014).

Another study reported the discovery of conjugated dienes, lipid hydroperoxides and malondialdehydes in the bacteria. These components are the intermediate products of the lipid peroxidation at different stages, therefore the authors claimed that this was due to the actions of graphene nanosheets towards bacterial cell membrane (Krishnamoorthy, Veerapandian, Zhang, Yun, & Kim, 2012). However, bacteria have a defense strategy against the violation of ROS towards its membrane through the protection offered by antioxidants (free radical scavenger) such as α-tocopherol which is situated inside the membrane. Pre-incubation of the bacterial cells with these antioxidants has prevented the membrane damage by removal of ROS thus further proving the importance of ROS in generating oxidative stress (Perreault et al., 2015).

Besides generation of ROS, other biological stress pathways in the bacterial cells too may induce oxidative stress. Liu *et al.* (2011) reported low levels of $O_2^{\bullet-}$ in the exposure medium, however, they noted that oxidation of glutathione took place regardless of the near-absence of ROS. The conductivity of graphene has been proposed to be the most probable stimulant of the oxidative stress experienced by the bacterial cells where rGO has demonstrated higher glutathione oxidation capability due to its better conductive nature than GO.

The authors further proposed that rGO may have acted as a conductive bridge to facilitate the release of cellular energy through the insulating lipid bilayer (Liu et al., 2011).

Similarly, in another study on the antibacterial actions of graphene film on conductor Cu, semiconductor Ge and insulator $SiO_2$, electron transfer was proposed to cause bacterial oxidative stress (Roman, 2015). In the electron transfer theory, graphene acts as an electron acceptor from the bacterial membrane and then passes on to the substrate. However, the insulating property of $SiO_2$ prevents the electron transfer which has led to the unharmed effects of the bacterial cells in comparison to membrane destruction of bacterial cells on the Cu and Ge substrate. Therefore, the authors proposed that oxidative stress is mediated by electron transfer from the microbial membrane which is facilitated by the graphene films (Roman, 2015).

**c. Phospholipid extraction**

The use of molecular simulations in determining the interactions between the graphene nanosheets and phospholipid bilayer of bacterial cell membrane have suggested that the lipid bilayer could be extracted out of the membrane formation through high hydrophobic interactions between the lipid bilayer and $sp^2$ carbons on graphene nanosheets (Tu et al., 2013). Therefore, Tu *et al.* (2013) investigated the molecular simulations theory through investigational means and demonstrated redistribution of hydrophobic tails of the lipid molecule onto the graphene nanosheets surface to further enhance hydrophobic interactions as shown in Figure 2.8.

This circumstance creates severe bacterial membrane damage through robust extraction of lipid molecules from the inner and outer membrane of the bacterial model thus effectively inhibiting the viability of the bacteria (Tu et al., 2013). Increase in the size and concentration of the graphene sheet is also found to increase the antibacterial property of the nanomaterial and therefore, this mechanistic actions of graphene should be researched further to understand the antibacterial nature of this material (Zou et al., 2016).

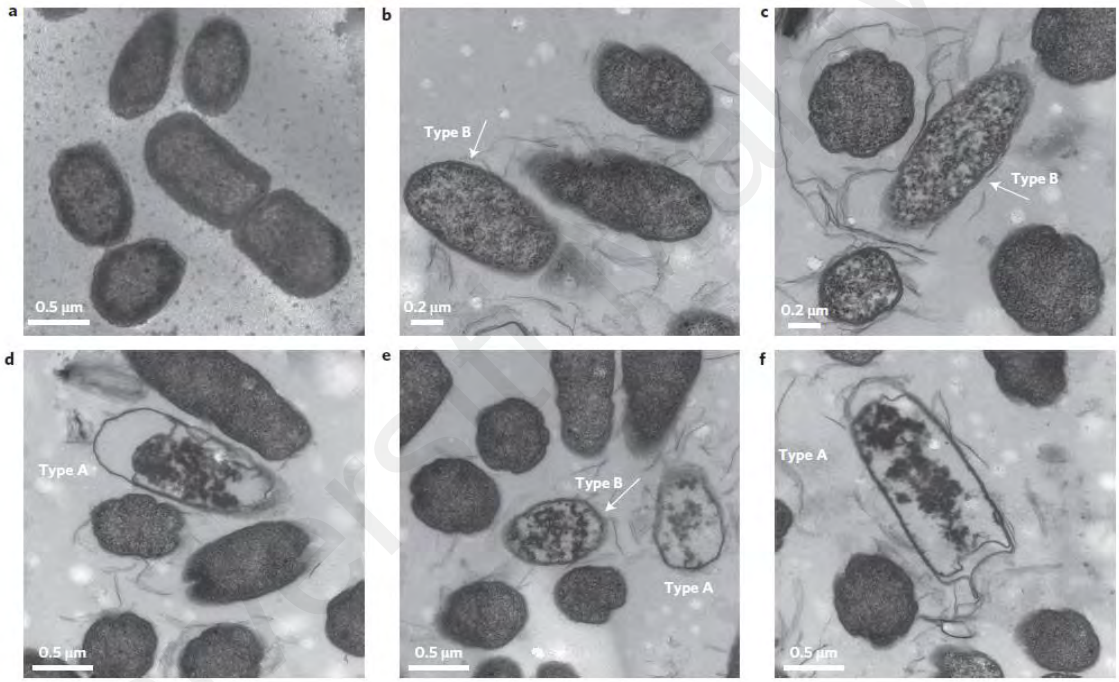


**Figure 2.8:** Phospholipid extraction of *E. coli* after treatment with graphene oxide nanosheets. (a) Bacterial cells at the initial period appeared to have intact cell membrane. Two types of phospholipid extraction mechanisms are observed. (d and f) Type A, where graphene nanosheets appear to have sliced off parts of bacterial membrane, (b and c) Type B, where graphene nanosheets have extracted phospholipids from cell membrane resulting in lower density of phospholipid bilayer. (e) Both types of mechanism are shown. Adapted from Tu *et al.* (2013) with permission from Springer Nature.

### 2.3.3 Contributing factors of GO

#### a. Size and length

The sheet size of GO was essential in determining the toxicity of graphene towards bacterial cells as GO's lateral size greatly influences the other physicochemical factor such as dispersibility, availability of edges and sharp corners and adsorption capacity for the inactivation of bacterial cells (Pumera, 2010). Size too plays an essential factor in determining the antibacterial effects of graphene. Antimicrobial potential of graphite, graphite oxide, GO and rGO were investigated against *E. coli* and under similar parameter settings. Among them, GO showed the highest bactericidal property and the authors attributed this phenomenon to the size of the GO itself as this graphene-based nanomaterial ranked as the smallest-sized material within the conducted study. Smaller GO sheets were able to puncture the bacterial cell membrane through its sharp edges and induced superoxide anion-independent oxidative stress (Liu et al., 2011).

The antimicrobial toxicity of graphene is regulated through its size and GO is influenced by its lateral size. Common methods of synthesizing GO often produces a mixture of GO sheets that are different in size, which can generally be in the range of 10 nm and 20 μm and the size variation of the GO sheets in the reaction mixture may not reveal the true bactericidal stimulator (Sanchez et al., 2012). A study that was conducted specifically to address this issue has demonstrated that larger GO sheets expressed more bactericidal effects compared to the smaller sheets in a suspension-based exposure medium against the *E. coli*. The larger GO sheets were shown to fully cover the external surfaces of *E. coli* thus preventing proliferation and the full wrapping of the cells too may have inhibited nutrient uptake for survival of the bacterial cells (Liu et al., 2012).

Contrastingly, smaller GO sheets exhibited stable antimicrobial potentials albeit slower response than the larger GO sheets in the suspension-based reaction medium. However, when the same set of study was replicated using higher concentration, smaller GO sheets were found to have higher antibacterial activity towards *E. coli* compared to the larger GO sheet (Liu et al., 2012). Similarly, Perreault *et al.* (2015) found that larger GO sheets were able to entrap and prevent the multiplication of the bacterial cells than smaller GO sheets in the suspension-based study as illustrated in Figure 2.9 (Perreault et al., 2015). Smaller GO sheets can adhere to bacterial cells without inhibiting their proliferation rate and therefore, application of smaller GO sheets for antibacterial surface coatings proves to offer the highest antibacterial potency (Liu et al., 2012; Perreault et al., 2015).

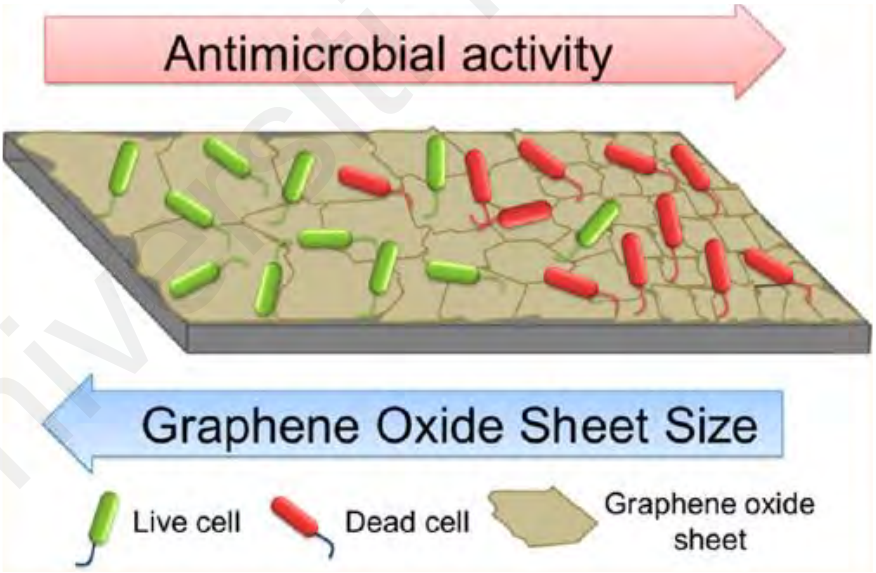


**Figure 2.9:** The effect of sheet size of graphene oxide towards bacteria. As the sheet size of graphene oxide reduces, the antibacterial activity of GO was shown to increase when tested in the form of antibacterial surface coatings. Adapted from Perreault *et al.* (2015) with permission from American Chemical Society.

The increase in the number of GO layers in bacterial inactivation process was investigated by masking of the GO edges. Deposition of GO through the Langmuir-Blodgett (LB) technique enables the GO sheet to be immobilized on a flat surface and it is less likely for the edges to come into contact with the bacterial membrane (Badhulika, Terse-Thakoor, Chaves Villarreal, & Mulchandani, 2015). LB method provides the opportunity for the GO sheets to be stacked in a layer-by-layer fashion, where the thickness parameter of the nanomaterial could be studied. Mangadlao *et al.* (2015) investigated this parameter and showed that increased GO layer (triple layer) had the highest antibacterial activity compared to singular layer of GO sheet. The increase in the antibacterial potential of the nanomaterial has been linked to an addition in the availability of basal planes to initiate interactions with the bacterial cells further (Mangadlao et al., 2015).

**b. Aggregation/Dispersivity**

High surface energy that is found on graphene, especially GO and rGO, enables these nanomaterials to be prone to aggregation in dispersions and therefore, the antimicrobial potentials of graphene tend to vary as the formation of aggregation differs according to the exposure medium (Endes et al., 2014). Sharp edges of GO are altered upon dispersion as adsorption capability of these nanomaterials is weakened and the mode of bacterial killing is different. GO dispersions often form layers of thin nanosheets that wrap individual bacterial cells compared to rGO which forms large aggregations and bacterial cells are observed to be embedded within the rGO aggregate (Liu et al., 2011). The presence of oxygen-containing functional groups in GO facilitates dispersion of GO in water, whereas in media with electrolytes, GO often forms aggregates thus formation of aggregate is highly dependent on pH and ionic strength (Male, Leung, Montes, Kamen, & Luong, 2012).

Hannukainen *et al.* (2012) investigated the interaction of GO and *E. coli* cell membrane and found that the only interactions that occur among GO and the bacterial cells are mediated through repulsive forces due to the negatively-charged cell membrane of *E. coli* and deprotonated carboxylic acid groups on the external surface of GO (Hannukainen, Suhonen, Savolainen, & Norppa, 2012). As only repulsive forces have been characterized between the GO and the bacterial cells, physicochemical trait-based antimicrobial assay may not be entirely appropriate for determining the bactericidal property of GO as only sporadic interactions were observed and that too may be due to bacterial lipopolysaccharide bridging event. Therefore, the authors suggested that the oxidative stress mechanism of bacterial inactivation of graphene could be more complicated than what is known (Hannukainen et al., 2012).

As experimental settings often require bacterial cells to be washed and re-suspended in aqueous solutions such as water or saline, these interchangeable conditions affect the aggregation factor of GO where the difference in the presence of ions in the solutions could influence the availability of GO's basal plane and edges for bacterial inactivation (Male et al., 2012). Existence of electrolytes in the reaction solutions are more prone to induce the formation of aggregates of GO and divalent cations such as calcium and magnesium ions causes the bridging of functional groups at the GO edges (Wu et al., 2013). Palmieri *et al.* (2017) reported that the efficiency of GO remains at optimal level at concentrations below 6 µg/mL regardless of the exposure medium, however, at higher concentrations, antibacterial activity of GO remains the same in water but decreases in salt-containing solutions.

This phenomenon is facilitated through blade-like effects of GO in water irrespective of the concentration and conversely formation of GO aggregates in ionic solutions shields the edge effect of GO and instead antimicrobial activity of GO in these reaction solutions are mediated through bacterial trapping mechanism which impedes the growth of the bacterial cells (Palmieri et al., 2017). Similar observations were recorded by Liu *et al.* (2012) where antibacterial effects of GO in ultrapure water is greater than observed for GO dispersion in saline where larger GO sheets were shown to have better efficiency in deionized water due to lower aggregation effects of GO in this aqueous medium (Liu et al., 2012). Additionally, aggregation of GO in saline could provide better trapping of bacterial cells and their growth inhibition within the aggregate, however, sonication of the saline-based exposure medium tends to mediate release of the trapped bacterial cells and these cells were then able to begin proliferation once again (Perreault et al., 2015).

Although the interaction between the bacterial cell and GO is attributed to their repulsive-nature, presence of cations in the reaction solution increases Z-potential and subsequently the repulsive forces between the interacting GO and bacteria decreases and this favors the occurrence of collision between the nanomaterial and the cells to enable the initiation of bacterial inactivation (Hannukainen et al., 2012; Palmieri et al., 2017). Moreover, the difference in the make-up of bacterial cell produces variations in bacterial inactivation efficiency among the Gram-positive and Gram-negative bacteria as outer membrane of Gram-negative bacteria plays a protective role by shielding the blade-like effects of GO (Deokar et al., 2013; Silhavy, Kahne, & Walker, 2010).

### c. Functionalization

Graphene's tendency to aggregate in liquid substances has prompted the need for surface modification of these nanomaterials as aggregation factor significantly reduce the chances of interaction with bacterial cells in the reaction medium. Therefore, researchers often bypass the agglomeration characteristics through covalent or non-covalent binding of the surface or the edge of graphene sheets (Sanchez et al., 2012). Basal surfaces of graphene may be subjected to functionalization with hydroxyl, carbonyl and epoxide groups which could accommodate the dispersion of GO in water and could be used in various real-world applications.

Akhavan & Ghaderi *et al.* (2012) reported that rGO performed well as an antimicrobial agent compared to GO. They proposed that the main difference in bactericidal potential could have risen due to the difference in surface modification between the two nanomaterials (Akhavan & Ghaderi, 2010). Additionally, rGO inhibits bacterial proliferation, whereas GO enhances bacterial adhesion and growth of the cells on its accessible surface area and hence, this leads to the utilization of GO in the fabrication of antibacterial surface coatings (Akhavan & Ghaderi, 2012).

Excellent adsorption properties of GO could inhibit its antibacterial properties of this nanomaterial as blocking of active interaction sites on the surface of GO could significantly limit its contact ratio with the bacterial cells. Researchers investigating the accessibility of GO's basal plane in context with bacterial inactivation proposed that blocking of the basal plane could mediate the decrease in cytotoxicity of the nanomaterial (Hui et al., 2014).

Supplementation of 10% of LB broth in the reaction medium completely hindered ~99% of the antimicrobial effects of GO as observed in saline and repetition of the experimental settings with BSA and tryptophan revealed that non-covalent adsorption on the basal planes of GO is the main inhibition contributor of bactericidal effects (Hui et al., 2014). Hence, the availability of GO's basal plane is one of the key factors that regulate the antibacterial effects of the nanomaterial through interaction with bacterial cells and limitation in the contact ratio may jeopardize antimicrobial potential of GO.

Disordered wrinkle can often be observed on atomically thin graphene sheets and it is contributory to the compression factor and also due to low bending rigidity of graphene. Advances in technology could be utilized to effectively manipulate the amplitude and size of the wrinkles on the surface through atomic force microscopy tips (Guo & Guo, 2012). The magnitude of the wrinkles may be important in determining the extent of the antibacterial activity of the nanomaterial as this is a unique feature that may have led to the inconsistencies in interpreting the bactericidal property of GO (Zou et al., 2016).

Bacterial adhesion onto the GO film depends on the surface roughness of the GO film as the similarities in the wrinkle size and bacterial diameter could enhance bacterial adhesion. The undulating surfaces of the GO were able to trap bacterial cells with matching diameters and it enhances the oxidative effects of GO through close-contact interactions with the cellular components (Zou et al., 2017). Cell membrane of bacteria may undergo membrane piercings and lacerations along the lipid bilayer and subsequent leakage of the intracellular compounds when these bacterial cells come into contact with the nanoscale wrinkles as shown in Figure 2.10.

Therefore, it has been proposed that wrinkles on the surface of GO acts as a trap to facilitate interactions with the bacterial cells through similarities among the diameter of GO-sink thus causing disruptions in the structural makeup of bacterial membrane and ultimately jeopardizes the mortality of the bacterial cells (Zou et al., 2017).

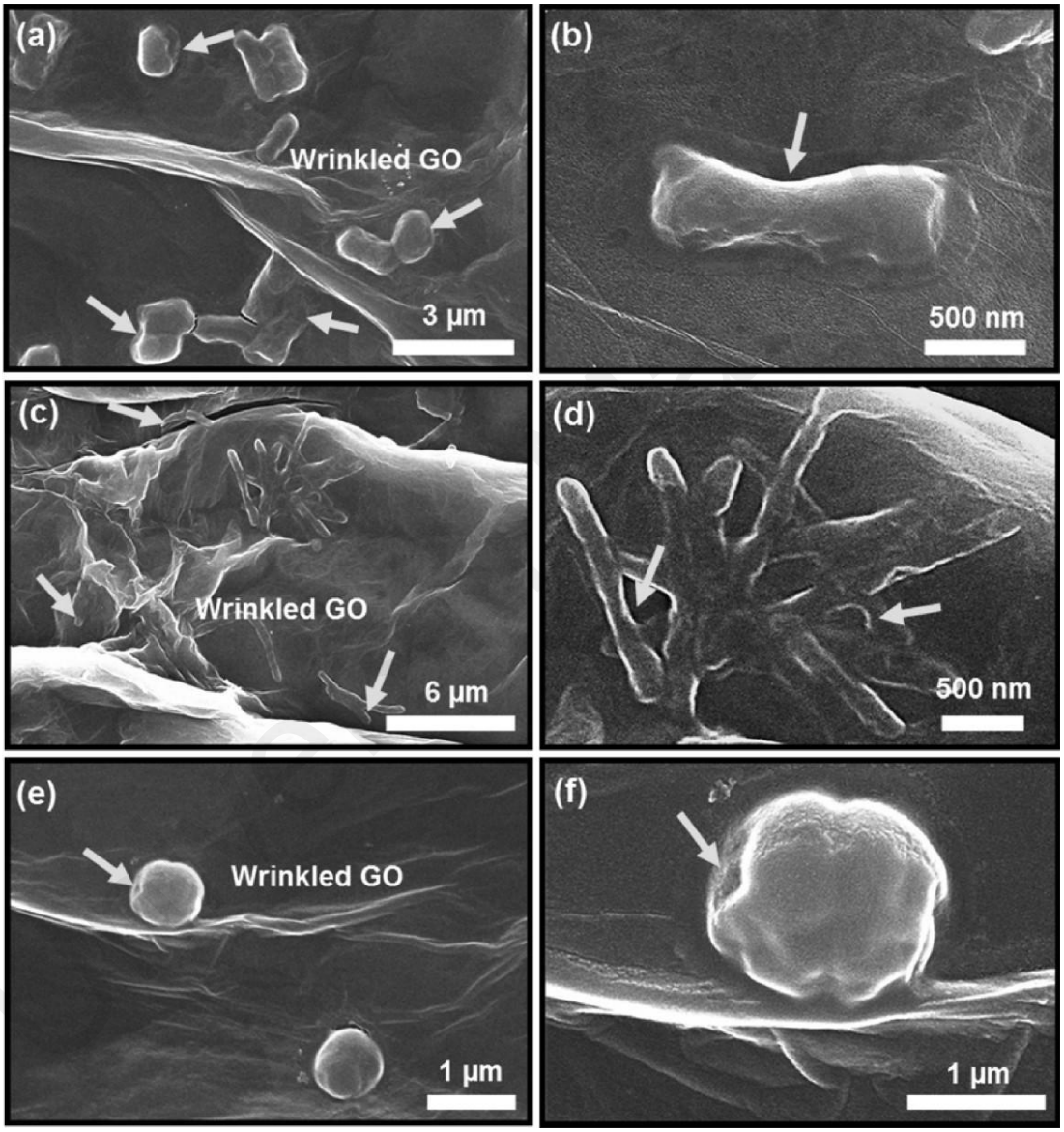


**Figure 2.10:** Antibacterial effects of wrinkled surfaced GO sheets towards (a, b) *E. coli*, (c, d) *M. smegmatis* and (e, f) *S. aureus* where interaction with wrinkled GO significantly disrupts bacterial membrane as peaks and valleys of wrinkled GO efficiently traps bacterial cell. Arrows on the images indicate disintegration of individual bacterial membrane. Adapted from Zou *et al.* (2017) with permission from American Chemical Society.

**d. Adsorption**

Adsorption of GO sheets on to the bacterial cells mainly in the suspension-based antimicrobial assay has been regarded as one of antibacterial mechanisms of GO. GO's flexible nature and its reputation as the thinnest film in the world have contributed to this adsorption behavior (Pumera, 2010; Zou et al., 2016). Wrapping of the bacterial cells is greatly dependent of the size of GO sheet and mainly larger GO sheets are found to be wrapped around the cells as visualized through atomic force microscopy (AFM) (Liu et al., 2012).

Another report which reported the similar wrapping mechanism proposed that graphene sheets inhibit the uptake of nutrients and bacterial proliferation by biological isolation of the bacteria from the growth medium (Akhavan & Ghaderi, 2010). However, smaller graphene sheets were found to adhere to the bacterial surface and exhibited weaker antimicrobial potential compared to larger GO sheets in suspension-based medium. Therefore, bacterial cells adhered to smaller GO sheets may still have uncovered active sites for sufficient nutrient uptake for survival. Larger GO sheets may have better bacterial adsorption rate due to the higher number of $sp^2$ carbon, which mediates hydrophobic interactions with the phospholipid bilayer of the bacterial membrane (Liu et al., 2012).

Viability of the bacterial cells in the graphene sheet could be prolonged up to 24 hours and these cell could then be reactivated when released from the nanosheets through sonication (Dong, Hirani, Colacino, Lee, & Roman, 2012). Similar circumstances were observed with the reactivated bacterial cells where no significant changes in bacterial growth profile were observed when compared to the control group (Perreault et al., 2015).

Therefore, based on these observation, antibacterial property of graphene through adsorption or wrapping mechanism is reversible and hence the effects of this mechanism of action is rather bacteriostatic than bactericidal (Male et al., 2012). In summary, the antimicrobial effect of graphene is attributed to its mechanistic aspects and physicochemical characteristics. A summary of the mechanism of antibacterial activities of graphene and derivatives are as described in Table 1.

## 2.4 Antibiotic adjuvants

Bacterial resistance to antibiotics can be lowered by reducing its prescription in the health sector and its use in the agriculture field for farm animals (Guillemot et al., 2005; Lee, Cho, Jeong, & Lee, 2013). Therefore, in order to preserve the use of 'last-resort' antibiotics such as colistin and daptomycin for critical uses only, conventional antibiotics may be used for treatment of non-severe bacterial infections (WHO, 2017). However, to minimize the selective pressure on bacteria caused by antibiotics, use of antibiotic adjuvant combined with conventional antibiotic is encouraged (Gill, Franco, & Hancock, 2015). Use of metal/metal oxide nanoparticles as antibiotic adjuvants has been widely reported in the literature for their synergistic antibacterial effects with antibiotics (Bellio et al., 2018; Hwang et al., 2012).

**Table 2.1**: Contributing factors and antibacterial mechanism of action of graphene-based nanomaterial.

| NM | Bacteria | Contributing factor | Mechanism of action | References |
|---|---|---|---|---|
| GO, rGO | *E. coli*, *S. aureus* | Sharp edges of GO<br>Improved charge transfer and sharp edges of rGO | Membrane damage | (Akhavan & Ghaderi, 2010) |
| Gt, GtO, GO, rGO | *E. coli* | Dispersion factor | Bacterial cell deposition on the nanomaterials, membrane damage through contact and cell death through oxidative stress | (Liu et al., 2011) |
| GO | *E. coli* | Increasing lateral size of GO masks bacterial cells | Inhibition of cell proliferation and nutrient uptake | (Liu et al., 2012) |
| GO<br>rGO | *E. coli* | More superoxide anions were discovered in rGO solutions compared to GO | Oxidative stress and DNA fragmentation | (Gurunathan et al., 2013) |
| GO | *E. coli* and *B. subtilis* | Non-covalent adsorption on GO basal planes | Bacterial inactivation | (Hui et al., 2014) |
| GO | *E. coli* | Smaller GO sheets had better antimicrobial properties | Membrane damage | (Perreault et al., 2015) |
| GO | *Streptococcus mutans*, *Porphyromonas gingivalis*, *Fusobacterium nucleatum* | Higher concentration of GO nanosheets | Destruction of cell wall and leakage of cell content | (He et al., 2015) |

**Table 2.1**, continued.

| NM | Bacteria | Contributing factor | Mechanism of action | References |
|---|---|---|---|---|
| GO | *E. coli*, *B. subtilis* | Reduced organic carbon concentration in phototransformed GO | Significant membrane damage and oxidative stress | (Hou et al., 2017) |
| GO | *E. coli* | Functional groups on the basal plane of the GO sheets that was immobilized on a PET substrate using Langmuir-Blodgett technique | Bacterial inactivation | (Mangadlao et al., 2015) |
| GO | *E. coli* | The increased density of carbon radical (•C) on the GO surface after the hydration process | Membrane damage due to lipid peroxidation | (Li et al., 2016b) |
| GO | *E. coli, Enterococcus faecalis* | GO sheet causes the release of adenine and protein | Disintegration of outer and inner bacterial membrane | (Nanda et al., 2016) |
| GO, rGO | *P. aeruginosa* | Generation of ROS species | Oxidative stress and DNA fragmentation | (Sodhi, 2016) |
| GO | *E. coli, Mycobacterium smegmatis and S. aureus* | Wrinkled GO surface traps bacteria and inactivates it | Membrane damage, release of intracellular components and cell death | (Zou et al., 2017) |
| GO | *E. coli, S. aureus* | Photophysical properties | Photothermal /photodynamic therapy effect | (Romero et al. 2020) |

These nanomaterials with bactericidal properties were also previously reported to act as an antibiotic carrier (Wang et al., 2017). This is mainly due to the relatively small size of the nanomaterial which makes it an attractive medium for drug delivery especially among drug-resistant bacteria due to antibiotic's poor membrane transport. Therefore, nanomaterials that can be loaded with antibiotics have been investigated to overcome this limitation of antibiotics (Ranghar, Sirohi, Verma, & Agarwal, 2014). Ag nanoparticles are the most commonly studied nanomaterial to increase the activity of antibiotics. Ag nanoparticles enhance the effects of antibiotics such as kanamycin and tetracycline against bacteria through synergistic effects. Ag nanoparticles form a complex with the antibiotic and this complex has better antibacterial activity by releasing more $Ag^+$ ions to inhibit the growth of bacteria as depicted in Figure 2.11 (Deng et al., 2016).

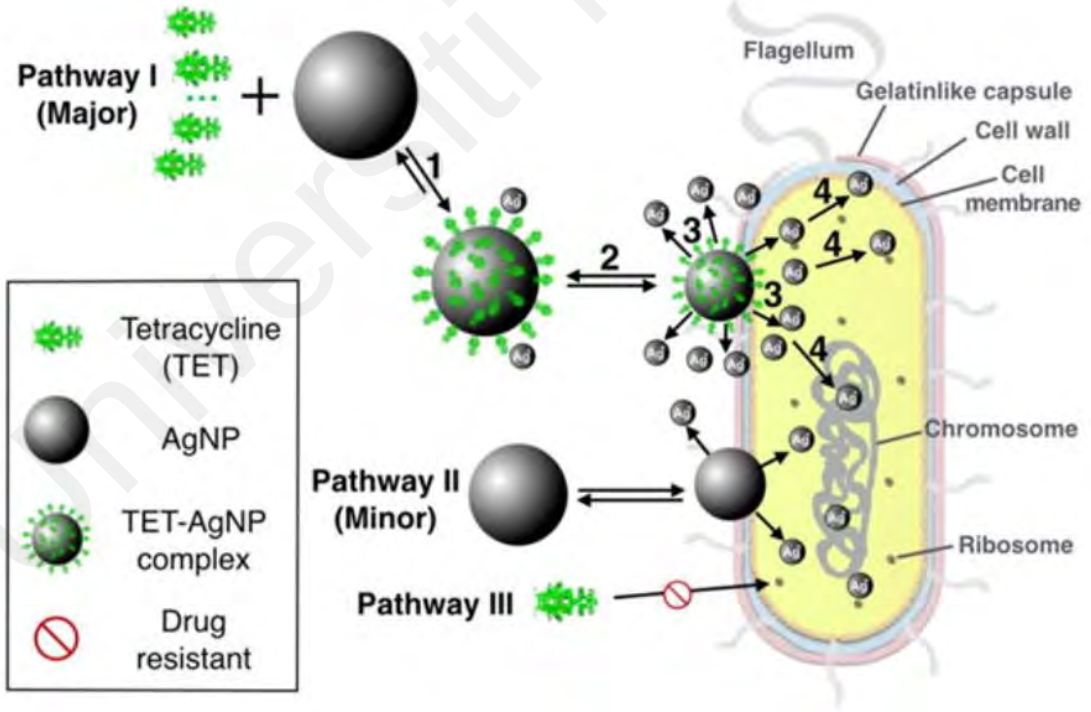


**Figure 2.11:** Synergistic antibacterial pathway of silver nanoparticles and tetracycline against multidrug-resistant *Salmonella* as illustrated in Pathway I. Pathway II is a minor antibacterial mechanism while pathway III is ineffective due to antibiotic resistance of *Salmonella*. Adapted from Deng *et al.* (2016) with permission from American Chemical Society.

As metal-based nanoparticles have been increasingly studied for their synergistic effects in enhancing antibacterial action of antibiotics, however, their safety for human use has become a concern (Allahverdiyev et al., 2011). Although GO has shown optimal antibacterial activity, studies on the combinatorial activity of GO with common antibiotics are still lacking. Gao *et al.* (2017) reported that GO acted as an antibiotic carrier when used in combination with lincomycin hydrochloride, chloramphenicol and gentamycin sulfate on *S. aureus* and *E. coli*. The authors postulated that this activity is dependent on the interaction between GO and antibiotic, the interaction between GO and bacteria and the susceptibility of bacteria to the respective antibiotic (Gao et al., 2017). Therefore, detailed investigations on the combinatorial activity of GO and antibiotics are still needed.

## 2.5 Cytotoxicity of GO

Physicochemical attributes of GO make it an attractive nanomaterial for its potential application in the medical sector (Wu, An, & Hulme, 2015). Increasing usage of this nanomaterial poses a risk of environmental exposure of GO towards humans. The *in vitro* cytotoxicity aspects of GO have been well studied and changes in the viability and morphology of the cells, membrane disruptions and DNA damages have been previously observed (Fujita et al., 2018; Lu et al., 2017). Reduction in the expression of genes that are responsible for cell membrane regulations including endocytosis, focal adhesion and actin cytoskeleton have been noted for derivatives of GO (Xu et al., 2016). GO was found to exhibit minimal toxic effects in human lung epithelial cells (A549) by inducing concentration-dependent oxidative stress and minor loss of cell viability when exposed to higher concentrations of GO as shown in Figure 2.12 (Chang et al., 2011; Hu et al., 2011).

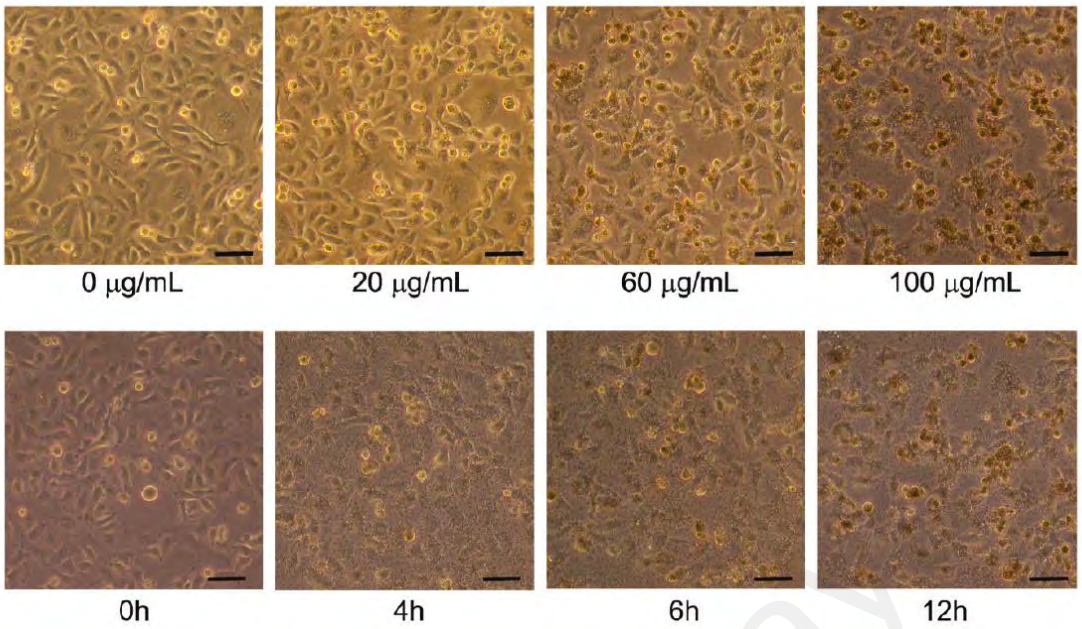


**Figure 2.12**: Cytotoxic effects of graphene oxide nanosheets against A549 cells. The viability of A549 cells gradually reduces when treated with increasing concentrations of graphene oxide (top). Viability of A549 cells is also affected when the cells were treated with 100 μg/mL of GO for different exposure periods (bottom). Adapted from Hu *et al.* (2011) with permission from American Chemical Society.

Cell uptake of GO in HeLa cells was observed to be the lowest when compared to multi-walled carbon nanotubes and nanodiamond. However, this ratio does not play a role in cytotoxicity as GO exhibited enhanced toxic effects in terms of generation of ROS and production of malondialdehyde and lactose dehydrogenase enzymes increased compared to nanodiamond (Zhang, Hu, Li, Tao, & Wei, 2012b).

### 2.5.1 Contributing factors

Concentration of GO plays a role in the cytotoxicity aspects towards *in vitro* cell studies as well. A study that investigated the effects of concentration of GO against A549 cells found that lower concentrations of GO (20 μg/mL) did not affect the viability of the cell line compared to higher concentration of GO (85 μg/mL).

The higher GO concentration was found to reduce the viability of the A549 cells by 50% after treatment period of 24 h (Hu et al., 2010). Similarly, Lv *et al.* (2012) demonstrated that no cytotoxic effects were observed for 96 h of treatment period when low concentrations of GO were exposed to human neuroblastoma SH-SY5Y cell line. However, the viability of the tested cell line decreased by 20% once treated with 100 mg/mL for the similar treatment time of 96 h (Lv et al., 2012).

Sizes of GO too contributes to its cytotoxicity towards cell lines. Lateral dimension of GO that is lower than <100 nm could enter the cell membrane, GO that is smaller than <40 nm are able to enter the cell nucleus and whereas GO that are smaller than <35 nm may cross the blood-brain barrier (Jennifer & Maciej, 2013). GO sheets with the lowest lateral size are often studied to experience higher levels of cell uptake and they induced the highest amount of oxidative stress when investigated in HeLa cell line (Zhang et al., 2013). However, another study showed that larger GO flakes were able to induce pro-inflammatory responses in macrophages by strong adsorption onto the plasma membrane. This resulted in reduced phagocytosis where better interaction with toll-like receptors and activation of NF-κB pathways occurred in comparison with smaller GO flakes (Ma et al., 2015).

Functionalization of GO has been shown to reduce its toxicity when tested against *in vitro* cell lines. Biocompatibility of GO was shown to improve when functionalized with polyethylene glycol (PEG), polyethylenimine (PEI) and lactobionic acid-polyethylene glycol (LA-PEG) and they were found to reduce the toxic effects induced by GO alone (Ma et al., 2015). Methods of preparing GO too have been reported to cause toxic effects among cell line as presence of impurities such as $Fe^{2+}$ and $Mn^{2+}$ may induce mutagenesis in cells (Wu et al., 2015).

GO sheets that were prepared with minimal impurity content showed no significant cytotoxic effect even at GO dosage of 100 µg/mL when tested *in vitro* (Ali-Boucetta et al., 2013).

The high surface energy of GO normally causes GO to interact with proteins that are found in the biological systems and form protein corona. This protein corona has been suggested to interfere in GO's circulation, toxicity aspects and distribution. Formation of protein corona in GO has helped to mitigate the toxic effects of GO by reducing the interaction with cell membrane when exposed in A549 cells (Duan et al., 2017; Hu et al., 2011). Therefore, toxicity aspects of GO are modulated through multiple aspects and more studies are required to reduce the toxic effects of GO.

### 2.5.2 Cytotoxic mechanisms of GO in cell lines

Interactions of GO with cell lines often lead to excessive generation of ROS which then contributes to oxidative stress in the particular cell line and may lead to mutagenesis and carcinogenesis (Ou et al., 2016). GO was found to induce DNA damage in human lung fibroblast (HLF) cells and also caused apoptosis in the cells. It was also noted that GO was responsible for causing severe genotoxic effects in the HLF cell lines compared to cytotoxic effects (Wang et al., 2013). Similarly, GO sheets induced short-term ROS generation in A549 and macrophage cell lines, however, this may contribute to genotoxicity effects that may trigger inflammatory responses in target cells (Horvath et al., 2013).

Mitochondria are the center of energy production of cell that are involved in numerous signaling pathways and the main stimulator of apoptosis. Therefore, effects on mitochondria after GO exposure in cell lines were investigated and it was found that the depolarization of mitochondrial membrane and the total amount of mitochondria were reduced when tested in HepG2 cell lines (Lammel, Boisseaux, Fernández-Cruz, & Navas,

2013). Stimulation of the apoptosis process through the mitochondrial pathway occurs when GO increases the coupled and uncoupled oxygen intake and affects the mitochondrial membrane potential. This was found to occur in alveolar macrophages and epithelial cells where GO increased the production of mitochondrial ROS by involving in redox reactions with constituents of the cell's electron transport chain (Duch et al., 2011). Formation of ·OH caused by GO in cell lines could affect the mitochondrial respiratory process; additionally, the acceptance of electrons from cell's redox proteins by the oxygen moieties on the surface of GO may also influence the activity of cell's mitochondria (Salas, Sun, L ttge, & Tour, 2010; Zhang et al., 2012).

High surface area and surface charge properties of GO often become the main culprit of the genotoxic effects of GO. For instance, GO may contribute to DNA damage by causing chromosomal fragmentation, point mutations and breakage in DNA strands (Chatterjee, Yang, & Choi, 2016; Ou et al., 2016). Interactions of GO with DNA may occur when the nuclear membrane breaks down for mitosis process as it is not possible for GO to enter the nucleus of a cell (Magdolenova et al., 2014; Ren et al., 2010). GO has been shown to stimulate inflammatory pathways through activation of TGF-β, MAPK and NF-κB signaling pathways and eventually trigger point mutations, chromosomal fragmentation and DNA adducts (Chatterjee, Eom, & Choi, 2014). As DNA damage may induce the development of cancer and possibly harm the next generation if the mutations were to arise in reproductive cells, it is imperative to thoroughly research the safety aspects of GO (Ciccia & Elledge, 2010). The use of GO in *in vitro* cell line is also found to induce apoptosis, a mechanism to self-destruct through gene regulation.

A study showed that GO was able to activate 3 types of apoptosis pathway; interaction with protein receptors that activate B-cell lymphoma-2 (Bcl-2) pathway which leads to ROS-dependent apoptosis; passive signal to activate apoptosis through protein receptor binding to activate ROS-independent pathway; finally, severe membrane damage which automatically triggers apoptosis (Ding, Zhang, Ma, & Chen, 2014).

Similarly, GO too may induce autophagy, a process of cell degradation of unwanted or dysfunctional components of the cell through a lysosomal pathway. The unnecessary cytoplasmic contents are usually isolated into an autophagosome that are fused with lysosomes. GO was reported to stimulate the accumulation of autophagosomes and also inhibits the conversion of microtubule-associated light chain 3 (LC3) which is a marker of autophagosomes (Wan et al., 2013). Additionally, GO too triggered the response of toll-like receptor (TLR) 4 and TLR 9 in macrophages and in CT2, a colon cancer cell line (Chen et al., 2012; Chen et al., 2014). In contrast, cell-death induced by inflammatory responses or injury to vital cell components are known as necrosis. Exposure to GO contributed towards macrophagic necrosis through activation of TLR4 signalling and partial stimulation of tumor necrosis factor (TNF)-α as illustrated in Figure 2.13 (Qu et al., 2013). Moreover, GO combined with chemotherapy drug such as cisplatin (CDDP) was reported to cause necrosis by reducing the levels of necrotic protein, RIP1, and increasing the levels of RIP3 proteins (Chen et al., 2015).

In summary, various cytotoxic studies have been conducted on GO, where the inflammatory signaling, oxidative stress and physical disruption are the key mechanisms that contributed to cell death. However, detailed investigations should be carried out to ensure biocompatibility aspects of GO.

Several factors such as physicochemical characterizations, experimental parameters, selection of cell lines, long-term fate of the GO-treated cells and mechanism of toxicity should be carefully researched to confirm the nanosafety features of GO.

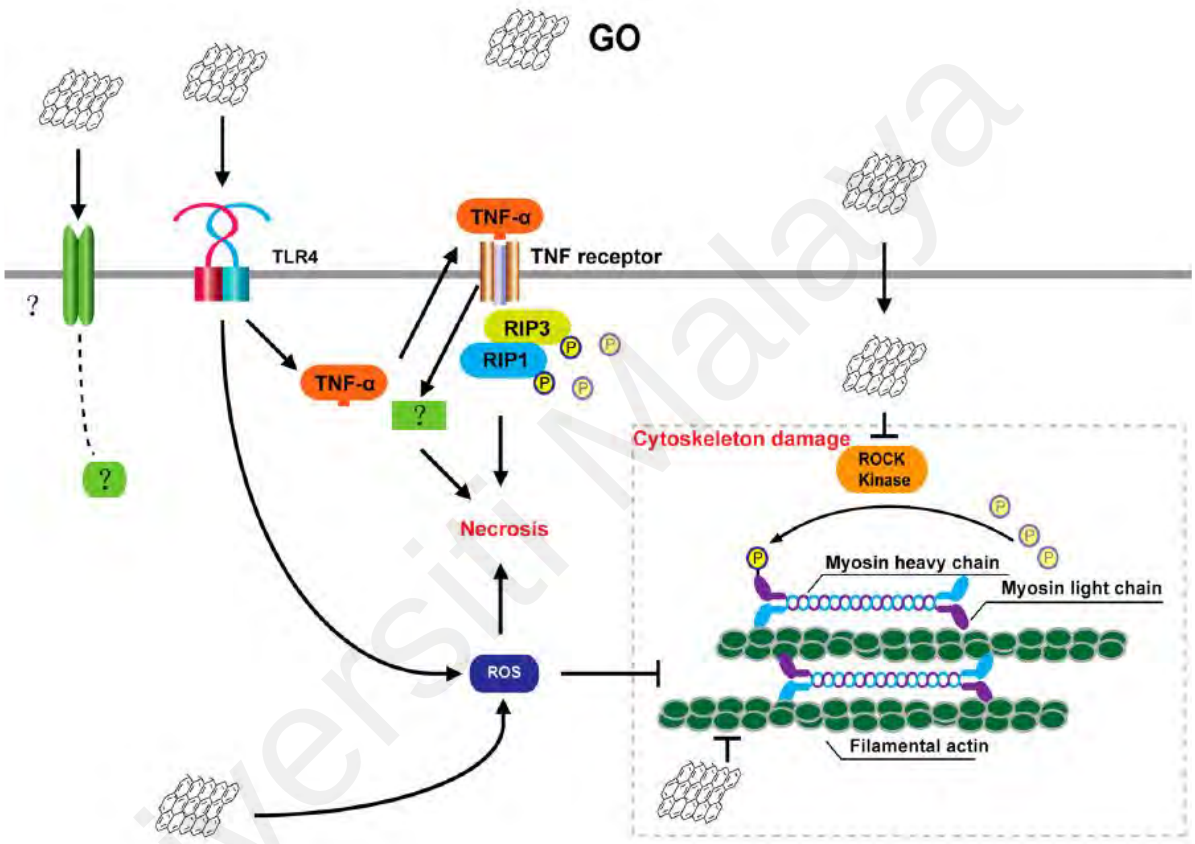


**Figure 2.13:** Mechanism of GO-induced cytotoxicity towards macrophages. TNF-R is produced when GO and TLR4 interacts and this causes programmed necrosis in macrophages. GO too induces cytoskeleton damage to the cell membrane and causes damage to vital functions associated with oxidative stress. Together, these factors caused cell death while additional factors such as TNF-R independent signalling and RIP-independent events too may have played a role. Adapted from Qu *et al.* (2013) with permission from American Chemical Society.

# CHAPTER 3: MATERIALS AND METHODS

## 3.1 Materials

GO was received from Nanotechnology and Catalysis Research Centre (NANOCAT), University of Malaya, Kuala Lumpur, Malaysia. Phosphate buffered saline (PBS) tablets was purchased from Sigma-Aldrich, USA and was used to prepare PBS. Dehydrated bacterial culture media of Tryptic Soy Agar (TSA) and broth (TSB) were purchased from BD Difco™, USA. Bacterial cultures of *S. aureus* ATCC 25923, *E. coli* ATCC 25922, *E. faecalis* ATCC 29212 and *P. aeruginosa* ATCC 27853 were obtained from the Laboratory of Biomedical Science's culture collection at University of Malaya, Kuala Lumpur, Malaysia. HaCaT cells were obtained from Industrial Biotechnology Research Centre, SIRIM Berhad, Shah Alam, Malaysia. LDH Cytotoxicity Assay kit was purchased from Thermo Fisher Scientific, Massachusetts, USA. Antibiotic powders of ampicillin, chloramphenicol and tetracycline, 3-(4,5-Dimethyl-2-thiazolyl)-2,5-diphenyl-2H-tetrazolium bromide (MTT) and 2′,7′-Dichlorofluorescein diacetate (DCFH-DA) were purchased from Sigma-Aldrich, USA. Dulbecco's modified Eagle's medium (DMEM) and Fetal Bovine Serum (FBS) were purchased from Gibco, USA. Penicillin/streptomycin (10,000 U/mL) was purchased from Thermo Fisher Scientific, Massachusetts, USA.

## 3.2 Characterizations of graphene oxide

### 3.2.1 Ultraviolet-visible spectroscopy of graphene oxide

Ultraviolet-visible (UV-Vis) spectroscopy techniques were carried out to measure the absorbance of GO. The adsorption spectra were obtained using Lambda 35 (Perkin-Elmer, USA) and the lamps were allowed to warm up for 15 minutes for stabilization. An aqueous solution of GO was used as the sample for UV-Vis and distilled water was used as the reference. The absorbance of the cuvette filled with distilled water (blank) was measured first. Then, followed by the aqueous solution of GO.

Wavelengths from 200 to 700 nm were collected to measure the absorbance of GO. Absorbance data of GO that was collected were used to draw a plot.

### 3.2.2 Raman spectroscopy of graphene oxide

Raman spectroscopy technique was carried out to determine the vibrational modes of GO. Raman spectra of GO sheets were obtained using a Renishaw inVia Raman microscope (UK) with an excitation laser wavelength of 325 nm. The excitation was conducted with a He-Ne laser in the regions of 1000 to 2200 $cm^{-1}$. The spectrum of the GO was obtained and plotted.

### 3.2.3 ATR-FTIR spectroscopy of graphene oxide

Functional groups of GO were determined using ATR-FTIR method. Initially, the background spectrum was collected and followed by the IR spectrum of GO. Briefly, a small amount of GO in powder form was collected using a metal spatula and placed under the detection probe. The probe was then locked into place by twisting it into place. The IR spectrum of GO was recorded and this measurement was repeated three times for accuracy. The probe was wiped with acetone once the IR spectra of GO were taken. The ATR-FTIR characterization of GO was conducted using Spectrum 400 IR spectrometer equipped with diamond crystal (Perkin Elmer, USA). The ATR-FTIR spectra were recorded with a resolution of ± 4 $cm^{-1}$ and a scan number of 12 in the range of 4000 to 400 $cm^{-1}$. The IR spectra of GO was obtained and plotted.

### 3.2.4 XRD analysis of graphene oxide

X-ray diffraction (XRD) studies were conducted using X-ray diffractometer (Bruker d8 ADVANCE) with primary monochromatic high-intensity CuKα radiation (λ = 0.15406 nm). The angle range 2θ between 5 to 80º were used to collect the XRD pattern. The obtained XRD analysis results were used to generate an XRD pattern for GO.

### 3.2.5 FESEM characterizations of graphene oxide

Double stick conducting carbon tape was placed on the sample stub using tweezers. The cover on the carbon tape was removed and GO in powder form was gently placed onto the carbon tape. Excess GO powder was blown off using a blower. Morphology of GO sheets was characterized using FESEM (FEI Quanta 650 FEG, Thermo Fisher Scientific, US) with an acceleration voltage of 20 kV and a 9 mm working distance.

### 3.2.6 TEM characterizations of graphene oxide

GO was suspended in 75% ethanol and was sonicated for 10 minutes. Ten µL of the GO suspension was pipetted out and dropped on the 400-mesh copper TEM grid. The droplet was then dried using filter paper by using gentle tapping method. Morphology of GO were viewed under the transmission electron microscopy (TEM) (LEO LIBRA 120, Carl Zeiss, Oberkochen, Germany) techniques as well. The TEM images of GO were observed using lower magnification of 170 k and at a higher magnification of 1250 k.

## 3.3 Bacterial isolates and culture conditions

The bacterial cultures of *S. aureus*, *E. coli, E. faecalis* and *P. aeruginosa* were revived by streaking on TSA media. The streaked culture plates were incubated at 37 °C for ~20 hours. Then, a single colony was picked from the overnight TSA plate and subsequently used to inoculate 10 mL of TSB. The inoculated TSB broth was incubated at 37 °C with agitation (150 rpm) for ~20 hours. The bacterial culture was subsequently used for the following experiments unless stated otherwise.

## 3.4 Antibacterial activity of graphene oxide against Gram-positive and Gram-negative bacteria in suspension

### 3.4.1 Concentration dependent activity through viability assay

Viability assay of bacterial cells treated with GO was conducted according to Liu *et al.* (2011). An aliquot of 5 mL of bacterial cultures ($10^8$ cfu) of *S. aureus*, *E. coli*, *E. faecalis* and *P. aeruginosa* were incubated with GO of varying concentrations ranging from 5 to 140 µg/mL for 4 h at 37 °C with agitation (150 rpm). At the end of the designated time period, an aliquot of 100 µL was withdrawn and serially diluted (1:10) in 0.8% saline solution. Serially diluted cell suspensions were plated onto the TSA and incubated overnight at 37 °C to determine the bacterial counts (cfu). The assay was carried out in triplicates of three independent experiments and the results were averaged. The degree of bacterial inactivation was calculated using the formula: $(T_0 - T)/ T_0$ where $T_0$ is the number of bacteria in the GO-free reaction and T is the residual bacteria in the reaction medium at a certain GO concentration. Three independent replicates were conducted for the assay.

### 3.4.2 Membrane integrity analysis through LDH cytotoxicity assay

LDH cytotoxicity assay according to Xiong *et al.* (2018) was conducted to determine the degree of membrane damage of bacteria once treated with GO. Membrane integrity of treated bacteria was evaluated using LDH Cytotoxicity Assay Kit (Thermo Fisher Scientific, Massachusetts, USA). Bacterial cultures of *S. aureus*, *E. coli*, *E. faecalis* and *P. aeruginosa* ($10^8$ cfu) were incubated with GO suspension of varying concentration ranging from 5 – 140 µg/mL for 4 h at 37 ºC with agitation (150 rpm). At the end of the time period, 50 µL of each reaction mixture were transferred to a 96-well plate and the assay was carried out according to the manufacturer's instructions. The absorbance was measured using a microplate spectrophotometer (Epoch-BioTek, Vermont, USA).

Untreated bacterial cultures were regarded as negative control and three independent experiments were performed with replicates and the results were averaged.

### 3.4.3 Time dependent activity through time-kill assay

Standardized bacterial cultures ($10^8$ cfu) of *S. aureus*, *E. coli, E. faecalis* and *P. aeruginosa* were incubated with 10 µg/mL of GO suspension at 37 °C with gentle agitation (100 rpm). At the end of selected time periods (2 h, 4 h, 6 h and 8 h), 100 µL of the bacterial culture was withdrawn and serially diluted (1:10) in 0.8% saline solution. Serially diluted cell suspensions were then plated onto the TSA and incubated overnight at 37 °C to determine the bacterial counts (cfu). Three independent experiments were carried out in triplicates and the results were averaged.

### 3.4.4 Visualization of the bacterial cell upon exposure to graphene oxide

#### a. Field-emission scanning electron microscopy technique

GO treated and untreated bacterial cultures of *S. aureus*, *E. coli, E. faecalis* and *P. aeruginosa* were retrieved from respective experiments for surface morphology observations using FESEM technique according to Zou *et al.* (2017). The GO treated and untreated bacterial cultures were harvested by centrifugation at 4500 x *g* for 15 min at RT. Briefly, 1 mL of the bacterial suspension (~ $10^8$ cfu/mL) was treated with 4 % glutaraldehyde (GLA) for more than 4 h. Then, the fixed bacterial cells were washed twice with cacodylate buffer and further fixed with 1% osmium tetroxide at 4 ºC for 1 h. The cells were washed twice in double-distilled water for 10 min each. The fixed bacterial cells were then gradually dehydrated with ethanol using increasing concentrations ranging from 30%, 50%, 70%, 80%, 90%, 95% and finally 100%. Each ethanol wash was performed for 15 minutes. Next, the bacterial cells were further dehydrated using mixtures of 100% ethanol and acetone at ratios of 3:1, 1:1 and 1:3 for 15 min, respectively.

The bacterial cells were dehydrated three times using acetone for 20 min, each time. Final dehydration of the bacterial cells was performed in critical point dryer (Leica EM CPD3000, Singapore) for 3 h. Lastly, the completely dried bacterial cells were sputter-coated with gold for FESEM observations (FEI, Quanta FEG 650) at a working distance around 9 mm, with an acceleration voltage of 20 kV.

**b. Transmission electron microscopy technique**

GO treated and untreated bacterial cultures of *S. aureus*, *E. coli, E. faecalis* and *P. aeruginosa* were retrieved from respective experiments for morphology observations using TEM technique according to Tu *et al.* (2013). The GO treated and untreated bacterial cultures were harvested by centrifugation at 4500 x *g* for 15 min at RT. Briefly, 1 mL of the bacterial suspension (~ $10^8$ cfu/mL) was treated with 4 % glutaraldehyde (GLA) for more than 4 h. Then, the fixed bacterial cells were washed twice with cacodylate buffer and further fixed in equal mixtures of osmium tetroxide and cacodylate buffer at 4 ºC for 2 h. The cells were washed twice with cacodylate buffer and stored overnight at 4 ºC. The next day, the bacterial cells were washed twice in double-distilled water for 5 min each. The fixed bacterial cells were then gradually dehydrated with ethanol using increasing concentrations ranging from 35%, 50%, 70%, 95% and finally 100% for 10 to 15 min each. Then, the bacterial cells were treated twice using propylene oxide for 15 min each. Next, the bacterial cells were further dehydrated using mixtures of propylene oxide and Epon at ratios of 1:1 and 1:3 for 1 h and 2 h, respectively. Finally, the cells were embedded in Epon for overnight, further embedded at 37 ºC and 60 ºC for 5 hours and 24 hours. Thin sections were cut through ultramicrotome, stained with uranyl acetate, air-dried and viewed under TEM. The GO treated bacterial isolates were also observed under TEM (Carl Zeiss, LEO LIBRA 120).

### 3.4.5 Interactions between bacterial cell membrane and graphene oxide at molecular level through ATR-FTIR characterizations

Bacterial cultures were treated with 10 µg/mL of GO for 4 h as described in the previous section. An aliquot of 100 µL of the GO-treated and untreated bacterial (control) cultures was aseptically dropped onto glass slides, respectively and left to dry. The thin film was analyzed through Spectrum 400 IR spectrometer equipped with diamond crystal (Perkin Elmer, USA). The spectra were recorded in the range of 4000 to 400 $cm^{-1}$ with a scan number of 12 and a resolution of ± 4 $cm^{-1}$ for free GO and antibiotic loaded GO.

## 3.5 Antibiofilm activity of graphene oxide against Gram-positive and Gram-negative bacteria

### 3.5.1 Concentration dependent activity through viability assay

An aliquot of 200 µL of bacterial cultures ($10^5$ cfu) of *S. aureus*, *E. coli*, *E. faecalis* and *P. aeruginosa* were resuspended in TSB into 96-well plates to form biofilm. Biofilm was left to mature for 24 h, 48 h and 72 h at 37 °C without agitation. At the end of respective biofilm growth period, TSB media was removed and the biofilm was washed twice with 1X PBS. Later, suspension of GO (5 to 200 µg/mL) in 0.8% saline solution were added to the biofilm for 24 h at 37 °C without agitation. Crystal violet assay was carried out according to Sharar *et al.* (2018) after the exposure time. Briefly, saline solution with GO in the 96-well plates was removed then washed twice with 1X PBS. The 96-well plates containing bacterial biofilm was heat-fixed for 30 min at 80 ºC. Staining of the biofilm cells was carried out using 0.5 % crystal violet solution and left at room temperature for 20 minutes. The 96-well plate was then washed twice with 1X PBS to remove the unbound dye. The destaining step was carried using ethanol:acetone (80:20%) solution and it was added to the wells and the plate was shaken for 5 minutes. The 96-well plate was quantified by a microplate reader (BioRad, USA) at 590 nm to determine the absorbance of the biofilm.

### 3.5.2 Membrane integrity analysis through LDH cytotoxicity assay

Bacterial cultures ($10^5$ cfu) of *S. aureus*, *E. coli, E. faecalis* and *P. aeruginosa* from overnight culture were resuspended in TSB into 96-well plates to form biofilm. Biofilm was left to mature for 24 h, 48 h and 72 h at 37 °C without agitation. At the end of respective biofilm growth period, TSB media was removed and the biofilm was washed twice with 1X PBS. Membrane integrity of GO treated biofilm cells was evaluated using LDH Cytotoxicity Assay Kit (Thermo Fisher Scientific, Massachusetts, USA).

Biofilm cells of *S. aureus*, *E. coli, E. faecalis* and *P. aeruginosa* of 24 h, 48 h and 72 h maturity period in the 96-well plates were incubated with 100 µg/mL of GO suspension at 37 °C without agitation. At the end of the time period, 50 µL of each reaction mixture was transferred to a 96-well plate and the assay was carried out according to the manufacturer's instructions. The absorbance was measured using a microplate spectrophotometer (Epoch-BioTek, Vermont, USA) at 590 nm. Untreated bacterial cultures were regarded as negative control and three independent experiments were performed with replicates and the results were averaged.

### 3.5.3 Time dependent activity through time-kill assay

Bacterial cultures ($10^5$ cfu) of *S. aureus*, *E. coli, E. faecalis* and *P. aeruginosa* from overnight culture were resuspended in TSB into 96-well plates to form biofilm. Biofilm was left to mature for 24 h, 48 h and 72 h at 37 °C without agitation. At the end of respective biofilm growth period, TSB media was removed and the biofilm was washed twice with 1X PBS. Biofilm cells of *S. aureus*, *E. coli, E. faecalis* and *P. aeruginosa* of 24 h, 48 h and 72 h maturity period in the 96-well plates were incubated with 100 µg/mL of GO suspension at 37 °C without agitation for different exposure periods of 3 h, 6h, 12h and 24h.

At the end of selected time periods (3 h, 6 h, 12 h and 24 h), crystal violet assay was conducted to study the viability of the biofilm at various GO exposure times. The biofilm was quantified by a microplate reader (BioRad, USA) at 590 nm.

## 3.6 Interactions between graphene oxide and antibiotics at molecular level

### 3.6.1 ATR-FTIR characterizations

Respective antibiotic solutions of ampicillin, chloramphenicol and tetracycline and GO dissolved in distilled water were prepared aseptically. 10 µg/mL of GO and 10 µg/mL of corresponding antibiotic solution were prepared and an aliquot of the GO-antibiotic mixture was aseptically dropped onto glass slides, respectively and left to dry. The thin film on the glass slide was subsequently analyzed using Spectrum 400 IR spectrometer equipped with diamond crystal (Perkin Elmer, USA). The spectra were recorded in the range of 4000 to 400 $cm^{-1}$ with a scan number of 12 and a resolution of ± 4 $cm^{-1}$ for free GO and antibiotic loaded GO.

### 3.6.1 UV-VIS characterizations

Respective antibiotic solutions of ampicillin, chloramphenicol and tetracycline and GO dissolved in distilled water were prepared aseptically. 10 µg/mL of GO and 10 µg/mL of corresponding antibiotic solution were prepared and an aliquot of the GO-antibiotic mixture was used as the sample for UV-Vis. The adsorption spectra were obtained using Lambda 35 (Perkin-Elmer, USA) and the lamps were allowed to warm up for 15 minutes for stabilization. An aqueous solution of GO-antibiotic mixture was used as the sample for UV-Vis and distilled water was used as the reference. The absorbance of the cuvette filled with distilled water (blank) was measured first. Then, followed by the GO-antibiotic mixture. Wavelengths from 200 to 700 nm were collected to measure the absorbance of GO-antibiotic mixture. Absorbance data that were collected were used to draw a plot.

### 3.7 Synergistic behaviour of GO with selected antibiotics against Gram-positive and Gram-negative bacteria in suspension

Bacterial cultures of *S. aureus*, *E. coli, E. faecalis* and *P. aeruginosa* were revived by streaking on TSA media and were incubated at 37 °C for overnight. A single colony from the overnight TSA plate was picked and used for the inoculation of 10 mL of TSB and incubated overnight at 37 °C with agitation (150 rpm). The bacterial culture broth was subsequently used for the following experiment. Synergistic antibacterial actions of GO and antibiotics were determined by treating standardized bacterial cultures ($10^8$ colony forming unit, cfu) of *S. aureus*, *E. faecalis*, *E. coli and P. aeruginosa* with a fixed concentration of GO along with different antibiotic solutions (ampicillin, chloramphenicol and tetracycline) according to Gao *et al.* (2017). The bacterial cultures were incubated with different antibiotics solutions of varying concentrations, ranging from 1 to 10 µg/mL in the presence or absence of 10 µg/mL of GO suspensions for 4 h at 37 °C with agitation (150 rpm). The GO exposure time was set at 4 h due to the presence of actively dividing cells which accommodates efficient antibacterial activity of antibiotics and additionally the concentration of GO was fixed at 10 µg/mL as this concentration has been previously reported to exhibit a "carrier effect" in delivering antibiotics to the bacterial cell membrane (Cogan, Brown, Darres, & Petty, 2012; Desai, Bühler, Weller, & Brown, 1998; Gao et al., 2017). After 4 h, an aliquot of 100 µL of the treated and untreated bacterial culture was retrieved and serially diluted in 0.8% saline solution. The diluted suspensions were then plated onto TSA plates and incubated for ~20 hours at 37 °C to determine the bacterial cell density (in cfu). The experiment was carried out in triplicates and the results were averaged. Untreated bacterial cultures were regarded as control samples.

### 3.8 Synergistic behaviour of GO with selected antibiotics against Gram-positive and Gram-negative bacteria in biofilm

Bacterial cultures ($10^5$ cfu) of *S. aureus*, *E. coli*, *E. faecalis* and *P. aeruginosa* from an overnight culture were resuspended in TSB into 96-well plates to form biofilm. Biofilm was left to mature for 24 h, 48 h and 72 h at 37 °C without agitation. At the end of the respective biofilm growth period, TSB media was removed and the biofilm was washed twice with 1X PBS. Biofilm in the 96-well plates was incubated with 100 µg/mL of GO suspension at 37 °C without agitation. The biofilm cells were incubated with antibiotics solutions (ampicillin, chloramphenicol and tetracycline) with varying concentrations from 2 to 10 µg/mL with or without 100 µg/mL of GO suspensions for 24 h at 37 °C without agitation. After 24 h, crystal violet assay was conducted to study the viability of the biofilm after exposure to antibiotics and GO-antibiotics. The study was carried out in three independent experiments with triplicates and the results were averaged.

### 3.9 Toxicological effects of graphene oxide against human epidermal keratinocytes

#### 3.9.1 Cell culture maintenance

The biocompatibility of GO among skin cells was conducted using HaCaT cells. These cells were cultured and maintained in DMEM supplemented with 10% heat-inactivated fetal bovine serum (FBS) (Gibco, USA) and 1% penicillin (100 U/mL)-streptomycin (100 µg/mL). The cells were incubated in a humidified incubator containing $CO_2$ (5%) at 37 °C. Trypan blue dye exclusion test was performed for cell counting prior to each experiment. HaCaT cells were seeded in the 96-well plates at 10,000 cells/well and incubated for 24 h before the experiment.

After 24 h, the confluence level of the cells was determined by viewing the seeded 96-well plate using the inverted microscope and used for subsequent experiments.

### 3.9.2 MTT viability assay

Viability of the HaCaT cells after treatment with GO was determined using the MTT assay according to Liao *et al.* (2011). Approximately ~ $10^4$ of HaCaT cells were seeded and cultured in DMEM complete medium using 96-well plates for 24 h. Subsequently, the medium was removed and the cells were then washed twice with PBS. A 100 µL of different concentrations of GO ranging from 0 to 1000 µg/mL was added to the cells in serum-free DMEM and incubated at 37 °C under $CO_2$ (5%) for 24 h. The cells were washed with PBS again to remove excess medium and 100 µL of 0.5 mg/mL of MTT was added to the cells and incubated at 37 °C under $CO_2$ (5%) for 4 h. MTT was removed and DMSO was added to the wells to dissolve the purple formazan. The plate was placed on a platform rocker (Corning Inc., USA) for 10 min and the absorbance was measured at 630 nm using spectrophotometer (FLUOstar Omega, BMG Labtech, USA). Viability of the HaCaT cells was determined by measuring the optical density of the GO treated cells against the untreated HaCaT cells.

### 3.9.3 Generation of reactive oxygen species

The generation of ROS was evaluated using ROS assay according to Horvath *et al.* (2013). Around ~ $10^4$ cells HaCaT cells were seeded and cultured using complete DMEM in a 96-well plate for 24 h. Then, the medium was removed and washed twice with PBS and incubated in the dark for 2 h with 100 µL of GO solution (0 to 1000 µg/mL) and 100 µL of DCFH-DA (Sigma-Aldrich, USA) solution in a serum-free DMEM. Subsequently, the medium was removed and washed twice with PBS to remove the excess probe.

A 100 µL of PBS was added into the well and the fluorescence intensity was measured at 485 nm of excitation and 530 nm of emission wavelengths using a fluorescence microplate spectrophotometer (FLUOstar Omega, BMG Labtech, USA). The increase in the fluorescence was expressed as ratio of GO-treated HaCaT cells relative to the untreated control cells.

### 3.9.4 LDH cytotoxicity assay

The release of LDH cytotoxicity assay was conducted to determine the degree of membrane damage of cells once treated with GO. Membrane integrity of the GO exposed HaCaT cells were evaluated using LDH Cytotoxicity Assay Kit (Thermo Fisher Scientific, Massachusetts, USA according to Gurunathan and Arsalan Iqbal *et al.* (2019). Around ~ $10^4$ of HaCaT cells were seeded and cultured in DMEM complete medium using 96-well plates for 24 h. Subsequently, the medium was removed and the cells were then washed twice with PBS. A 100 µL of different concentrations of GO ranging from 0 to 1000 µg/mL was added to the cells in serum-free DMEM and incubated at 37 °C under $CO_2$ (5%) for 24 h. At the end of the time period, 50 µL of each reaction mixture was transferred to a 96-well plate and the assay was carried out according to the manufacturer's instructions. The absorbance was measured using a microplate spectrophotometer (Epoch-BioTek, Vermont, USA). Untreated HaCaT cells were regarded as negative control and three independent experiments were performed with replicates and the results were averaged.

### 3.9.5 Cell surface morphology analysis

GO treated and untreated HaCaT cells were retrieved from the viability assay for surface morphology observations using FESEM technique. The GO treated and untreated HaCaT cells were harvested by centrifugation at 1500 rpm for 15 min at RT.

Briefly, 1 mL of the HaCaT cell suspension (~ $10^4$) was treated with 4 % glutaraldehyde (GLA) for more than 4 h. Then, the fixed HaCaT cells were washed twice with cacodylate buffer and further fixed with 1% osmium tetroxide at 4 ºC for 1 h. The cells were washed twice in double-distilled water for 10 min each.

The fixed HaCaT cells were then gradually dehydrated with ethanol using increasing concentrations ranging from 30%, 50%, 70%, 80%, 90%, 95% and finally 100%. Each ethanol wash was performed for 15 minutes. Next, the HaCaT cells were further dehydrated using mixtures of 100% ethanol and acetone at ratios of 3:1, 1:1 and 1:3 for 15 min, respectively. The cells were dehydrated three times using acetone for 20 min, each time. Final dehydration of the HaCaT cells was performed in critical point dryer (Leica EM CPD3000, Singapore) for 3 h. Lastly, the completely dried HaCaT cells were sputter-coated with gold for FESEM observations (FEI, Quanta FEG 650) at a working distance around 9 mm, with an acceleration voltage of 20kV.

### 3.10 Statistical analysis

All data were expressed as mean ± SD. Student's unpaired t-test was used to analyze experimental data of different treatment groups. The statistical analysis was performed using the GraphPad Prism 6 software (Prism, San Diego, CA, USA). A value of P less than 0.05 was accepted as statistically significant.

# CHAPTER 4: RESULTS

## 4.1 Characterizations of graphene oxide

### 4.1.1 Characterization of graphene oxide using UV-VIS spectroscopy

The prepared GO sheets were characterized using ultraviolet adsorption spectroscopy. As seen from Figure 4.1, a peak which corresponds to the π - π* plasmon was observed at around 240 nm. This is due to $sp^2$ clusters of the GO and linking units such as C=C, C=O, and C-O bonds. The shoulder band from 290 nm to 300 nm is attributed to the n – π* transitions of C = O bonds (Guo et al., 2017; Gurunathan et al., 2013). This observation is consistent with the findings reported by Gupta *et al.* (Gupta, Sharma, Singh, Arif, & Singh, 2017) and Luo *et al.* (Luo, Lu, Somers, & Johnson, 2009).

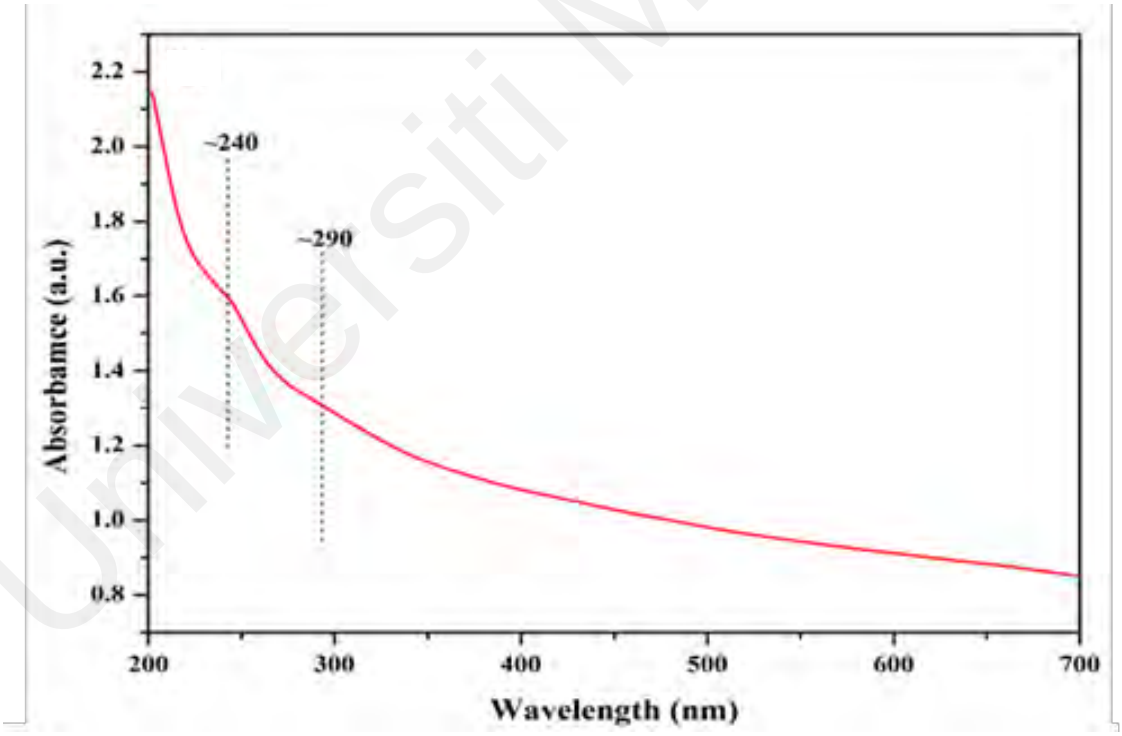


**Figure 4.1:** Characterization of synthesized GO using UV-Vis spectroscopy. UV-Vis spectrum of GO; absorbance peak of π - π* plasmon is observed at 240 nm.

### 4.1.2 Characterization of graphene oxide using Raman spectroscopy

The Raman spectrum of graphene oxide is shown in Figure 4.2. Two clear bands at 1416 $cm^{-1}$ and 1598 $cm^{-1}$ are the dominant vibrational modes corresponding to the D and G bands of carbon, respectively (Nanda et al., 2016). The intense G band at 1598 $cm^{-1}$ is common to all $sp^2$ carbon forms and is attributed to the optically allowed $E_{2g}$ phonon. The weak D band at 1416 $cm^{-1}$ is ascribed to the mode of the κ-point phonons of $A_{1g}$ symmetry (Zhou, Gui, Hu, Jiang, & Tang, 2016), reflecting the degree of defects found on the structure. Raman spectroscopy is mostly used to acquire structural data on carbon materials (Chaiyakun et al., 2012). The strong band (G) is due to the $sp^2$-bonded carbon regions while the weaker band (D) reflects the degree of defects found on the structure (Perreault et al., 2015).

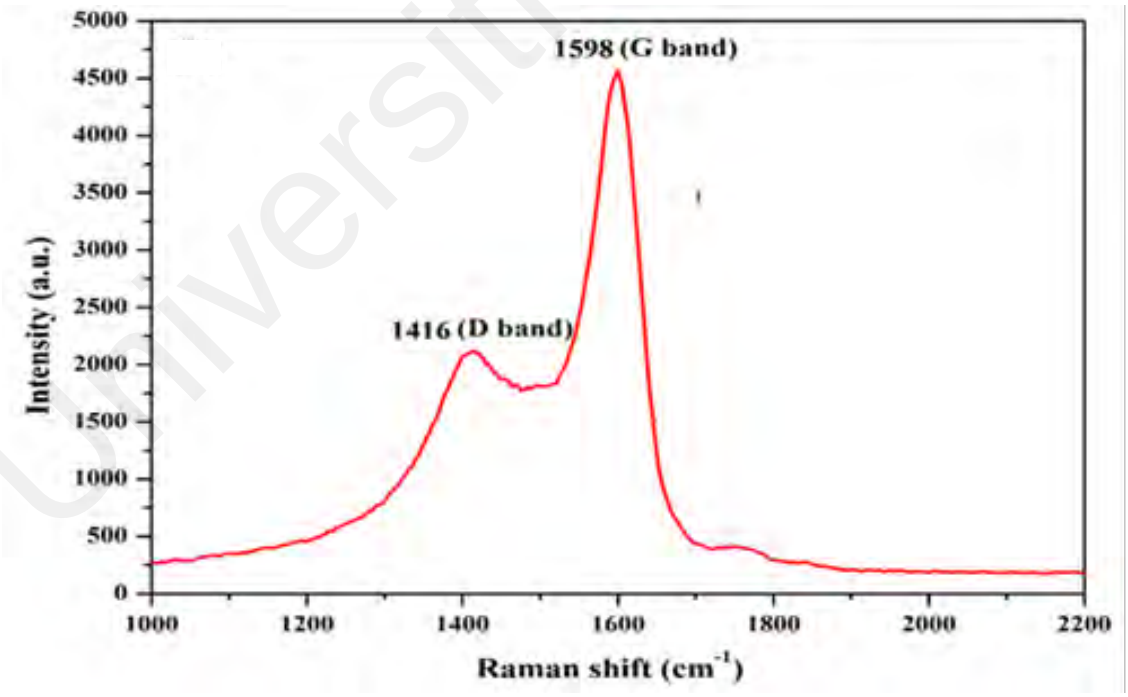


**Figure 4.2:** Raman spectrum of GO. G band arises due to the $sp^2$-bonded carbon regions and the D band reflects the degree of defects found on GO.

### 4.1.3 Characterization of graphene oxide using ATR-FTIR analysis

The ATR-FTIR spectrum of GO is shown in Figure 4.3. The presence of the bands in this spectrum is associated with the functional groups of GO. Vibration modes that are based on the configuration of oxygen which include the OH, C-OH, COOH and C-O functional groups are observed in the GO spectrum. The broad peak observed around 3224 $cm^{-1}$ could be attributed to the presence of carboxyl O-H stretching vibration mode. This peak appeared broad as it overlaps with absorption peaks that correspond to stretching vibrations of hydroxyl groups (O-H) on the plane, which is due to the presence of absorbed water molecules and alcohol groups (Nyquist & Kagel, 2012).

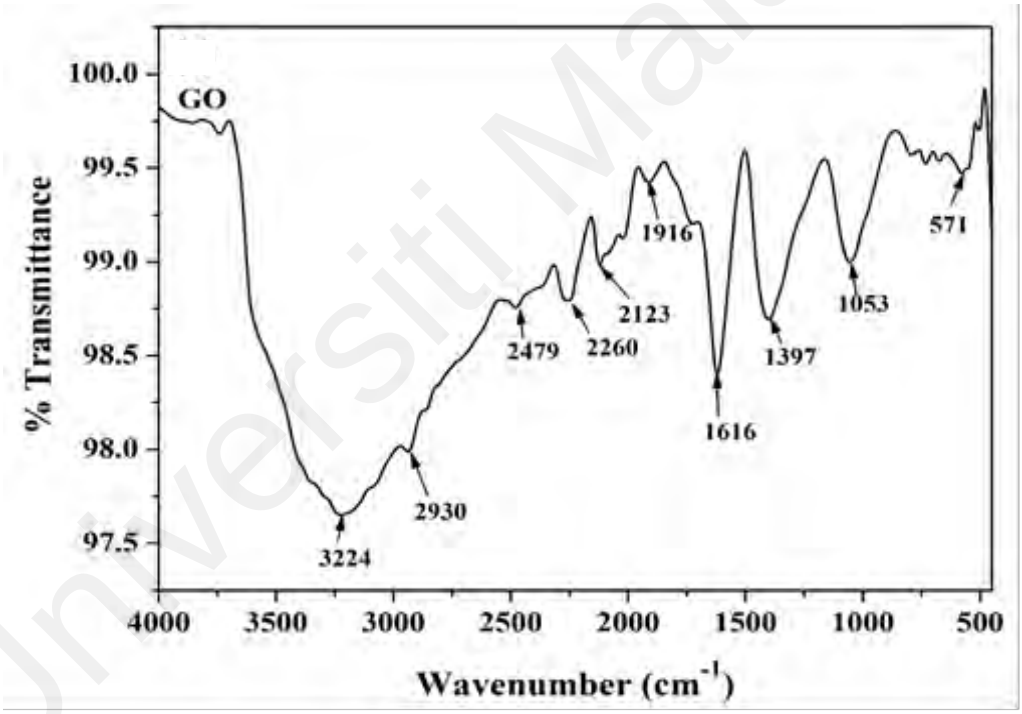


**Figure 4.3:** ATR-FTIR spectrum of GO. Functional groups of OH, COOH, C-OH and C-O are indicated at 3224 $cm^{-1}$, 1735 $cm^{-1}$, 1397 $cm^{-1}$ and 1053 $cm^{-1}$, respectively.

The asymmetric $CH_2$ stretching of GO appears at 2930 $cm^{-1}$ and the small peak located at 2479 $cm^{-1}$ is attributed to carbon dioxide. The band that appears as a shoulder peak at 1735 $cm^{-1}$ is attributed to C=O stretch of carboxyl groups located at the edges of the GO sheets (Valentini, Bon, Monticelli, & Kenny, 2012). The sharp peak appeared at 1616 $cm^{-1}$ is corresponds to the aromatic C=C bonds and the bands at 1397 $cm^{-1}$ and 1053 $cm^{-1}$ corresponds to C-OH and C-O stretching vibrations, respectively (Thirunavukkarasu et al., 2013).

### 4.1.4 Characterization of graphene oxide using XRD analysis

Figure 4.4 shows the XRD peak of graphene oxide.

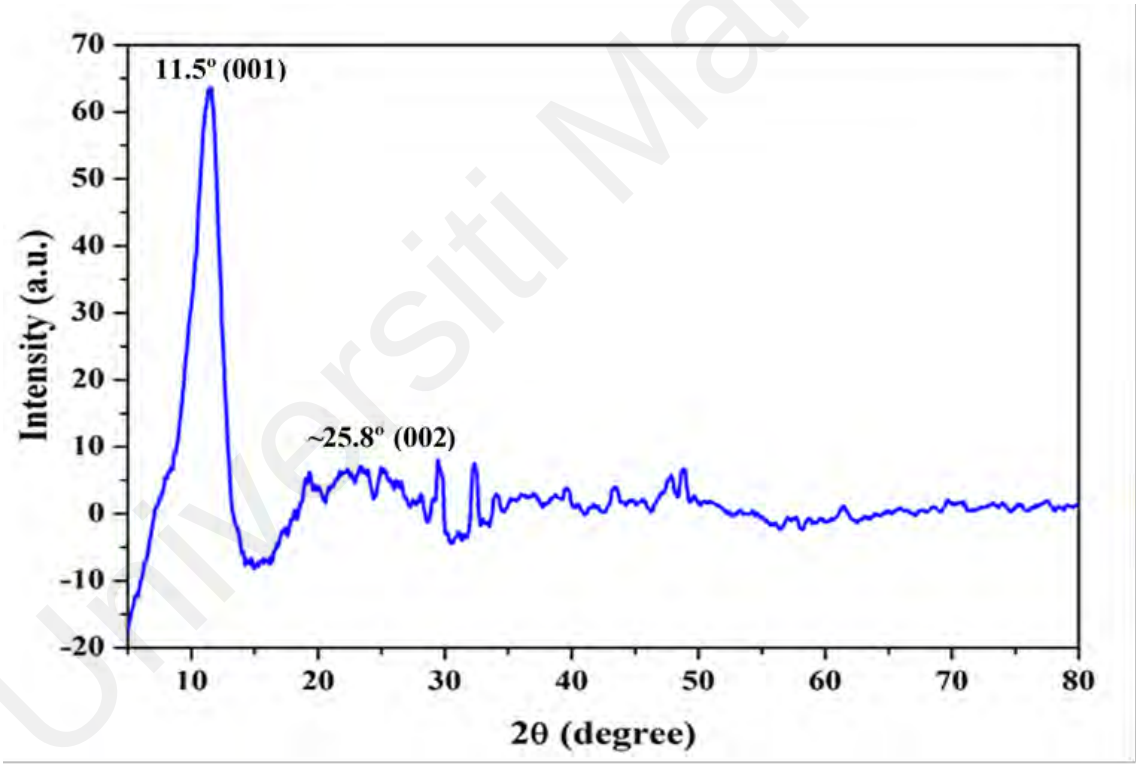


**Figure 4.4:** XRD of graphene oxide (GO). The peak at 2θ = 11.5° corresponds to the oxygen functional group and the broad peak at ~25.8 ° designates random packing of graphene sheet in GO.

The signal exhibited a very strong peak at 2θ = 11.5° which corresponded to the (001) plane with the inter-layer spacing (d) of 0.77 nm. This peak designates the oxygen functional group due to the hydration and exfoliation of graphene in aqueous medium (Yilbas, Ibrahim, Ali, Khaled, & Laoui, 2018). The broad peak at ~25.8 ° which corresponds to a random packing of graphene sheet in the GO (Gupta et al., 2017).

### 4.1.5 Characterization of graphene oxide using electron microscopy techniques

The topology of the synthesized GO was observed from FESEM images as shown in Figure 4.5.

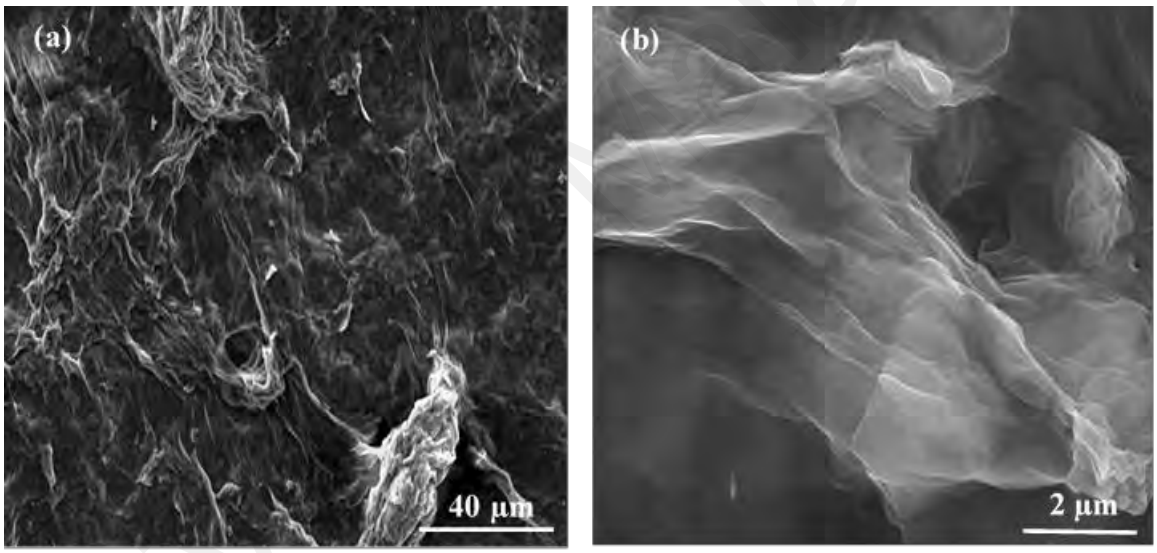


**Figure 4.5:** FESEM images of the synthesized GO at (a) lower magnification (2500x) showing a sheet-like layer formation of GO with multiple folds and at (b) high magnification (40,000 x) indicating an ordered layer structure which has been exfoliated into layers of GO sheets.

The FESEM image in Figure 4.5(a) shows the morphology of the 2D nanosheets of GO with randomly aggregated, thin and crumpled layers structure (Saleem, Haneef, & Abbasi, 2018). The oriented sheet-like layer formation of GO with multiple folds gives the appearance of a wrinkled thin film due to its oxidation. Figure 4.5(b) shows the GO appeared as a flat smooth surface with an ordered layer structure which has exfoliated into mono or multi-layer GO sheets. This image reveals that the wrinkles on the GO sheet which evidently emphasizes its sharp edge.

Figure 4.6 (a) and (b) show the morphology and nanostructure of the graphene oxide at the magnification of 170 k and 1250 k respectively. As expected, Figure 4.6(a) clearly shows the presence of thin graphene nanosheets (Gabriel et al., 2018). The high-resolution TEM image (Figure 4.6(b)) clearly demonstrates the multi-layers of graphene sheets which is consistent with the XRD result.

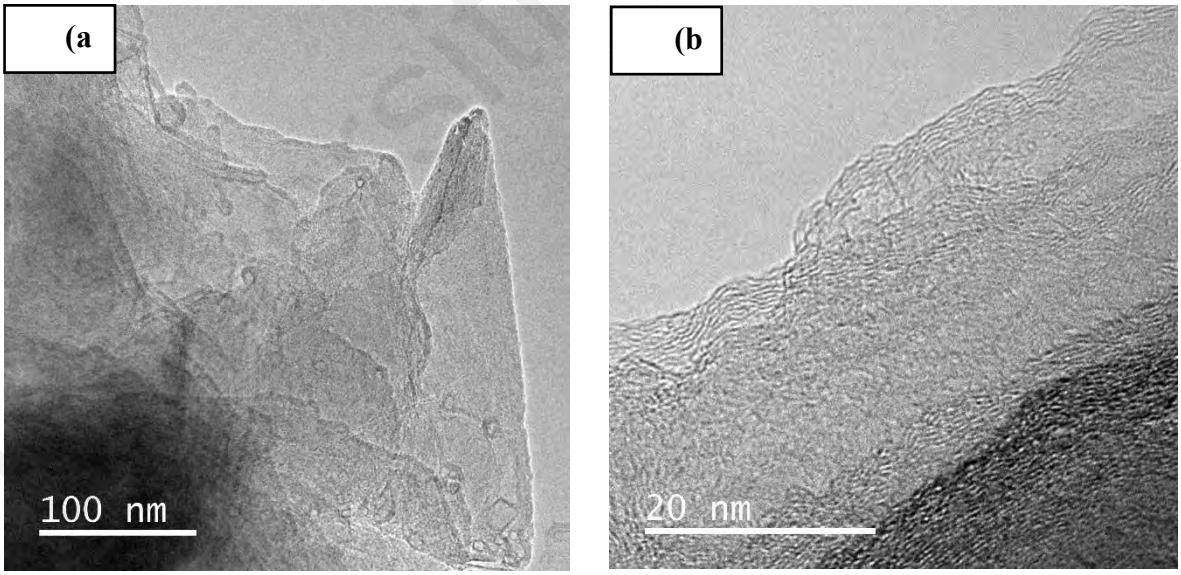


**Figure 4.6:** TEM image of synthesized GO at (a) lower magnification (170 k) which shows thin graphene nanosheets and at (b) multi-layers of graphene sheets could be observed at a higher magnification of 1250 k.

## 4.2 Antibacterial activity of graphene oxide against Gram-positive and Gram-negative bacteria in suspension

### 4.2.1 Concentration dependent activity through viability assay

The antibacterial activity of GO was assessed by exposing selected Gram-positive and Gram-negative bacteria to various concentrations of an aqueous suspension of GO ranging from 0 to 140 µg/mL for a fixed time-period (4 hours). Two Gram-positive bacteria *S. aureus* and *E. faecalis* and two Gram-negatives *E. coli* and *P. aeruginosa* have been tested in this study. The line graph in Figure 4.7 clearly depicts the reduction in the number of bacterial cells when treated with an increasing GO concentration for all bacterial strains.

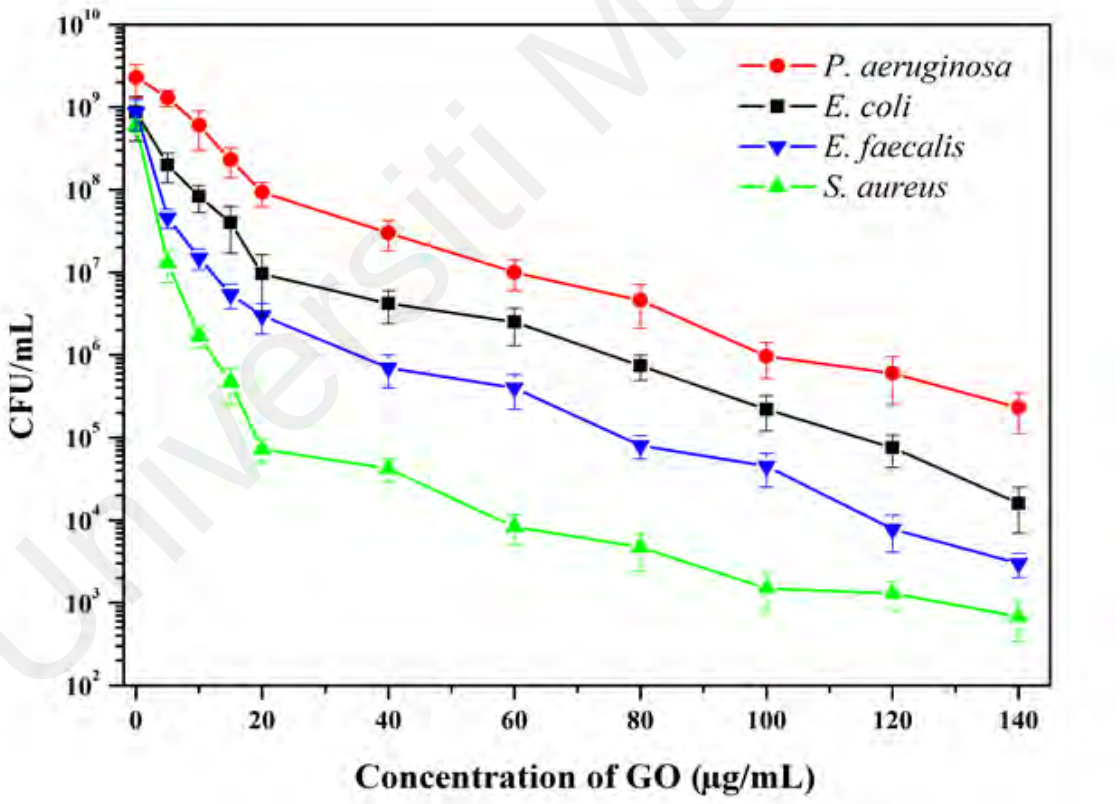


**Figure 4.7:** Viability curve of bacteria after exposure to GO for 4 h. A sharp decrease in the viability was observed at GO concentration of 10 µg/mL and deteriorates further as the concentration of GO increases.

The cfu counts indicated that GO has almost completely inhibited the bacterial growth of all strains as seen in the line graph, but the inactivation rate differed among individual bacteria at lower concentrations. The degree of bacterial inactivation followed the order; *S. aureus* > *E. faecalis* > *E. coli* > *P. aeruginosa* in a descending trend. More than 90% of all bacteria were inactivated at GO concentration of 15 µg/mL, whereas *S. aureus* was almost fully inactivated at GO concentrations of 5 µg/mL compared to other strains. At GO concentration of 10 µg/mL, loss of viability was 99.4% for *S. aureus,* 96% for *E. faecalis*, 73.6% for *E. coli* and 63% for *P. aeruginosa*.

As GO concentrations of 10 µg/mL was able to inactivate more than 60% of live cells, this concentration was selected for subsequent experiments. More than 99.9% reduction (> 3 log reductions) in colony counts signifies the bactericidal effect of the GO sheets. Increasing GO concentrations resulted in a reduction in the viability of all strains most notably for *S. aureus* and the least towards *P. aeruginosa*, therefore the bactericidal activity of GO is concentration dependent.

### 4.2.2 Membrane integrity analysis through LDH cytotoxicity assay

Membrane integrity of GO treated bacterial cultures was measured by monitoring the release of LDH into the reaction medium after treatment using the LDH cytotoxicity assay. This assay is commonly used to evaluate the loss of membrane integrity of cells after treatment with toxic compounds (Venkatasubbu, Baskar, Anusuya, Seshan, & Chelliah, 2016). It was found that the exposure of bacteria to increasing concentrations of GO enhanced the levels of LDH detected in the medium. This observation was noted for all bacteria when exposed to increasing GO concentrations. However, differences in the levels of detectable LDH among the bacterial cultures were noted as shown in Figure 4.8.

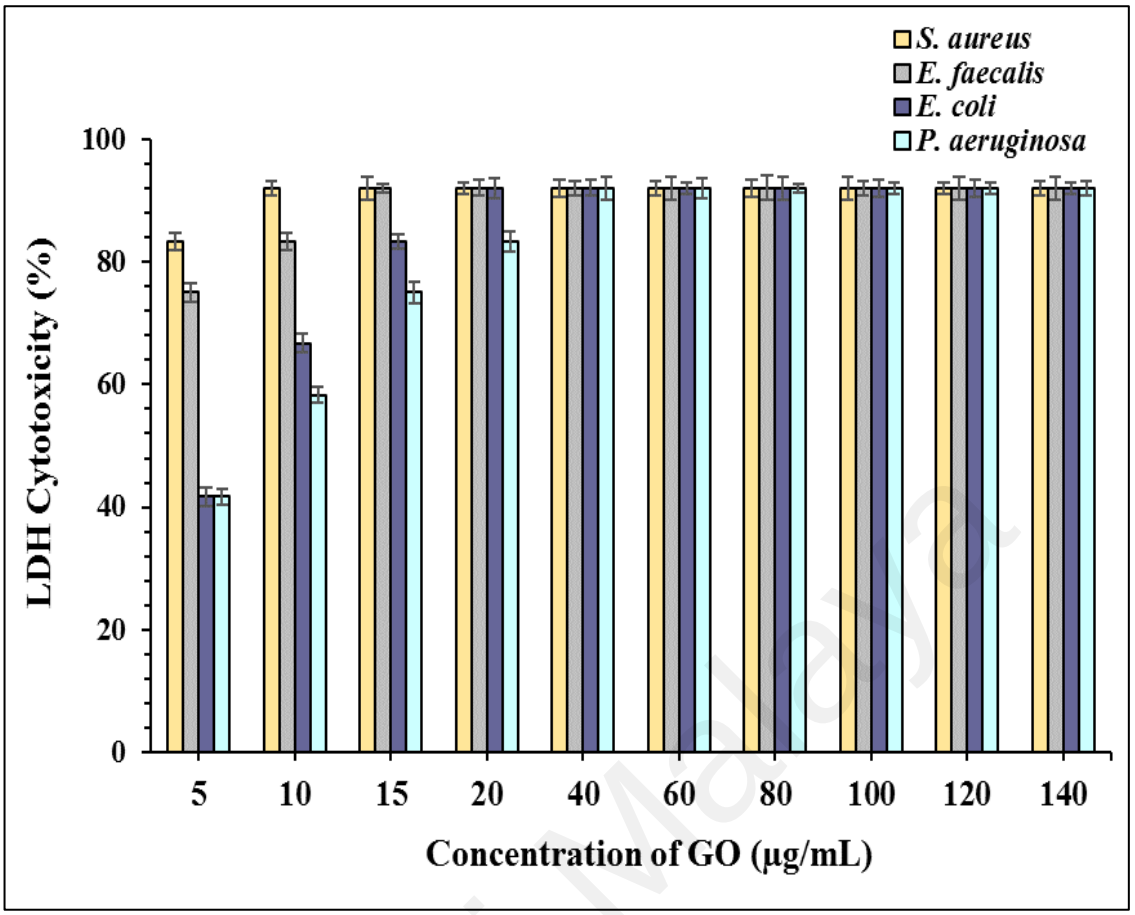


**Figure 4.8:** LDH cytotoxicity analyses of bacterial cells in suspension after exposure to GO for 4 h. Increased levels of LDH was measured for increasing concentrations of GO which indicated elevated membrane damage upon exposure to GO.

Apparent differences in the concentration of LDH detected in the medium was noted when the bacteria were exposed to 20 µg/mL of GO or lower. Higher release of LDH was observed for the Gram-positive isolates (*S. aureus and E. faecalis*) compared to the Gram-negative isolates (*E. coli and P. aeruginosa*) for the lower concentration levels of GO. LDH cytotoxicity for *S. aureus* and *E. faecalis* for GO concentration of 5 µg/mL were 83.3% and 75%, respectively. Meanwhile, 41.7% of LDH cytotoxicity was measured for both *E. coli* and *P. aeruginosa.*

At 10 µg/mL of GO, 92% and 83.3% of cytotoxicity level were noted for *S. aureus* and *E. faecalis* respectively while cytotoxicity levels of 66.7% and 58.3% were noted for *E. coli* and *P. aeruginosa*, respectively. On the other hand, LDH cytotoxicity levels for *S. aureus, E. faecalis, E. coli and P. aeruginosa* were measured to be similar among all bacteria for higher GO concentrations. Levels of LDH cytotoxicity were measured to be 92% for all the tested GO concentrations of 40 – 140 µg/mL as shown in Figure 4.8.

### 4.2.3 Time dependent activity through time-kill assay

The role of time in influencing the bactericidal effects of GO towards bacteria was investigated using the time dependant assay. This assay was performed for 8 h with a 2-hour interval time at a fixed GO concentration (10 µg/mL) for all the tested strains. Loss of viability was noted to increase with a longer period of incubation as all strains recorded the highest amount of cell death at the 8$^{th}$ hour (Figure 4.9) compared to the 2$^{nd}$ hour. Notably, *S. aureus* recorded the highest percentage for loss of cell viability for all tested exposure time, whereas *P. aeruginosa* was affected the least compared to all other bacteria. Longer incubation period with graphene oxide induced higher death rate among all the tested bacteria. This time-dependent assay also followed the same order of inactivation; *S. aureus* > *E. faecalis* > *E. coli* > *P. aeruginosa.*

At the 4$^{th}$ hour of incubation period, loss of viability was 99.4% for *S. aureus,* 96% for *E. faecalis*, 73.6% for *E. coli* and 63% for *P. aeruginosa*. A large portion of cell death occurred at 4 h of incubation and this time-period was used in the subsequent investigations in this work to explore the interactions of GO. It was noted that increase in the exposure period of GO against bacteria escalated the antibacterial activity of GO. Therefore, the antibacterial activity of GO was found to be time dependent.

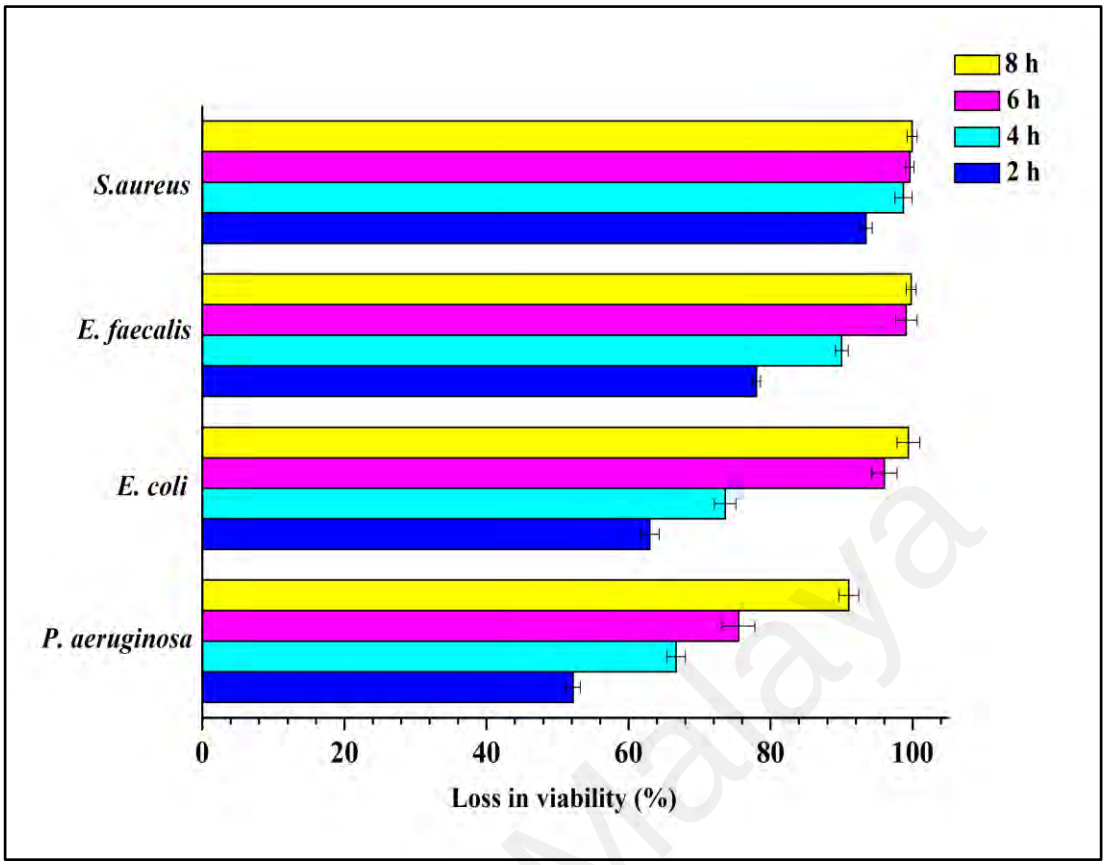


**Figure 4.9.** Time kill assay of bacteria after exposure to GO for several time periods (2 h, 4 h, 6 h and 8 h). Increase in the incubation time improves bacterial cell contact with GO and this leads to higher percentage of cell death.

### 4.2.4 Visualization of the bacterial cell upon exposure to graphene oxide

#### a. Field-emission scanning electron microscopy technique

FESEM characterizations were conducted to investigate the interactions between the bacterial cell membrane and GO sheets. Figure 4.10 (A – D) represent untreated bacterial cells while Figure 4.10 (E – H) show the treated cells. FESEM images revealed that untreated bacterial cells were observed to have intact cell membrane compared to bacterial cells that were treated with GO. Treated bacteria cells showed deformed shapes for all strains which indicated compromised membrane integrity and resulted in eventual cell death.

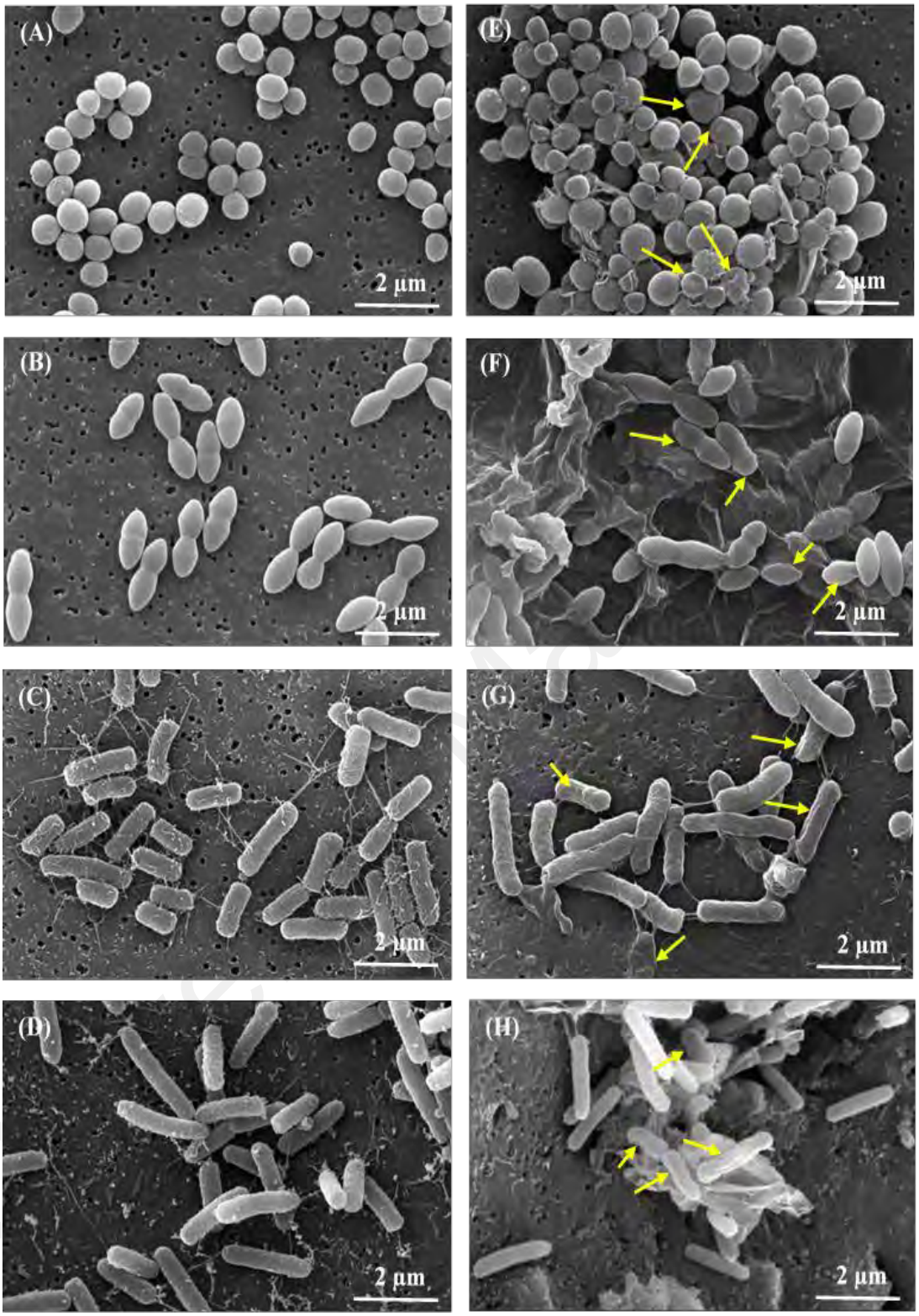


**Figure 4.10:** FESEM images of bacteria cells before and after exposure to GO. A to D represent untreated bacteria and E to H represent GO-treated bacterial cells. (A and E; *S. aureus*, B and F; *E. faecalis*; C and G; *E. coli*, D and H; *P. aeruginosa*.) Yellow arrows indicate membrane damage that was observed under FESEM analysis for GO-treated cells only.

However, the degree of membrane disruptions observed among the GO treated bacteria and the mechanism of action vary according to the type of bacteria. A clear difference in the degree of membrane damage and methods of GO interactions could be observed in the FESEM analyses among Gram-positive *S. aureus* and *E. faecalis* and Gram-negative *E. coli* and *P. aeruginosa*. Large clusters of Gram-positive *S. aureus* and *E. faecalis* appeared to be entrapped by numerous GO sheets in Figure 4.10 (E) and (F) images. In contrast, the Gram-negative bacteria suffered hollows and dents on their membrane surface and did not appear to be severely trapped under GO sheets, unlike the Gram-positive cells as observed in Figure 4.10 (G) and (H). Although membrane corrugations have been mainly observed for the Gram-negative bacteria only, loss of viability among *E. coli* and *P. aeruginosa* were lower compared to Gram-positive bacteria. Additionally, reduction in the number of pili was observed among cells of *E. coli* and *P. aeruginosa* that were treated with GO compared to the control group of bacteria. The Gram-positive *S. aureus* and *E. faecalis* were actively isolated in large clusters of cells from their nutrient due to the wrapping mechanism of GO.

**b. Transmission electron microscopy technique**

TEM analyses were carried out to monitor morphological changes among the Gram-positive *S. aureus* and *E. faecalis* and Gram-negative *E. coli* and *P. aeruginosa*. bacterial cells after treatment with GO. Figure 4.11 (A – D) show the TEM images of untreated control group of bacteria while Figure 4.11 (E – H) show the TEM images of GO treated group of bacteria. As observed with the FESEM analyses that were conducted for the same group of bacteria, differences in the mechanism of action of GO towards Gram-positive and Gram-negative bacteria were also observed in the TEM analyses.

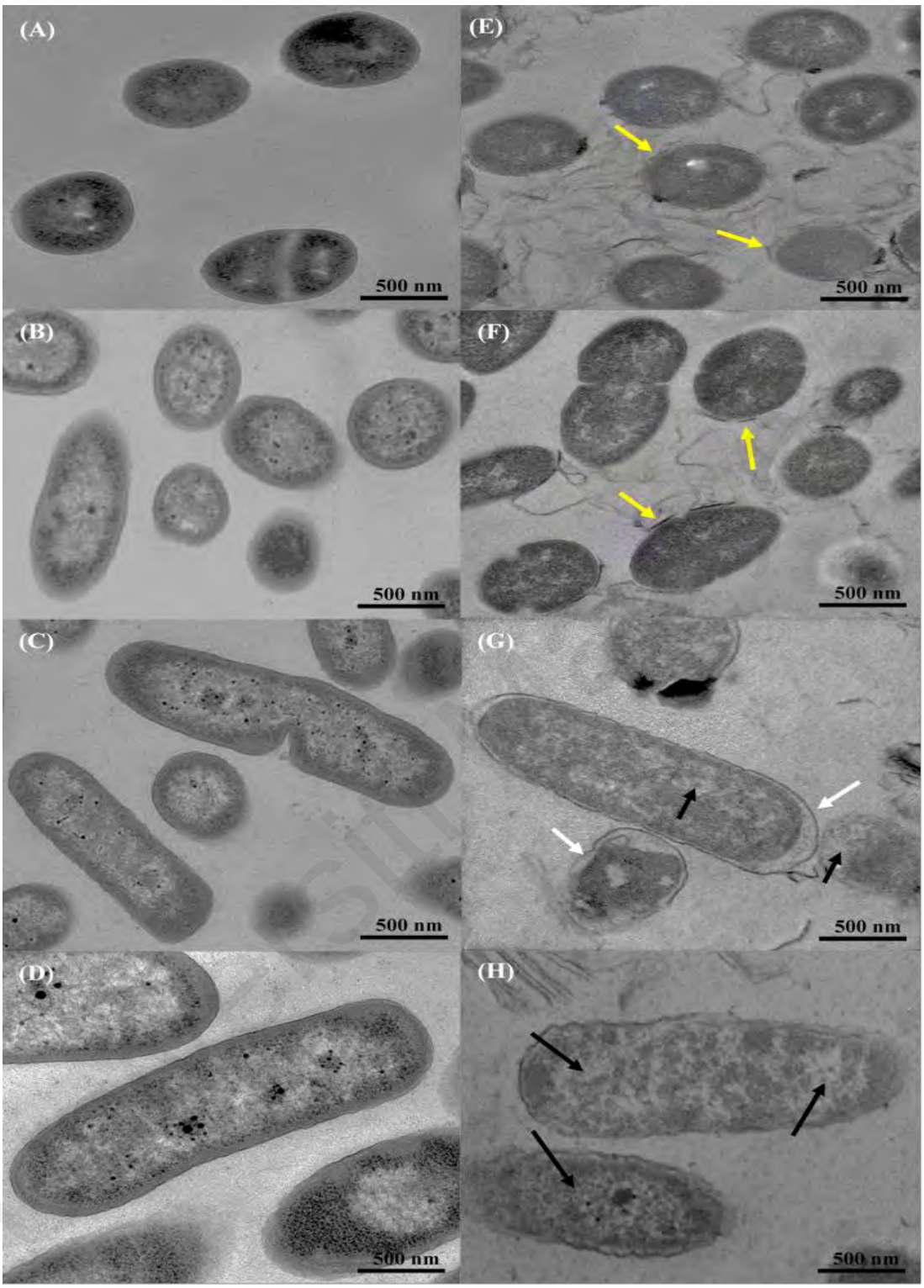


**Figure 4.11:** TEM analysis of bacterial cells before and after exposure to GO. A - D represent untreated bacteria and E to H represent GO-treated bacteria. (A and E; *S. aureus*, B and F; *E. faecalis*; C and G; *E. coli*, D and H; *P. aeruginosa*). Yellow arrows indicate attachment of GO sheets onto bacterial cells to potentiate antibacterial mechanism. White arrows show detachment of cell membrane that may have been caused by leakage of cell content. Black arrows indicate lower density of lipids that may have been caused by partial membrane damage.

In comparison to the control bacteria for the Gram-positive category, GO treated *S. aureus* and *E. faecalis* were observed to be surrounded by GO characterized by their long sheets. This is clearly shown in Figure 4.11 (E) and (F) where the GO sheets are seen to accumulate around the bacterial cells. However, this phenomenon was not observed among the Gram-negative *E. coli* and *P. aeruginosa* in Figure 4.11 (G) and (H). In contrast, the TEM images of the Gram-negative *E. coli* and *P. aeruginosa* bacteria in Figure 4.11 (G) and (H) were observed to display a decrease in intracellular density compared to the control group of bacteria in Figure 4.11 (C) and (D).

Additionally, *E. coli* was observed to display a slight loss in cytoplasmic content among the GO treated group. Gaps or empty spaces existed between the cytoplasm and cell wall in the TEM image of Figure 4.11 (G). This observation was not found among the GO treated *P. aeruginosa* cells. The GO treated *P. aeruginosa* cells were only noted to display a reduction in the intracellular density compared to GO treated *E. coli* cells.

### 4.2.5 Interactions between bacterial cell membrane and graphene oxide at molecular level

Figure 4.12 showed the ATR-FTIR characterizations of untreated and GO treated bacterial cultures. Amongst the bands that exhibited clear differences, the 2344 $cm^{-1}$ band in GO-*S. aureus* was assigned to the O-H stretching due to the carboxylic acid which is also present in the GO framework (Kannan, 2014). However, the intensity of the peak was reduced and the peak was observed to be shown at 2260 $cm^{-1}$ in the bare GO spectrum (Figure 4.3). The primary and secondary amides (region II) of *S. aureus* occurred at 1622 $cm^{-1}$ and 1538 $cm^{-1}$, respectively due to the stretching vibrations of C=O and N-H (Bhat, 2013).

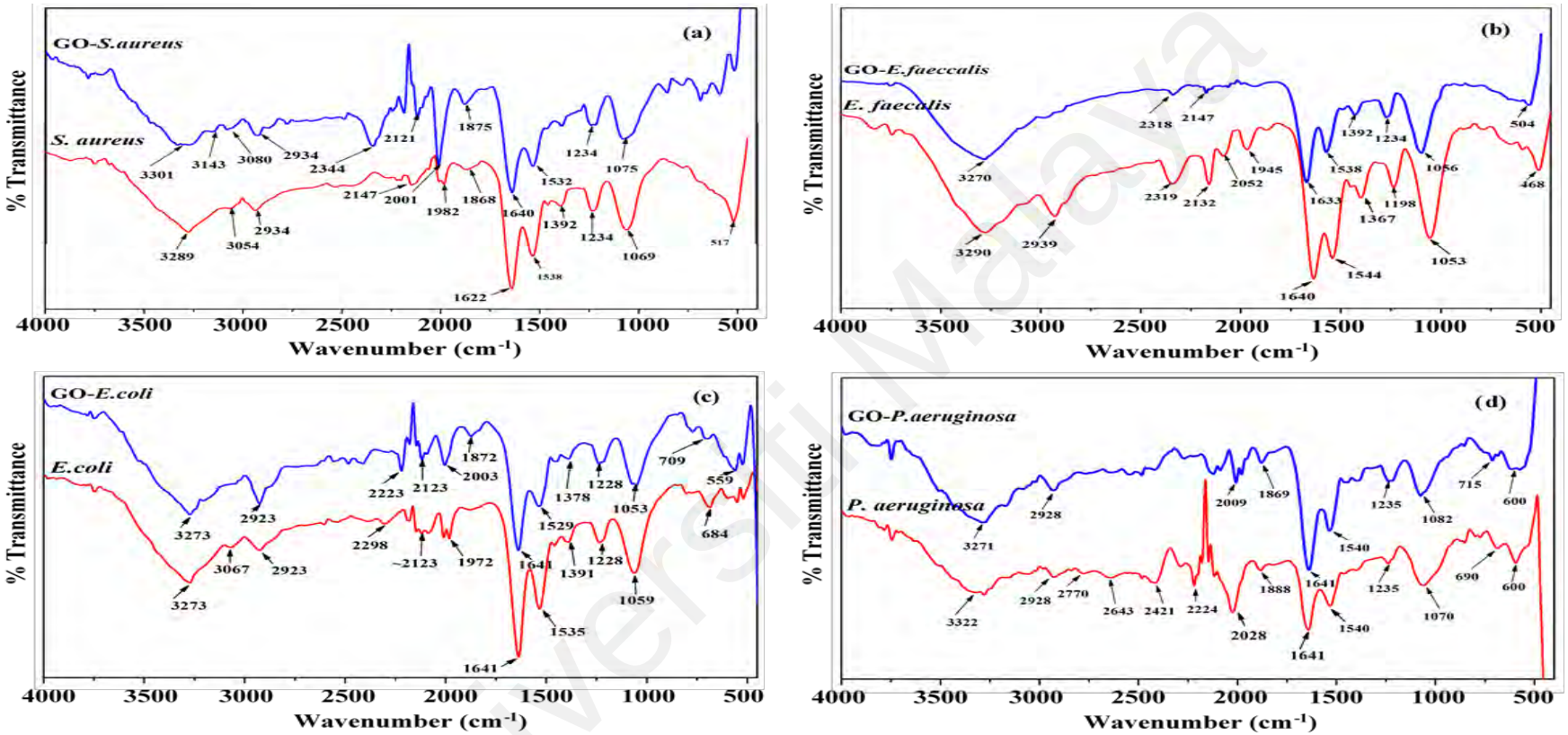


**Figure 4.12:** ATR-FTIR characterizations of untreated and GO treated bacterial cultures. The spectra show the differences in the intensity of functional groups that are present on the surface of bacterial cell wall before and after treatment with GO. (a) ATR-FTIR spectra of untreated and treated *S. aureus*; (b) ATR-FTIR spectrum of untreated and treated *E. faecalis*; (c) ATR-FTIR spectrum of untreated and treated *E. coli*; (d) ATR-FTIR spectrum of untreated and treated *P. aeruginosa*.

The intensity of both C=O and N-H bands decreased after the introduction of GO. Additionally, the presence of amino acid functional group at 517 $cm^{-1}$ (region V) which is due to the $COO^-$ and the symmetric C=O stretching of amino acids at 1392 $cm^{-1}$ (region III) were diminished in the GO-*S. aureus* spectrum as shown in Figure 4.12(a) (Garip, Bozoglu, & Severcan, 2007).

The ATR-FTIR spectra of *E. faecalis* and GO-*E. faecalis* are shown in Figure 4.12 (b). The presence of the characteristic bands of C-H asymmetric of $CH_2$ in fatty acids at 2939 $cm^{-1}$ in GO-*E. faecalis* spectrum has almost disappeared (Kannan, 2014). Furthermore, the O-H stretching vibration due to carboxylic acid at 2319 $cm^{-1}$ and C≡C stretching vibration of monoalkyl acetylene at 2132 $cm^{-1}$ have also been reduced in GO-*E. faecalis* spectrum (Thirunavukkarasu et al., 2013). Figure 4.12 (c) shows the ATR-FTIR spectra of *E. coli* and *E. coli* treated with GO. The peak at 2923 $cm^{-1}$ in *E. coli* spectrum is due to the presence of C-H stretching in aliphatic compounds of cell walls such as lipids mainly along with a minor contribution from proteins, carbohydrates and nucleic acids (Thirunavukkarasu et al., 2013). This peak, however, has intensified in the GO - *E. coli* and GO -*P. aeruginosa* spectra as well. The intensity of amide II (protein N-H bend, C-N stretch) peak at 1535 $cm^{-1}$ in GO-*E. coli* spectrum has noticeably reduced (Suzuki et al., 2013). Moreover, the peak attributed to COO- symmetric stretch in amino acid side chains and fatty acids at 1391 $cm^{-1}$ slightly reduced and have shifted to 1378 $cm^{-1}$.

Furthermore, a P=O asymmetric stretching band which appeared at 1228 $cm^{-1}$ is mainly due to nucleic acids with some influence from phospholipids (Lebedeva et al., 2015). These peaks do not fluctuate before and after the treatment.

The strong absorption band that appeared at 1059 $cm^{-1}$ may be associated with $PO^{2-}$ symmetric stretching from nucleic acids and phospholipids and this band decreases in intensity after GO treatment (Wong, Wong, Caputo, Godwin, & Rigas, 1991). Similarly, the $PO^{2-}$ symmetric stretching band appeared at 1070 $cm^{-1}$ for *P. aeruginosa* and this band decreased in intensity after GO exposure. The ATR-FTIR spectra of *P. aeruginosa* and GO-P. *aeruginosa* is shown in Figure 4.12 (d). In contrast to other bacteria, the amide I and amide II bands of *P. aeruginosa* after the GO treatment have intensified.

## 4.3 Antibiofilm activity of graphene oxide against Gram-positive and Gram-negative bacteria

### 4.3.1 Concentration dependent activity through viability assay

Bactericidal activity of GO against 24 h-, 48 h- and 72 h-biofilm of *S. aureus*, *E. faecalis*, *E. coli* and *P. aeruginosa* were evaluated using various concentrations of aqueous suspensions of GO ranging from 0 to 200 µg/mL for a fixed time-period of 24 h. Changes in the mass of biofilm were determined using crystal violet staining assay. The results indicated that the viability of the biofilm cells increased when treated with GO up to 200 µg/mL for all isolates regardless of the biofilm maturity. Although GO was noted to decrease the viability of the bacterial cells in suspension, however the reverse was observed for the biofilm cells. Increase in the viability of the biofilm cells upon exposure to GO is as indicated in Figure 4.13.

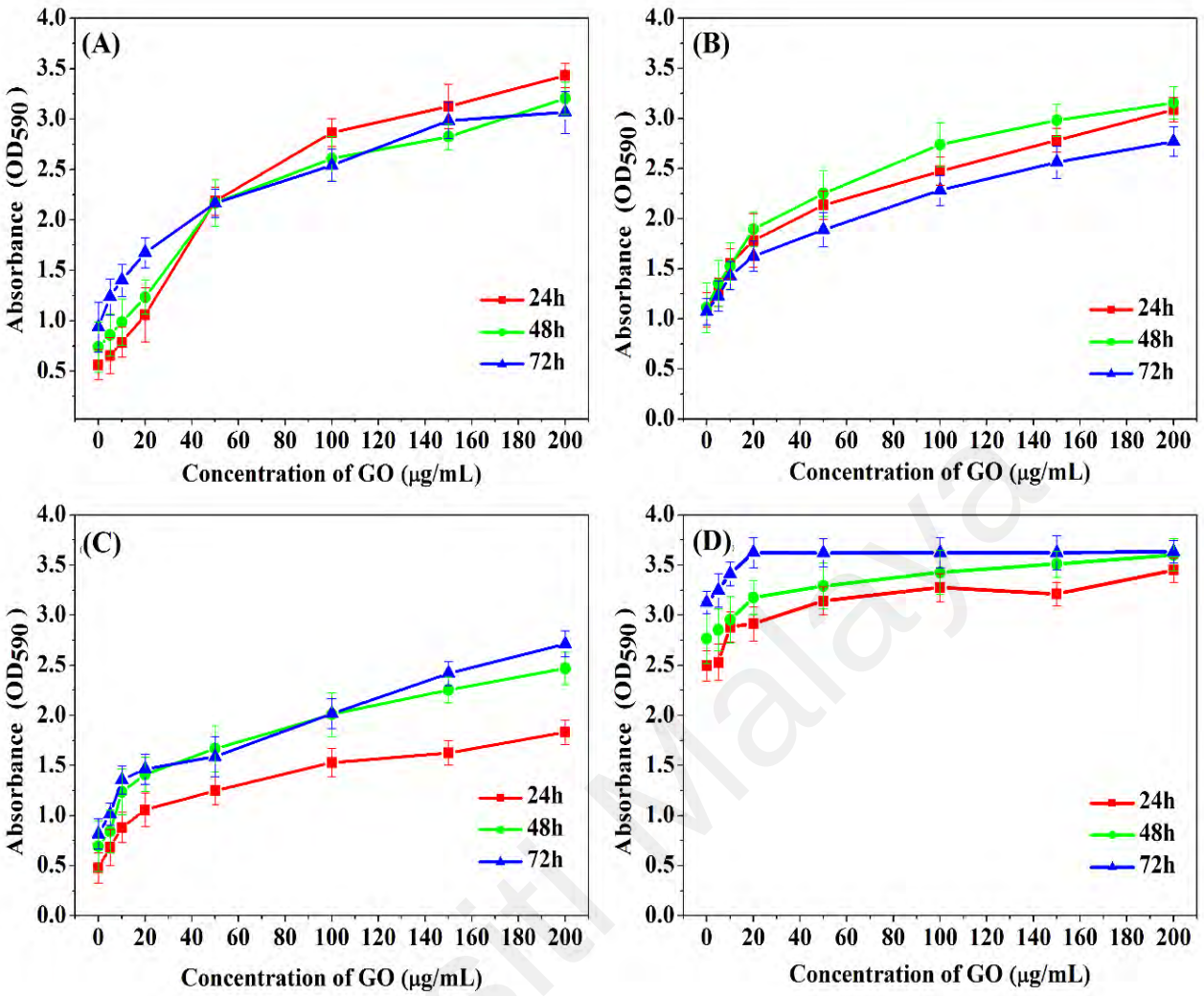


**Figure 4.13:** Viability of biofilm cells of *S. aureus* (A), *E. faecalis* (B), *E. coli* (C) and *P. aeruginosa* (D) upon exposure to various concentrations of GO. GO enhances the viability of the biofilm cells by providing additional surface area for attachment and growth.

However, the ability to form biofilm in the presence of GO varied among the different bacterial strains that were used in this study. 24 h-biofilm of *S. aureus* was able to form additional biofilm of more than 500% when exposed to 200 µg/mL of GO. Similarly, 24 h-biofilm of *E. faecalis*, *E. coli* and *P. aeruginosa* were only able to continue to produce biofilm up to 184 %, 284 % and 38 %, respectively when treated with 200 µg/mL of GO.

Subsequently, continuous production of biofilm for the 48 h-biofilm of *S. aureus* (334 %), *E. coli* (255 %) and *P. aeruginosa* (30 %) reduced but remained similar for *E. faecalis* (184 %) after treatment with 200 µg/mL of GO compared to the 24 h-biofilm cells of the same bacteria. The ability to continuously produce biofilm by the 72 h-biofilm cells of *S. aureus* (227 %), *E. faecalis* (158 %), *E. coli* (232 %) and *P. aeruginosa* (16 %) was also reduced after treatment with 200 µg/mL of GO compared to 24 h- and 48 h-biofilm of the same bacteria.

### 4.3.2 Membrane integrity analysis through LDH cytotoxicity assay

Membrane integrity of GO treated 24 h-, 48 h- and 72 h-biofilm of *S. aureus, E. faecalis, E. coli* and *P. aeruginosa* was measured by monitoring the release of LDH into the reaction medium using LDH cytotoxicity assay. The 24 h-, 48 h- and 72 h-biofilm cells were treated with various concentrations (5 - 200 µg/mL) of GO for 24 h. The release of LDH enzyme into the biofilm reaction medium after GO treatment was measured. Figure 4.14 describes the levels of LDH cytotoxicity induced by GO treatment for the 24 h-, 48 h- and 72 h-biofilm of *S. aureus, E. faecalis, E. coli* and *P. aeruginosa*.

Levels of LDH cytotoxicity measured for all biofilm cells after treatment with GO considerably varied according to the maturity of the biofilm. The 72 h-biofilm of *S. aureus, E. faecalis, E. coli* and *P. aeruginosa* released the least amount of LDH into the growth medium compared to 48 h- and 24 h-biofilm of the same tested bacteria.

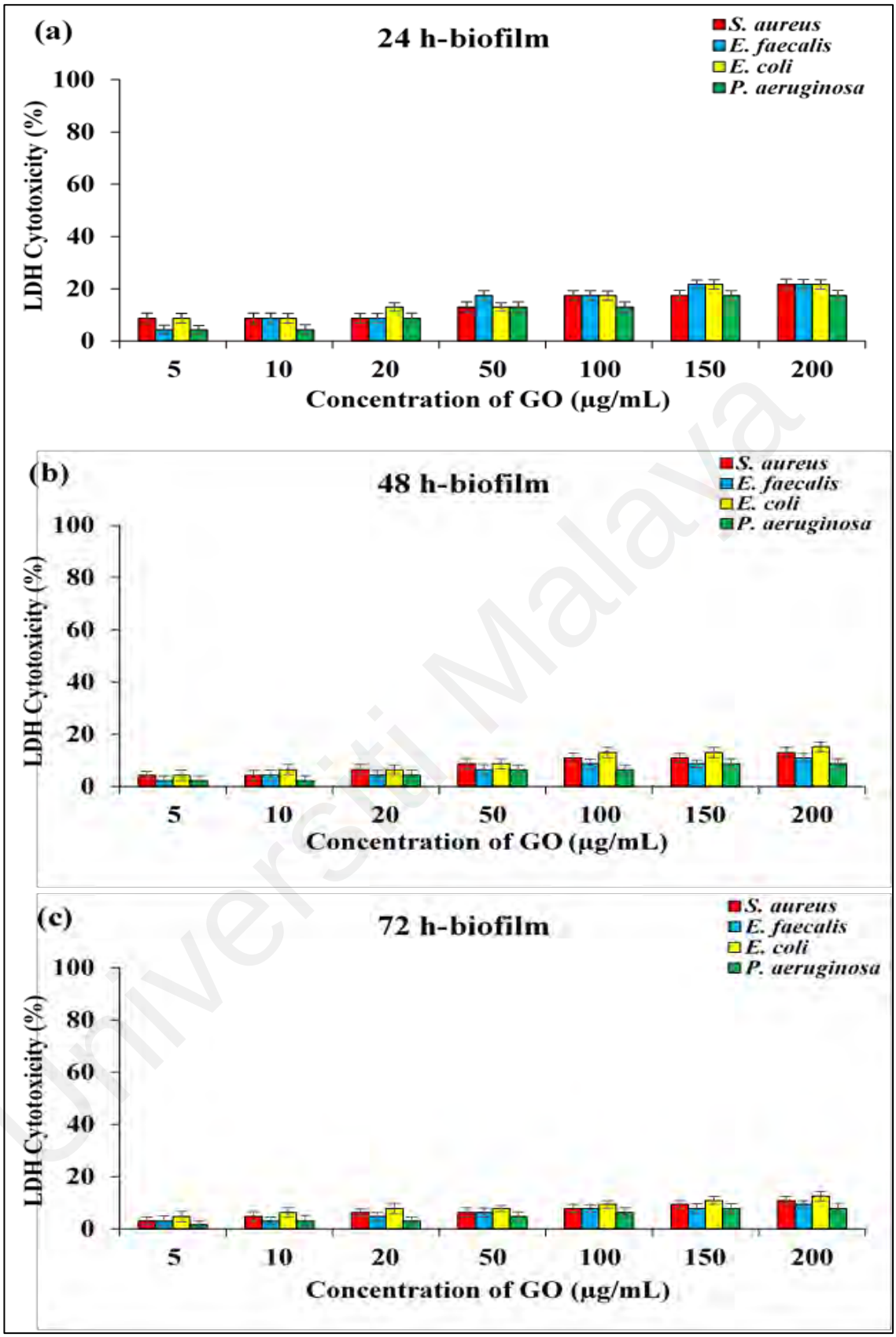


**Figure 4.14:** LDH cytotoxicity analyses of biofilm cells of bacteria after exposure to GO for 24 h. (a) LDH leakage assay of 24 h biofilm cells; (b) LDH leakage assay of 48 h biofilm cells; (c) LDH leakage assay of 72 h biofilm cells. Levels of LDH detected differs depending on the maturity of the biofilm.

Comparatively, 24 h-biofilm cells recorded LDH cytotoxicity values of 21.7 % for *S. aureus, E. faecalis* and *E. coli* and 17.4 % for *P. aeruginosa* when treated with 200 µg/mL of GO for 24 h. However, these percentages reduced to 13 % for 48 h-biofilm cells of *S. aureus*, 10.9 % for 48 h-biofilm cells of *E. faecalis,* 15.2 % for 48 h-biofilm cells of *E. faecalis* and 8.7 % for 48 h-biofilm cells of *P. aeruginosa*. Similarly, these percentages dropped lower for all 72 h-biofilm cells of bacteria. Briefly, 10.9 % for *S. aureus*, 9.4 % for *E. faecalis,* 12.5 % for *E. faecalis* and 7.8 % for *P. aeruginosa*.

### 4.3.3 Time dependent activity of through time-kill assay

Time-dependent assay was carried out against 24 h-, 48 h- and 72 h-biofilm cells of *S. aureus*, *E. faecalis*, *E. coli* and *P. aeruginosa* using a fixed concentration of GO at 100 µg/mL. These time-dependant assays were performed with an interval period of 3 h, 6 h, 12 h and 24 h for all biofilm of 24 h, 48 h and 72 h maturity period. The results indicated that the viability percentage of 24 h-, 48 h- and 72 h-biofilm cells of all bacteria increased consistently with longer GO treatment period as shown in Figure 4.15. Briefly, the viability of 24 h-biofilm cells of *S. aureus* when treated for a time period of 3 h was 70.2 % and this value increased to 408.2 % when the GO treatment time was extended to 24 h. Similarly, the viability of 48 h-biofilm cells of *E. faecalis* when treated with GO for 3 h was 22.2 % and this value increased to 146.1 % when they were treated with GO for 24 h.

Although increase in the percentage of viability was noted for all biofilm cells with increasing exposure time, however differences in the rate of increase among the bacteria were observed too. Biofilm cells of *S. aureus* were able to continue to produce more biofilm in the presence of GO with increasing exposure time compared to biofilm cells of other bacteria.

24 h-biofilm cells of *P. aeruginosa* was only able to increase the formation of biofilm from 3.8 % (3 h exposure to GO) to 31.2 % (24 h exposure to GO) only. Therefore, the mass of biofilm increased with time of exposure for all bacteria when the biofilm cells were exposed to GO for longer exposure time.

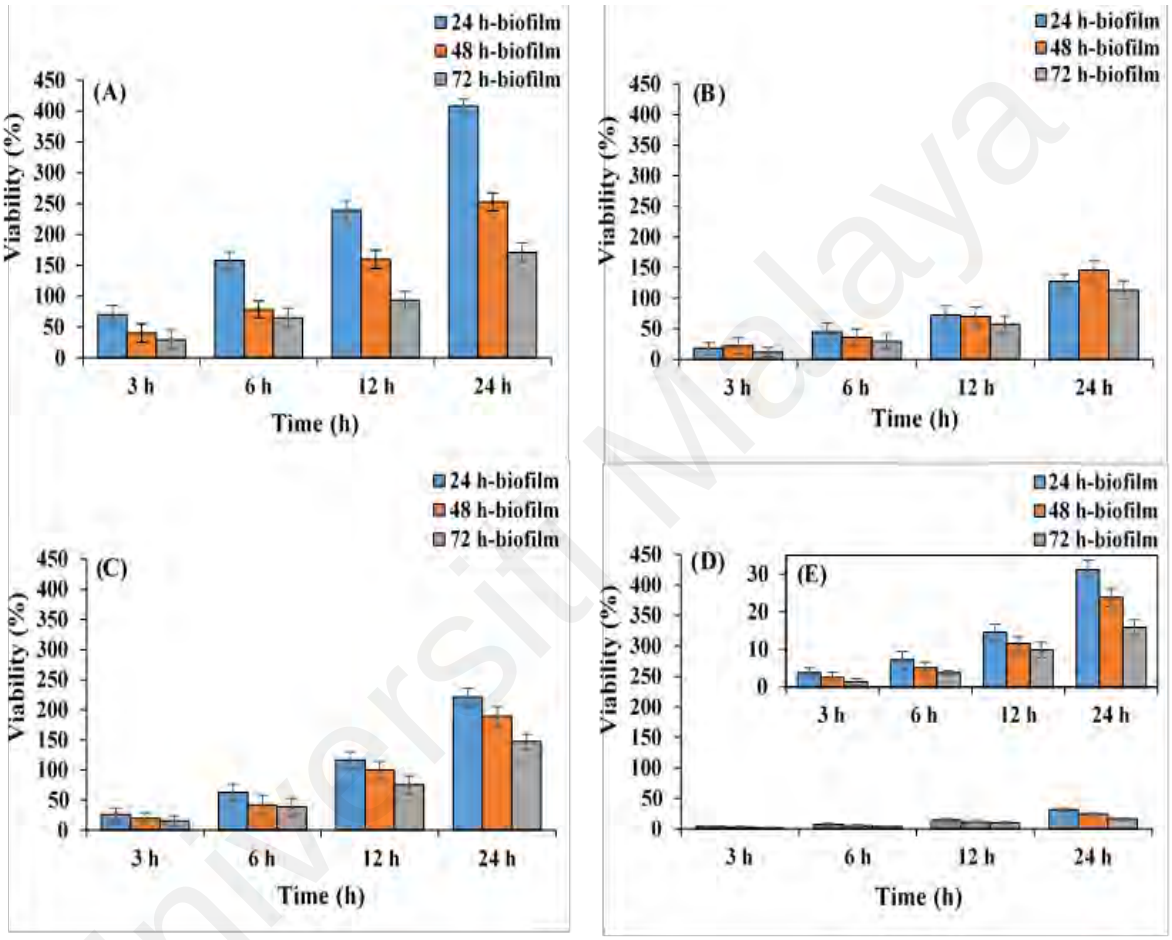


**Figure 4.15:** Time dependent assay of biofilm cells of *S. aureus* (A), *E. faecalis* (B), *E. coli* (C) and *P. aeruginosa* (D) and (E) magnified chart of *P. aeruginosa*) upon exposure to GO for selected time periods (3 h, 6 h, 12 h and 24 h). Longer incubation time improves the viability of the biofilm cells.

## 4.4 Interactions between graphene oxide and antibiotics at molecular level

### 4.4.1 ATR-FTIR characterizations

ATR-FTIR were conducted to analyse the interaction between GO and the antibiotics. The molecular changes on the GO loaded antibiotics, bare GO and antibiotic alone were analysed using ATR-FTIR as shown in Figure 4.16. Figure 4.16(a) showed that the ATR-FTIR spectra of free ampicillin, bare GO and GO loaded with ampicillin in the whole spectral range of 4000-400 $cm^{-1}$. In the spectrum of ampicillin, the peak 1762 $cm^{-1}$ and 1690 $cm^{-1}$ were attributed to the -C=O of the β-lactam ring and the amide carbonyl group respectively (Nairi, Medda, Monduzzi, & Salis, 2017). The asymmetric stretching of -COOH was as observed at 1398 $cm^{-1}$. The peak at 1520 $cm^{-1}$ can be assigned to the $-NH_2$ bending vibration (Bravo & Anacona, 1998). The peak observed at 3219 $cm^{-1}$ could be ascribed to the carboxyl O-H stretching vibration mode. This peak seemed to have broadened since it overlapped with absorption peaks which corresponded to O-H stretching in the presence of absorbed water molecules and alcohol groups.

The peak at 1616 $cm^{-1}$ was associated with C=C from $sp^2$ hybrid domain. The bands at 1397 $cm^{-1}$ and 1053 $cm^{-1}$ corresponded to C-OH and C-O stretching vibrations respectively. The peaks that occurred in the spectrum of the bare GO and free ampicillin have also occurred in the ATR-FTIR spectrum of GO loaded ampicillin sample. However, some of the peaks in the range of 1800-1300 $cm^{-1}$ were embedded within the broad bands of GO. For instance, a week signal at 1398 $cm^{-1}$ (asymmetric stretching of –COOH) in the ampicillin spectrum have also occurred in the ATR-FTIR spectrum of GO and GO loaded ampicillin sample.

The ATR-FTIR spectra of free chloramphenicol, bare GO and GO loaded with chloramphenicol are shown in Figure 4.16(b). The ATR-FTIR spectrum of free chloramphenicol showed a peak at 2970 $cm^{-1}$ that was assigned to aromatic C-H stretching. The vibrational peaks at 1684 and 1551 $cm^{-1}$ were attributed to C=O and N-O stretching respectively (Trivedi et al., 2015). Additionally, the C-Cl stretching was observed at 631 $cm^{-1}$ (Trivedi et al., 2015). A medium signal at 879 $cm^{-1}$ has appeared due to the stretching of C-N bond (out of plane NH-bending) (Karthikeyan, 2013). The ATR-FTIR spectrum of GO treated with chloramphenicol showed broad absorption peaks at ~ 3270 $cm^{-1}$ which is considered due to the presence of O-H and N-H stretching vibrations. The peaks that appeared at 1684 $cm^{-1}$ and 1551 $cm^{-1}$ were observed in similar frequency region in GO loaded chloramphenicol, however these peaks overlapped with GO functional group and have appeared as an intense peak. Figure 4.16(c) showed the ATR-FTIR spectra of free tetracycline, bare GO and GO loaded with tetracycline. The ATR-FTIR spectrum of free tetracycline showed only two major bands at 891 $cm^{-1}$ and 764 $cm^{-1}$ which were assigned to C-N stretching and C-C stretching or aromatic C-H out-of-plane bending respectively. The ATR-FTIR spectrum of GO loaded tetracycline showed that the absorption peaks for N-H and O-H stretching were at 3308 $cm^{-1}$.

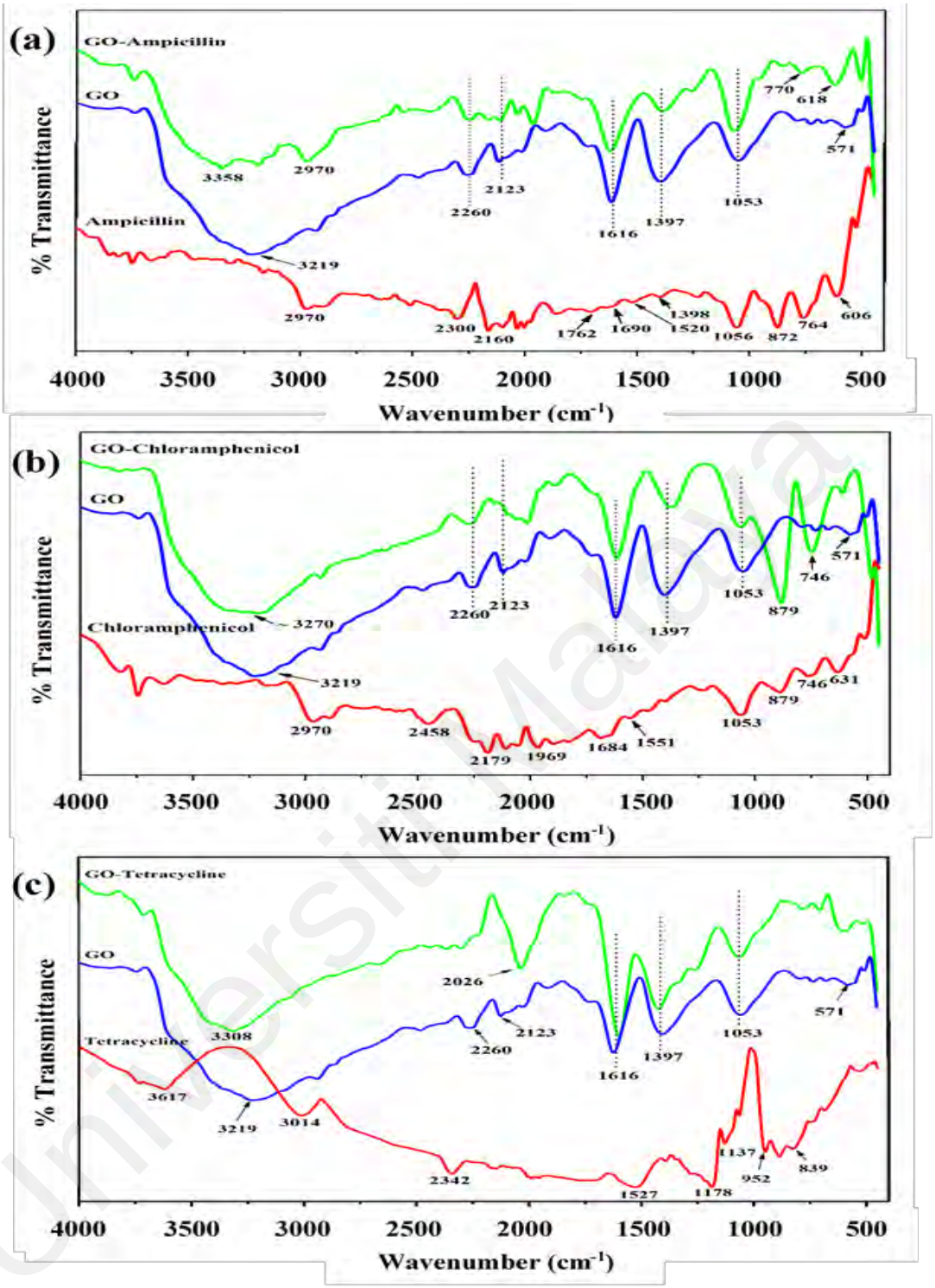


**Figure 4.16:** Spectra of antibiotics, GO and antibiotics loaded GO as determined by ATR-FTIR (a) ATR-FTIR spectrum of ampicillin, GO and ampicillin loaded GO; (b) ATR-FTIR spectrum of chloramphenicol, GO and chloramphenicol loaded GO; (c) ATR-FTIR spectrum of tetracycline, GO and tetracycline loaded GO. Green line indicates spectra of antibiotic loaded GO, blue line indicates the spectra of free GO and the red line indicates spectra of respective antibiotic.

### 4.4.2 UV-VIS characterizations

The UV-Vis spectra of the GO, antibiotics and treated samples of antibiotics are shown in Figure 4.17. In all the spectrum the GO show peaks at 240 nm and 290 nm which are attributed to the standard absorbance bands of GO due to the $\pi$ - $\pi^*$ plasmon and n - $\pi^*$ transitions respectively. Figure 4.17(a) shows the free ampicillin together with treated ampicillin with GO. Since ampicillin is colourless, it has no absorption in the range of 250-500 nm, thus it appears at $\lambda_{max}$ = 207 nm (Xu, Wang, & Xiao, 2004). There are slight changes in $\lambda_{max}$ as compared to control, which indicated that the functional groups had been altered and the result has well corroborated with the ATR-FTIR results.

Figure 4.17(b) showed that the spectral measurements were carried out on chloramphenicol and GO treated chloramphenicol. The peak showed that there were no substantial changes in the lambda max ($\lambda_{max}$) of the treated sample as compared to the free chloramphenicol (275 nm). However, the intensity of the absorbance values has been changed, indicated that there were slight changes in the chromophore of the chloramphenicol group after the treatment process. The UV-Vis of the free tetracycline and treated sample of tetracycline are as shown in Figure 4.17(c). Both the spectra showed three similar pattern of UV absorbance at 357 nm, 275 nm and 216 nm which indicated no changes in the chromophore group (Trivedi et al., 2015).

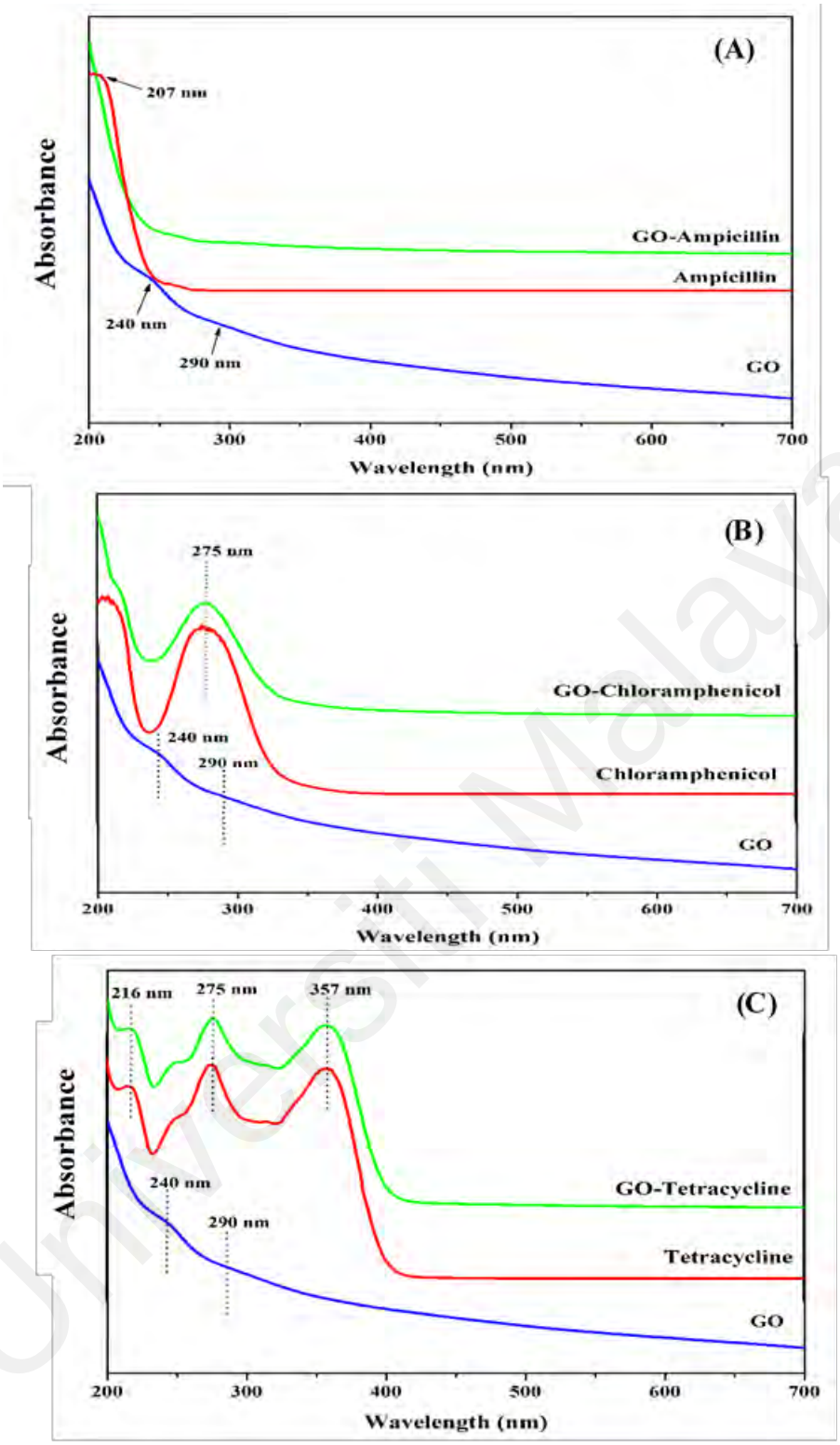


**Figure 4.17:** UV-Vis spectra of antibiotics, GO and antibiotics loaded GO (a) UV-Vis spectrum of ampicillin, GO and ampicillin loaded GO; (b) UV-Vis spectrum of chloramphenicol, GO and chloramphenicol loaded GO; (c) UV-Vis spectrum of tetracycline, GO and tetracycline loaded GO. Green line indicates spectra of antibiotic loaded GO, red line indicates the spectra of respective antibiotic and the blue line indicates spectra of free GO.

## 4.5 Synergistic behaviour of GO with selected antibiotics against Gram-positive and Gram-negative bacteria in suspension

The use of GO as an adjuvant in combination with broad-spectrum antibiotics have been explored in this study. *S. aureus*, *E. faecalis*, *E. coli* and *P. aeruginosa* have been treated with ampicillin, chloramphenicol and tetracycline in combination with GO. Increasing concentrations of antibiotics (1 - 10 µg/mL) in combination with GO (10 µg/mL) were tested for ampicillin, chloramphenicol and tetracycline against both the Gram-positive and Gram-negative bacteria.

Figures 4.18, 4.19 and 4.20 illustrate the increase in the antibacterial action of antibiotic + GO compared to antibiotic alone or GO only for all the tested bacteria. Use of ampicillin alone at 10 µg/mL to treat *S. aureus*, *E. faecalis*, *E. coli* and *P. aeruginosa* were measured to have significantly lower log-reduction values compared to combined treatment of 10 µg/mL of GO and 10 µg/mL of ampicillin. A 5.07 log-reduction value was noted for 10 µg/mL of ampicillin when exposed to *S. aureus* compared to 6.26 log reduction value when treated with a combination of ampicillin and GO (10 µg/mL each). Similarly, higher log-reduction values for *E. faecalis*, *E. coli* and *P. aeruginosa* were observed when treated with combined GO and ampicillin treatment compared to ampicillin or GO alone.

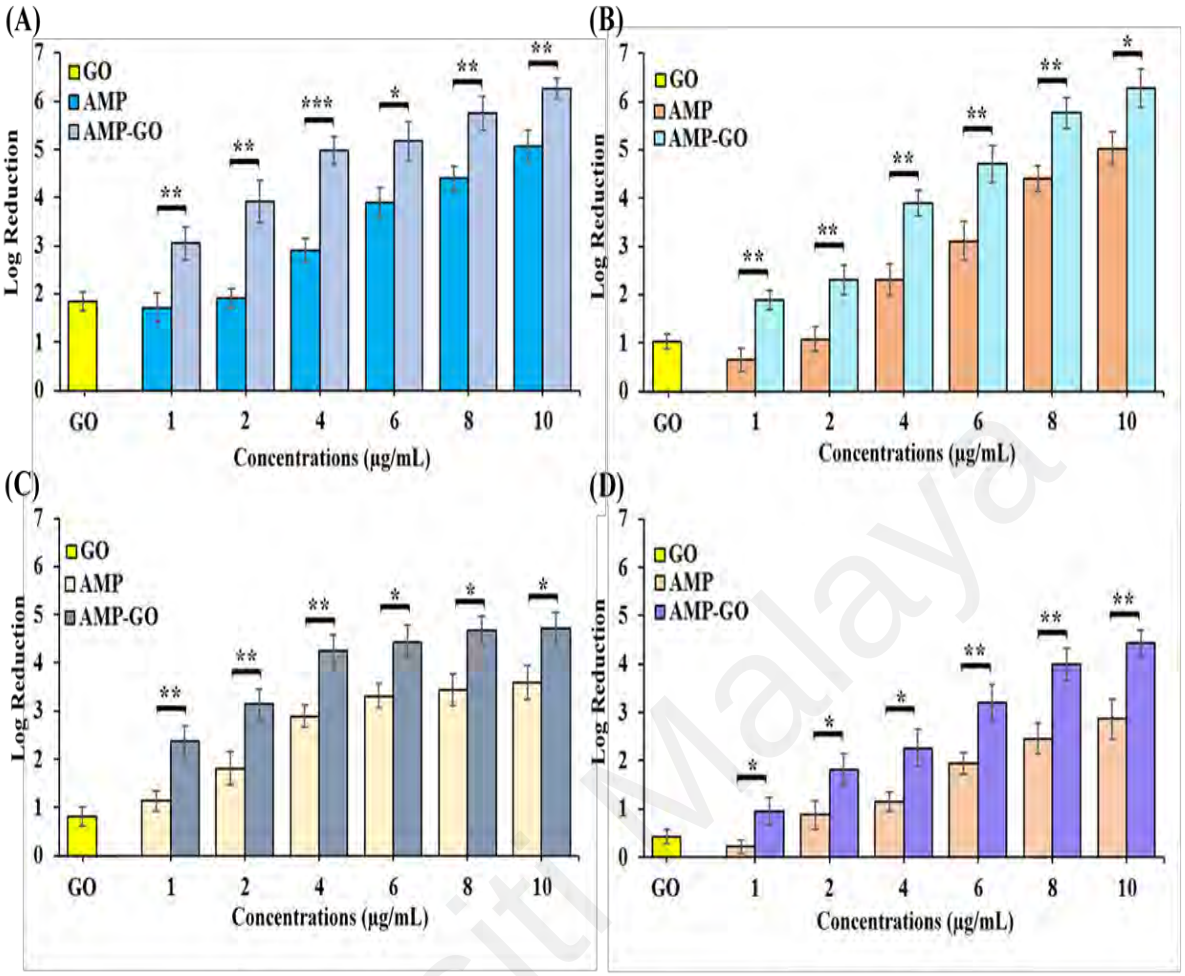


**Figure 4.18:** Log reduction graph of *S. aureus* (A), *E. faecalis* (B), *E. coli* (C) and *P. aeruginosa* (D) after treatment with GO (10 µg/mL), ampicillin (AMP) and ampicillin-GO (AMP-GO). Data shown as mean ± SD *$p \leq 0.05$, **$p \leq 0.01$, ***$p \leq 0.001$ compared to cells treated with antibiotics only.

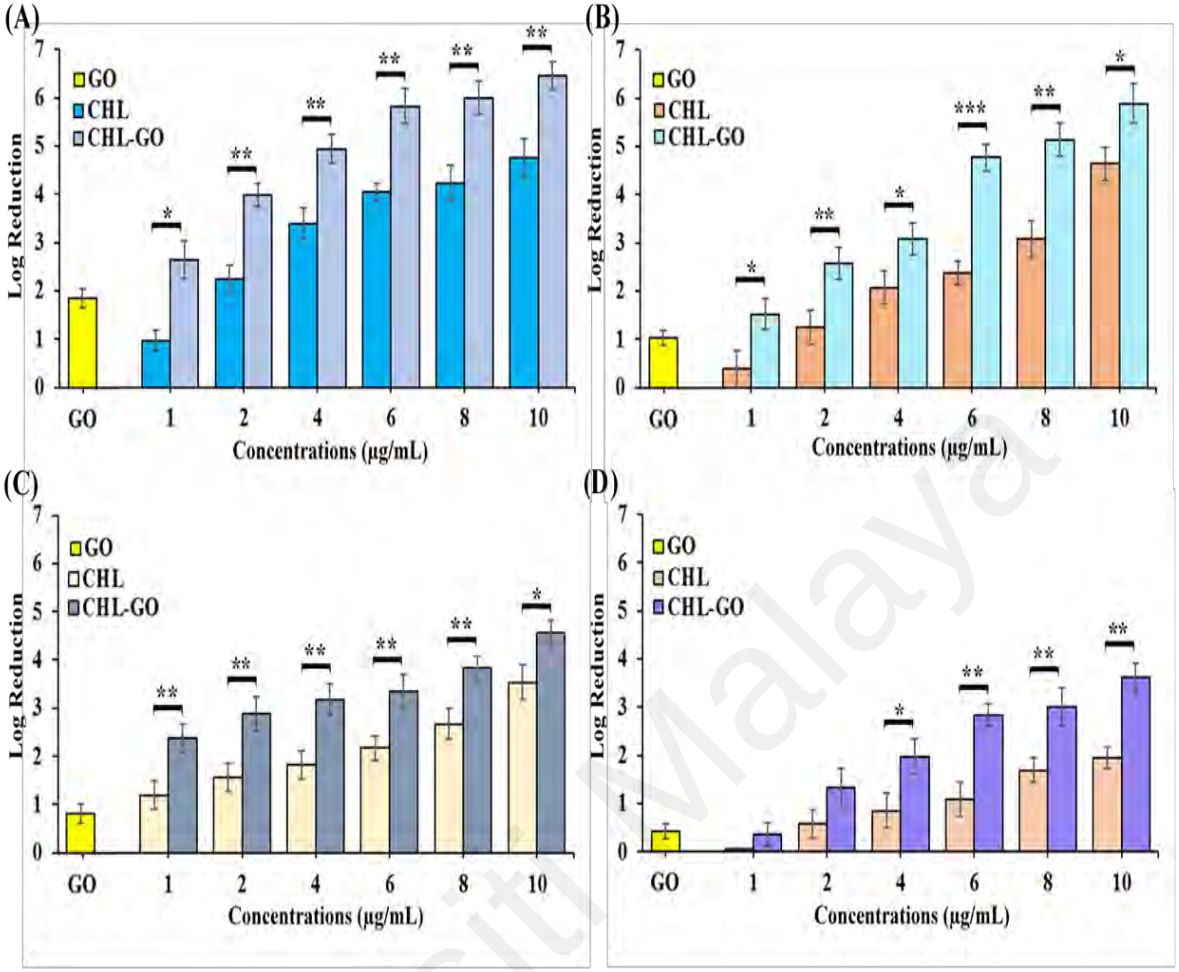


**Figure 4.19:** Log reduction graph of *S. aureus* (A), *E. faecalis* (B), *E. coli* (C) and *P. aeruginosa* (D) after treatment with GO (10 µg/mL), chloramphenicol (CHL) and chloramphenicol-GO (CHL-GO). Data shown as mean ± SD *p ≤ 0.05, **p ≤ 0.01, ***p ≤ 0.001 compared to cells treated with antibiotics only

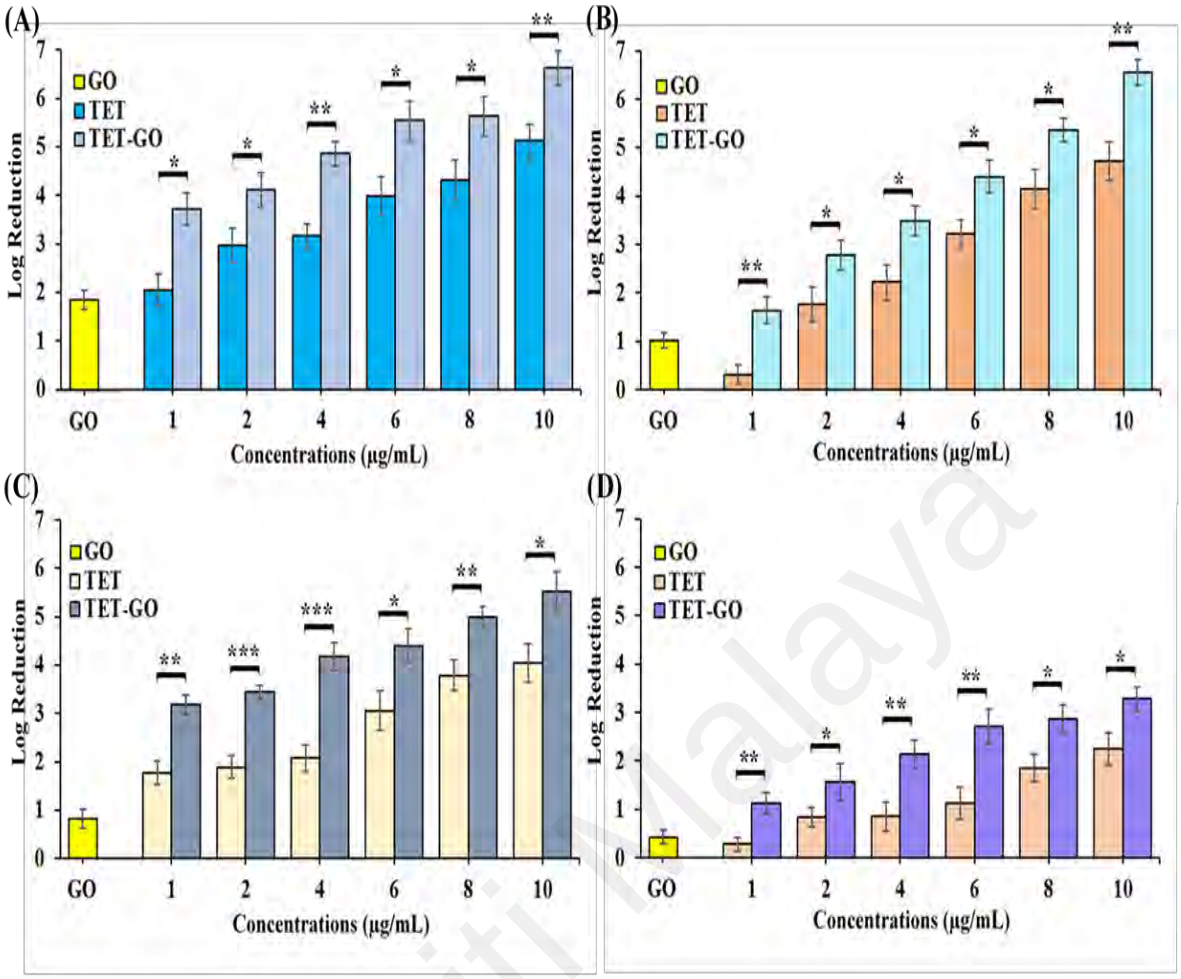


**Figure 4.20:** Log reduction graph of *S. aureus* (A), *E. faecalis* (B), *E. coli* (C) and *P. aeruginosa* (D) after treatment with GO (10 µg/mL), tetracycline (TET) and tetracycline-GO (TET-GO). Data shown as mean ± SD *p ≤ 0.05, **p ≤ 0.01, ***p ≤ 0.001 compared to cells treated with antibiotics only.

A 10 µg/mL of chloramphenicol was used to treat *S. aureus*, *E. faecalis*, *E. coli* and *P. aeruginosa*, it was found that the log-reduction values of chloramphenicol alone were lower compared to treatment with a combination of 10 µg/mL of GO and 10 µg/mL of chloramphenicol. Combined treatment of GO and chloramphenicol at 10 µg/mL each, was observed to be log-reduction value of 6.45 compared to 4.75 (10 µg/mL of chloramphenicol alone). A similar observation was noted for *E. faecalis*, *E. coli* and *P. aeruginosa* as shown in Figure 4.19.

Combined treatment of 10 µg/mL of tetracycline and 10 µg/mL of GO towards *S. aureus*, *E. faecalis*, *E. coli* and *P. aeruginosa* were also observed to have significantly higher log-reduction values compared to treatment with 10 µg/mL of tetracycline alone. Briefly, a 5.12 log-reduction value was measured for *S. aureus* when treated with 10 µg/mL of tetracycline compared to a log-reduction value was 6.63 for combined treatment of tetracycline and GO at 10 µg/mL each. A similar observation was noted for *E. faecalis, E. coli* and *P. aeruginosa* too as depicted in Figure 4.20.

Nevertheless, significant log-reduction values too have been noted for almost all combinations of GO and antibiotics ($p < 0.05$) which indicates synergistic antibacterial effects of GO and antibiotics among the 4 bacterial species. On the contrary, non-significant differences between antibiotic treatment and combined antibiotic treatment of antibiotic and GO were observed for combinations of 10 µg/mL of GO with 1 µg/mL of chloramphenicol and 10 µg/mL of GO with 2 µg/mL of chloramphenicol during the treatment of *P. aeruginosa* only.

Additionally, it was also observed that the antibacterial action of GO + antibiotics worked better among the Gram-positive bacteria (*S. aureus* and *E. faecalis*) as compared to the Gram-negative bacteria (*E. coli* and *P. aeruginosa*) as indicated in Figures 4.18, 4.19 and 4.20. Log-reduction values of *S. aureus* and *E. faecalis* when treated with a combination of ampicillin and GO (10 µg/mL each) were 6.26 and 6.28, respectively compared to 4.72 and 4.44 for *E. coli* and *P. aeruginosa*, respectively. Similar observations were also observed among the log-reduction values of *S. aureus*, *E. faecalis, E. coli* and *P. aeruginosa* when treated with combinations of GO and chloramphenicol/tetracycline (all GO + antibiotic combinations).

## 4.6 Synergistic behaviour of GO with selected antibiotics against Gram-positive and Gram-negative bacteria in biofilm

The use of GO as an adjuvant in combination with broad-spectrum antibiotics has been explored in this study against the 24, 48 and 72 h-biofilm cells of *S. aureus*, *E. faecalis*, *E. coli* and *P. aeruginosa*. Biofilm cells of these bacteria were treated with ampicillin, chloramphenicol and tetracycline in combination with GO. Increasing concentrations of antibiotics (2 - 10 µg/mL) in combination with a fixed concentration of GO (100 µg/mL) were tested for ampicillin, chloramphenicol and tetracycline against both the Gram-positive and Gram-negative bacteria.

It was observed that the activity of GO + antibiotic combinations seemed to be hindered when in contact with 24 h-, 48 h- and 72 h-biofilm cells as shown in Figures 4.21, 4.22 and 4.23. GO was found to be an antibiotic adjuvant when tested against the bacterial cells in suspension, however, the use of GO with antibiotic against the biofilm cells was found to be obstructing the antibacterial activity of the antibiotics tested. This observation was based on the constant increase noted among the absorbance values of the GO + antibiotic treated biofilm cells of all bacteria compared to treatment with antibiotics alone as shown in Figure 4.21, 4.22 and 4.23. Increase in absorbance value indicates increase in the concentration of bacteria present in the tested reaction medium. For an instance, the absorbance value of 24 h-biofilm cells of *S. aureus* when treated with 10 µg/mL of ampicillin was 0.5 and this value increased to 3.3 when treated with a combination of 10 µg/mL of ampicillin and 100 µg/mL of GO.

Although the absorbance values of biofilm cells treated with combinations of antibiotics and GO increased for all bacteria regardless of the antibiotic used and biofilm maturity, the increase observed among the 24 h-, 48 h- and 72 h-biofilm cells of *E. coli* was lower compared to other biofilm cells.

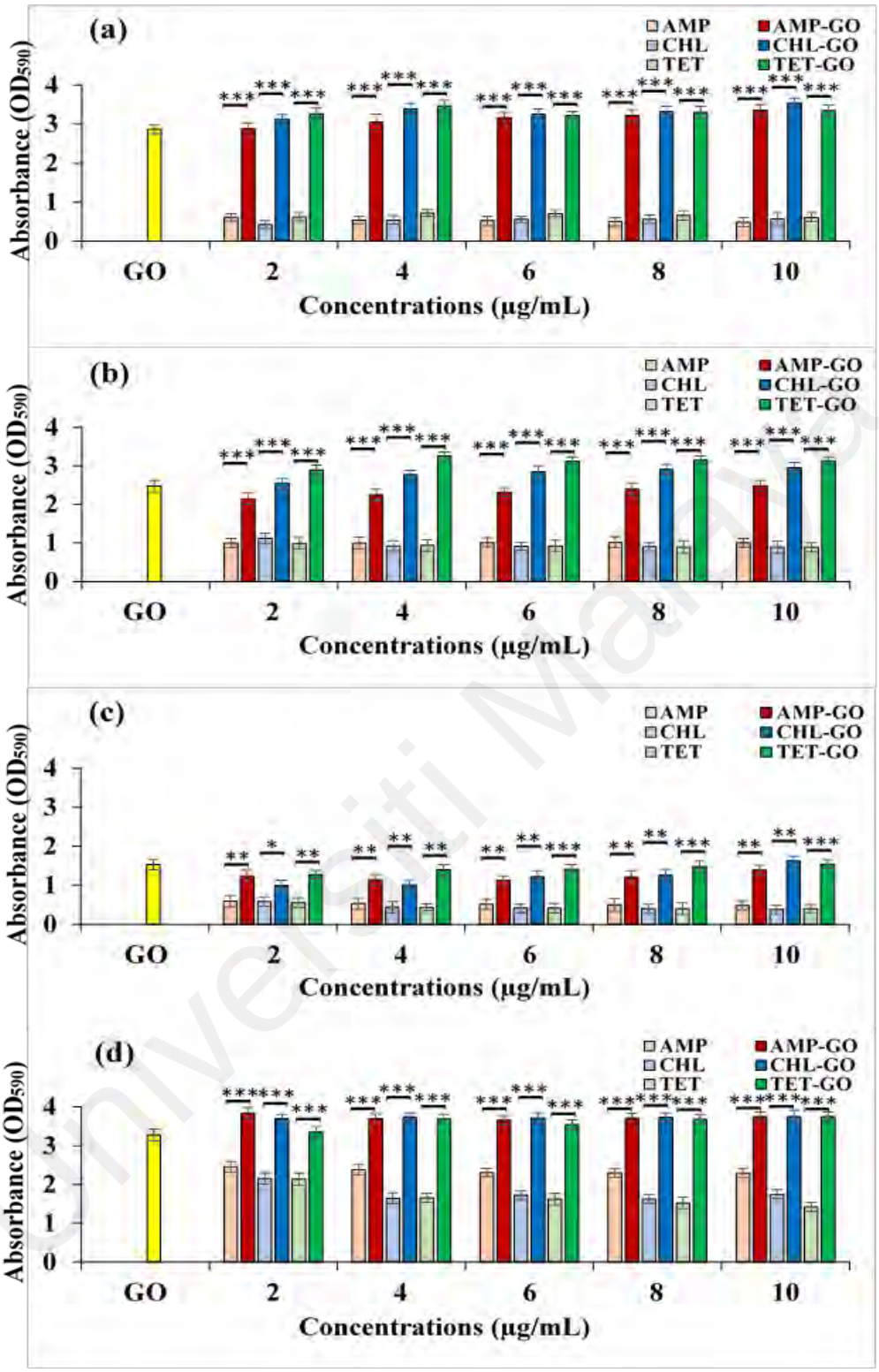


**Figure 4.21:** Viability graph of the 24 h-biofilm cells of *S. aureus* (a), *E. faecalis* (b), *E. coli* (c) and *P. aeruginosa* (d) after treatment with GO (100 µg/mL); ampicillin (AMP) and ampicillin-GO (AMP-GO), chloramphenicol (CHL) and chloramphenicol-GO (CHL-GO) and tetracycline (TET) and tetracycline-GO (TET-GO). Data shown as mean ± SD *$p \leq 0.05$, **$p \leq 0.01$, ***$p \leq 0.001$ compared to cells treated with antibiotics only.

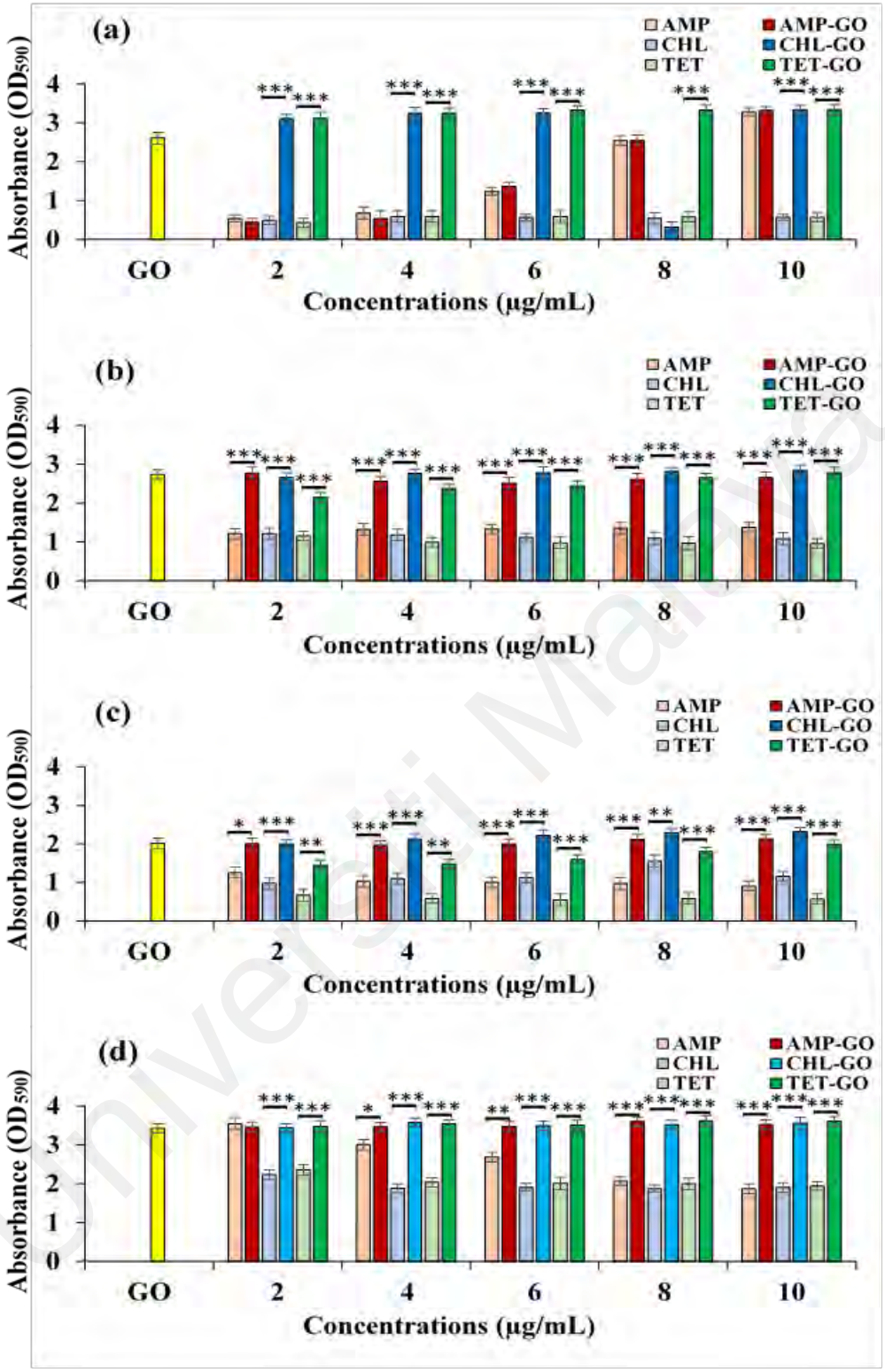


**Figure 4.22:** Viability graph of the 48 h-biofilm cells of *S. aureus* (a), *E. faecalis* (b), *E. coli* (c) and *P. aeruginosa* (d) after treatment with GO (100 µg/mL); ampicillin (AMP) and ampicillin-GO (AMP-GO), chloramphenicol (CHL) and chloramphenicol-GO (CHL-GO) and tetracycline (TET) and tetracycline-GO (TET-GO). Data shown as mean ± SD *$p \leq 0.05$, **$p \leq 0.01$, ***$p \leq 0.001$ compared to cells treated with antibiotics only.

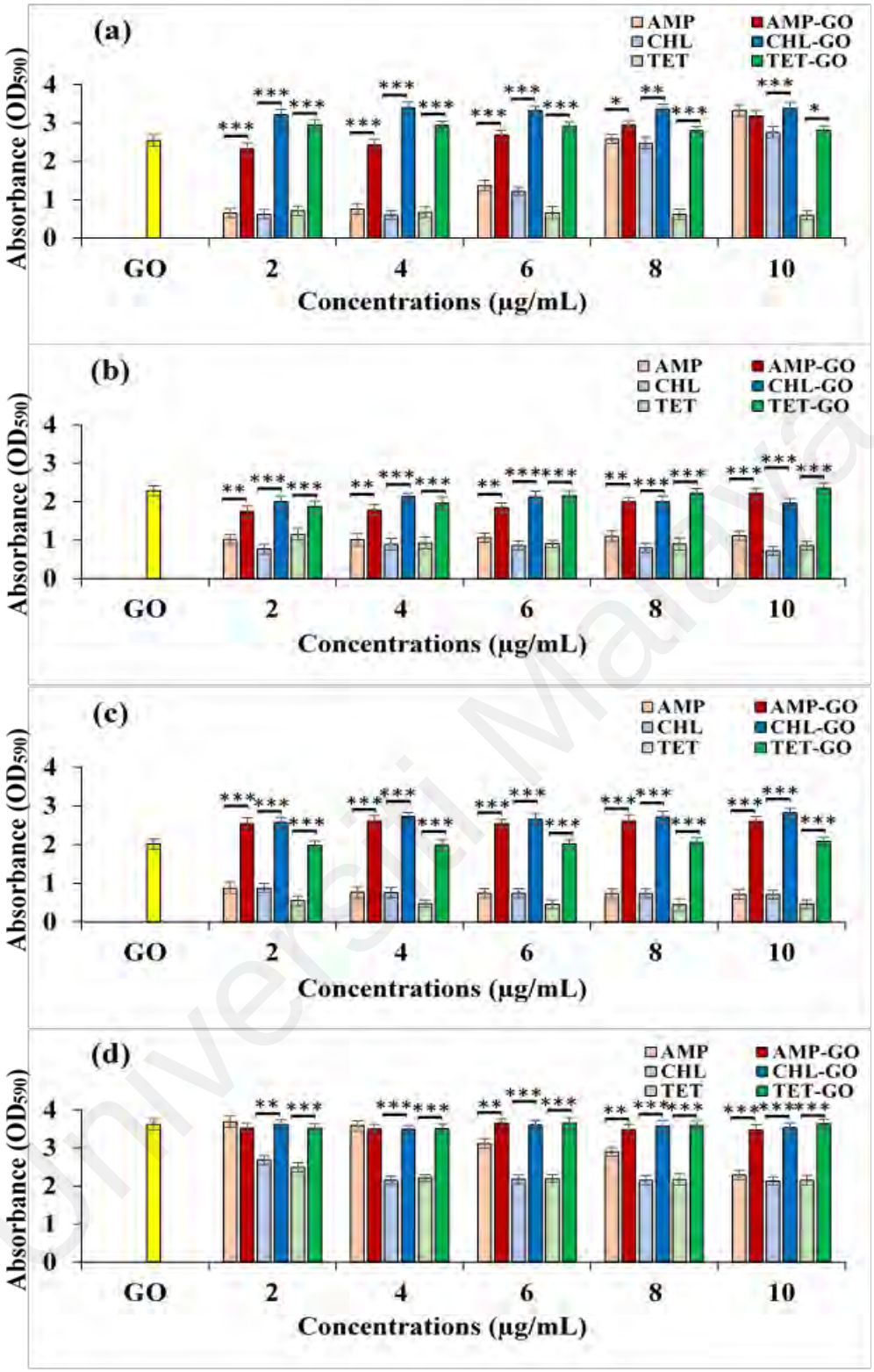


**Figure 4.23:** Viability graph of the 72 h-biofilm cells of *S. aureus* (a), *E. faecalis* (b), *E. coli* (c) and *P. aeruginosa* (d) after treatment with GO (100 µg/mL); ampicillin (AMP) and ampicillin-GO (AMP-GO), chloramphenicol (CHL) and chloramphenicol-GO (CHL-GO) and tetracycline (TET) and tetracycline-GO (TET-GO). Data shown as mean ± SD *$p \leq 0.05$, **$p \leq 0.01$, ***$p \leq 0.001$ compared to cells treated with antibiotics only.

Briefly, the absorbance value for 24 h-biofilm cells treated with 10 µg/mL of ampicillin was 0.5 while the absorbance value for combined treatment of 10 µg/mL of ampicillin and 100 µg/mL of GO was 1.4 only. This trend was observed for 24 h- and 48 h-biofilm cells of *E. coli* only.

As shown in Figure 4.21, 4.22 and 4.23, the absorbance values of biofilm cells of *S. aureus*, *E. faecalis*, *E. coli* and *P. aeruginosa* were observed to be higher when treated with combinations of antibiotics and GO compared to treatment with antibiotics alone. Briefly, the absorbance value measured for 48 h-biofilm cells of *E. faecalis* when treated with 10 µg/mL of tetracycline and 100 µg/mL of GO was 2.8 while the absorbance value for treatment with 10 µg/mL of tetracycline alone was only 1.0. This similar trend was noted for all other biofilm cells regardless of the biofilm maturity, type of bacteria and type of antibiotic. This indicated that combinatorial therapy for the treatment of biofilm cells was not effective in reducing the formation of biofilm cells.

Moreover, the activity of GO + antibiotic treatment for the biofilm cells was found to be similar to the activity of GO alone in respect to the maturity of the biofilm and bacterial strain. The absorbance value for GO alone when treated against 48 h-biofilm cells of *P. aeruginosa* was 3.4 while the absorbance value for treatment with combination of 10 µg/mL of tetracycline and 100 µg/mL of GO was 3.6. This trend was also noted to be similar with other biofilm cells regardless of bacteria, type of antibiotic and biofilm maturity.

## 4.7 Toxicological effects of graphene oxide against human epidermal keratinocytes

### 4.7.1 MTT viability assay

Since GO enhanced the antibacterial activity of antibiotics, it is interesting to explore the nanosafety of GO for biomedical applications. Here, the cytotoxicity of GO towards HaCaT cell line using MTT cytotoxicity assay has been studied. HaCaT cell line was used in this work mainly as it is a representative cell line for cutaneous toxicity-based studies (Crosera et al., 2015; Li et al., 2016). The HaCaT cells wells were treated with various concentrations of GO ranging from 5 to 1000 µg/mL for 24 h. No significant changes in the viability of the HaCaT cells were observed for lower concentrations of GO (<100 µg/mL) compared to the untreated HaCaT cells as shown in Figure 4.24.

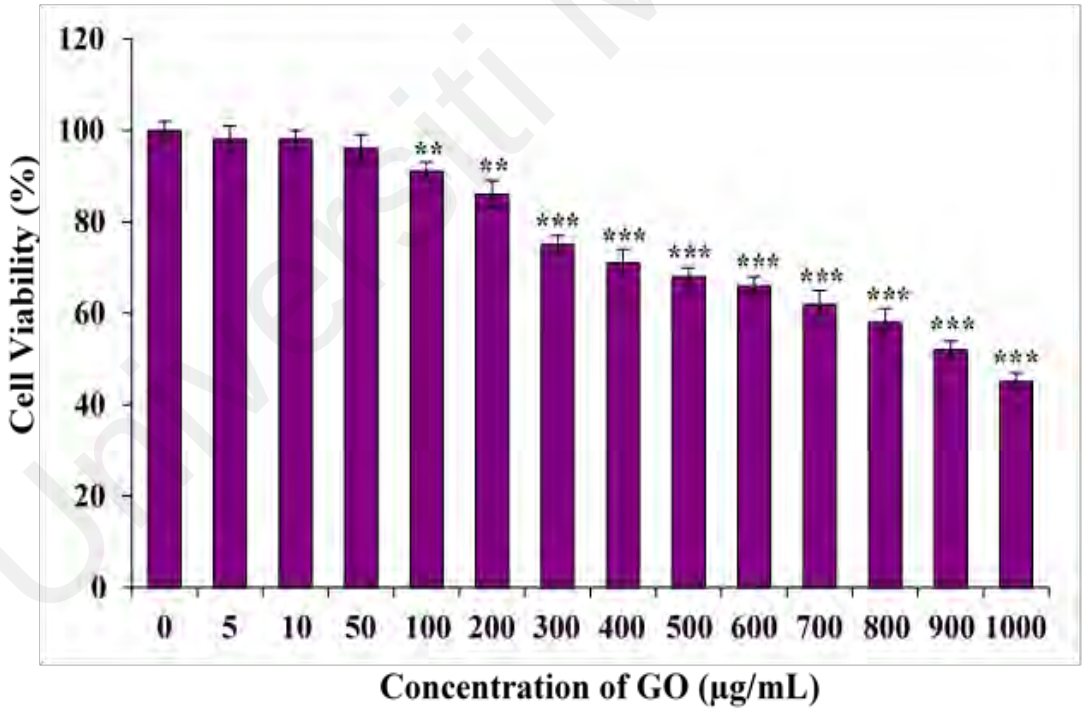


**Figure 4.24:** MTT cytotoxicity assay of GO towards HaCaT cell line. Viability of the HaCaT cells was significantly affected from GO concentration of 100 µg/mL onwards. Data shown as mean ± SD *p ≤ 0.05, **p ≤ 0.01, ***p ≤ 0.001 compared to untreated cells.

A 98 % of cell viability was noted for GO concentrations of 5 and 10 µg/mL while 96 % of cell viability was observed for 50 µg/mL of GO. Subsequent GO concentrations were observed to significantly reduce HaCaT cell viability. Hundred µg/mL of GO was noted to decrease cell viability to 91 % while 500 µg/mL of GO was noted to decrease cell viability to 68 %. A 50% of decrease in cell viability was only noted at GO concentration of 900 µg/mL. Therefore, the half-maximal inhibitory concentration ($IC_{50}$) of GO towards HaCaT cells was measured at 900 µg/mL. The highest concentration of GO tested against HaCaT cells at 1000 µg/mL was noted to reduce the cell viability up to 45 % as observed in Figure 4.24.

### 4.7.2 Generation of reactive oxygen species

Additionally, to investigate the ability of GO in inducing oxidative stress among the HaCaT cells, the generation of ROS was measured among the HaCaT cells upon exposure to this nanomaterial. This is because ROS is an indication of cell damage and the amount of ROS correlate with the increase in cell death. Specific ROS amount that was produced was detected using DCFH-DA fluorescence assay. Relative frequency unit (RFU) of the untreated HaCaT cells were fixed at RFU. The HaCaT cells wells were treated with various concentrations of GO ranging from 5 to 1000 µg/mL for 2 h.

No significant changes in the RFU were observed for GO concentrations of 5, 10 and 50 µg/mL compared to the untreated HaCaT cells. As depicted in Figure 4.25, GO significantly increased generation of ROS from concentration of 100 to 1000 µg/mL after 2 h of exposure period. Briefly, at GO concentration of 900 µg/mL, which was the $IC_{50}$ of GO against HaCaT cells, RFU measured was at 708, 7-fold higher than the untreated HaCaT cells. At GO concentration of 100 µg/mL, RFU was observed to be at 179, while RFU was noted to 550 at 500 µg/mL of GO.

Finally, the maximum GO concentration of 1000 µg/mL was observed to record a RFU value of 796 when exposed to the HaCaT cells.

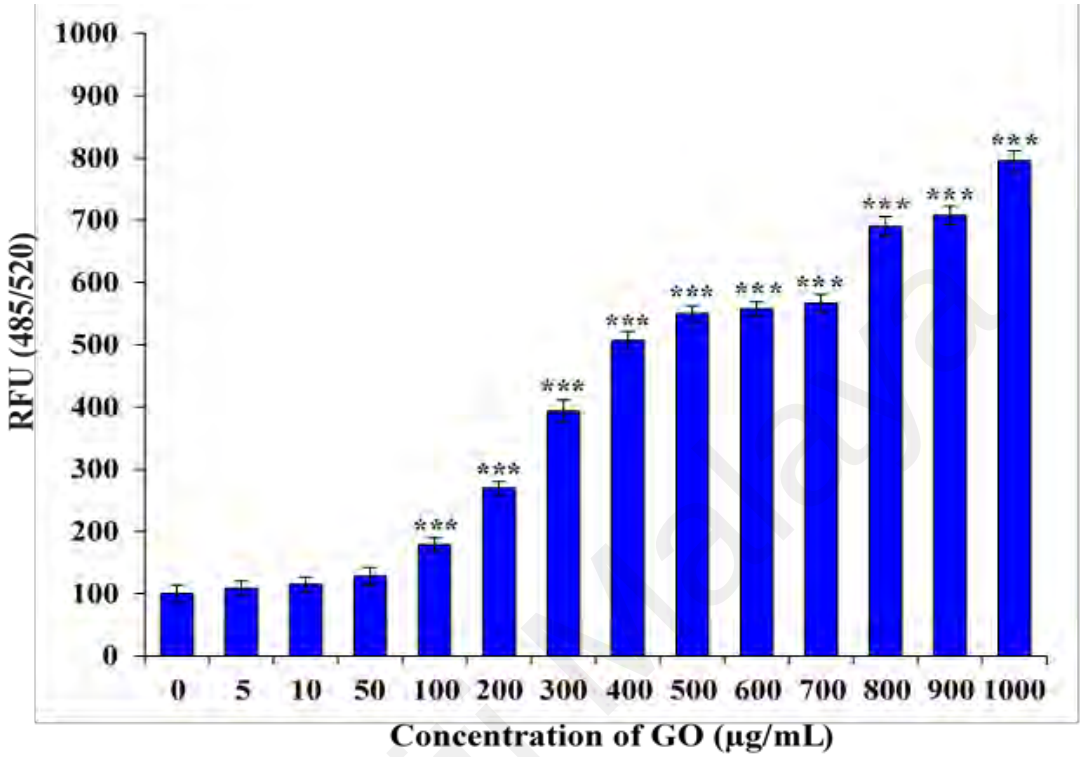


**Figure 4.25:** ROS generation assay of GO towards HaCaT cell line. Generation of ROS was observed to significantly increase according to GO concentration of 100 µg/mL onwards. Data shown as mean ± SD *p ≤ 0.05, **p ≤ 0.01, ***p ≤ 0.001 compared to untreated cells.

### 4.7.3 Membrane integrity analysis

The integrity of the HaCaT cell membrane was investigated by measuring the concentration of LDH enzyme in the cell medium after GO exposure. The HaCaT cells wells were treated with various concentrations of GO ranging from 5 to 1000 µg/mL for 24 h. It was found that the concentration of LDH detected in the cell culture medium increases with the rise in the concentration of GO that was exposed to the HaCaT cells.

Similar to the MTT viability assay and generation of ROS assay, it was found that significant cytotoxic effect was only noted for GO concentrations higher than 100 µg/mL as shown in Figure 4.26.

GO concentrations of 5, 10 and 50 µg/mL was noted to induce LDH cytotoxicity at 4%, 4 % and 6 %, respectively. Concentrations of GO from 5 to 50 µg/mL did not induce significant production of LDH enzyme into the HaCaT cell culture medium. Significant toxicity of GO towards the HaCaT was only noted at GO concentration of 100 µg/mL and the LDH cytotoxicity level was at 9%. Meanwhile, at GO concentration of 900 µg/mL, which was the $IC_{50}$ of GO against HaCaT cells, LDH cytotoxicity was 42%. Only 49% of LDH cytotoxicity effect was noted for the highest tested GO concentration of 1000 µg/mL.

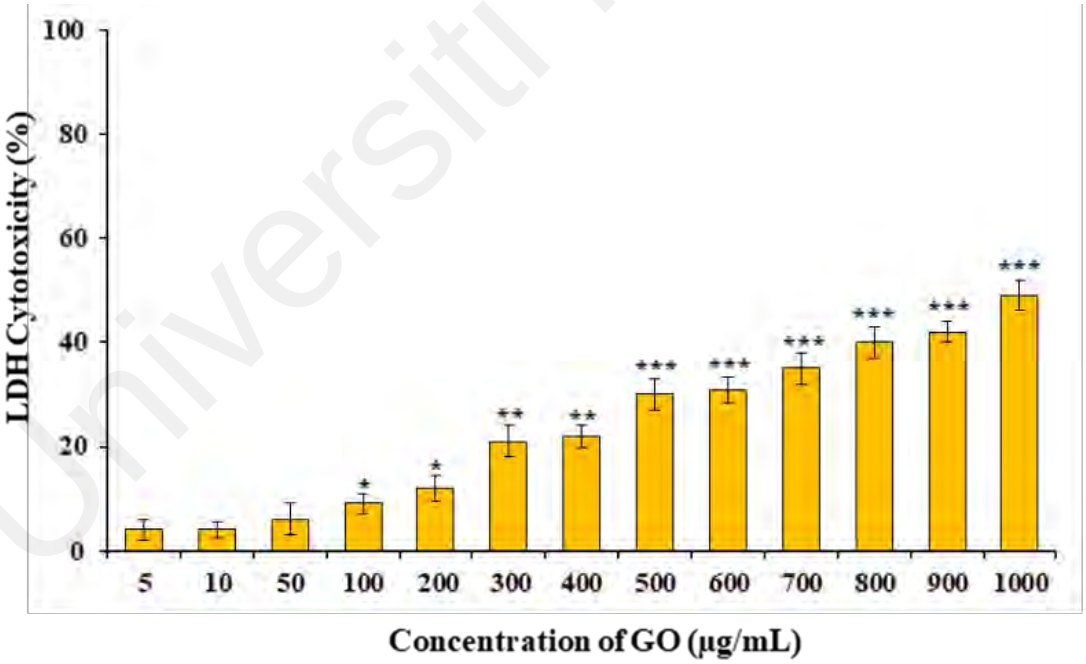


**Figure 4.26:** LDH cytotoxicity assay of GO towards HaCaT cell line. LDH leakage assay determines cell membrane integrity once exposed to GO. Data shown as mean ± SD *p ≤ 0.05, **p ≤ 0.01, ***p ≤ 0.001 compared to untreated cells.

### 4.7.4 Cell surface morphology analysis

Membrane integrity of HaCaT cells was observed through the FESEM characterization technique after treatment with GO concentration of 100 and 200 µg/mL. Figure 4.27 (A) clearly showed the intact cells of HaCaT cell line with a clear presence of microvilli structures surrounding the individual cells. However, the appearance of GO treated HaCaT cells goes through some changes when treated with 100 µg/mL of GO. The microvilli structures were observed to be reduced and some cells were noted to be partially covered by GO sheets as shown in Figure 4.27 (B). No apparent damage was noted on the membrane integrity of HaCaT cells when treated with GO concentration of 100 µg/mL.

Additionally, Figure 4.27 (C) showed the appearance of the HaCaT cell after exposure to 200 µg/mL of GO. Compared to untreated HaCaT cells, these cells appear to have suffered membrane damage compared to the untreated HaCaT cells. The HaCaT cell appeared to have distorted shape along with disoriented microvilli structure surrounding the HaCaT cell. The external microvilli structure too appears to have reduced compared to the untreated HaCaT cells. Moreover, GO sheets were observed to be trapping the cell partially while the HaCaT cell appeared to be in a distorted shape compared to the untreated HaCaT cells in Figure 4.27 (A).

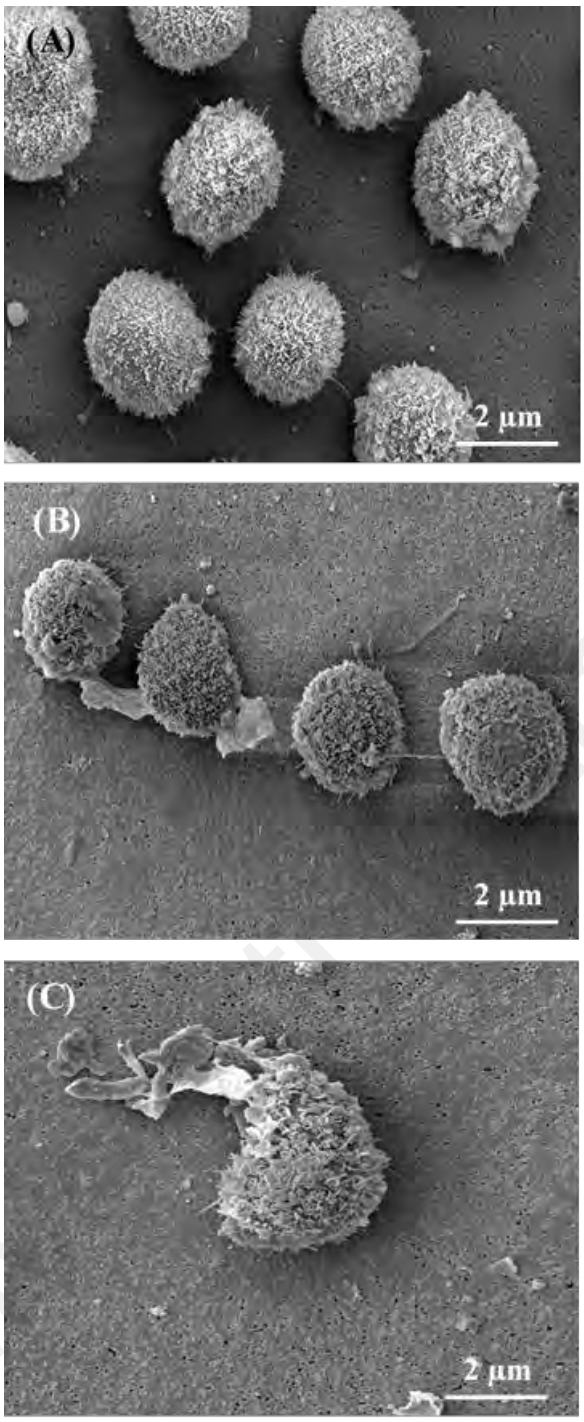


**Figure 4.27:** FESEM images of HaCaT cells before and after exposure to GO. A represent untreated cells, B represent 100 µg/mL of GO treated cells and C represent 200 µg/mL of GO treated cell. GO sheets can be seen to partially entrap the GO treated HaCaT cells.

# CHAPTER 5: DISCUSSIONS

## 5.1 Characterizations of graphene oxide

The GO that was provided for this study was characterized using UV-Vis spectroscopy techniques. UV-Vis light was passed through diluted GO suspension to detect the differences in intensity between transmitted light and incident light to determine the wavelength at maxima absorption. This wavelength was used to identify the presence of certain chromophores in GO. The two peaks at 240 nm and 290 nm attributed to the $\pi \rightarrow \pi^*$ and $n \rightarrow \pi^*$ transitions respectively (Gurunathan et al., 2013). Thus, the UV-Vis spectroscopy technique was very useful to monitor the structural changes during the modification or chemical reduction of GO.

Raman spectroscopy is another powerful non-destructive technique and is a very useful optical approach to distinguish the ordered and disordered structure of carbonaceous materials (Shi et al., 2012; Zhang, Yan, Li, Jing, & Xie, 2015). The technique was mostly used to acquire structural data on carbon materials (Chaiyakun et al., 2012). The Raman spectrum of GO showed two main bands which appeared due to the Stokes phones energy shift caused by laser excitation. The G (1598 $cm^{-1}$) and D (1416 $cm^{-1}$) bands are a primary in-plane vibrational mode and second-order overtone of a different in-plane vibration, respectively (Nanda et al., 2016). The level of disorder in GO can be determined by using the ratio of peak intensities $I_D/I_G$. The intensity of the G band was higher compared to the D band, indicating that the prepared graphene h as a low defect content (Jorio et al., 2010).

The successful oxidation of graphite to GO was confirmed by ATR-FTIR characterization. The broad peak that appeared at 3224 $cm^{-1}$ showed the presence of different types of oxygen functionalities in GO which was attributed to the O-H stretching vibrations of C-OH groups and water molecules (Nyquist & Kagel, 2012). Hence, it could be concluded that the sample had strong hydrophilicity.

The inter-layer spacing d = 0.77 nm was calculated based on the XRD result using Bragg's Law which showed that the large numbers of polar groups were produced between the layers of graphite during oxidation. The covalent bonding between oxygen and carbon atoms tend to increase the graphite's crystal lattice along axis c (Galpaya et al., 2014). Based on the XRD result of GO, it can be concluded that the diffraction peak of graphite disappeared completely indicating that the graphite had been completely oxidized during the preparation of GO.

The secondary electrons emitted by GO was observed as a topology image from the FESEM analyses. By using this topology image, the lateral dimension of the GO can be quantified, however it was difficult to quantify the thickness of the sheet. The FESEM images of the prepared GO showed 2D nanosheet morphologies with wrinkled and multiple folded textures with irregular edges, rough surfaces, and crumpling (Saleem et al., 2018). TEM technique uses electrons that passed by the GO with contrast resulting from differences in electron density, thus it is recognized as a valuable tool for distinguishing single-layer and multilayer GO sheets. The multiple sheets appeared darker relative to single sheets which was consistent with the XRD result.

## 5.2 Antibacterial activity of graphene oxide against Gram-positive and Gram-negative bacteria in suspension

### 5.2.1 Concentration dependent activity through viability assay

In this study, two Gram-positive bacteria, *S. aureus* and *E. faecalis* and two Gram-negatives, *E. coli* and *P. aeruginosa* were used to investigate the concentration dependent antibacterial activity of GO. It was indicated that the degree of bacterial inactivation followed the order; *S. aureus* > *E. faecalis* > *E. coli* > *P. aeruginosa* in a descending trend.

Increasing GO concentrations resulted in a reduction in the viability of all strains most notably for *S. aureus* and the least towards *P. aeruginosa*. Similar observations were made by Akhavan *et al.* (Akhavan & Ghaderi, 2010) who reported that *S. aureus* cells have higher susceptibility to GO nanowalls compared to *E. coli*. They reported that the RNA efflux was higher for *S. aureus* than for *E. coli* when exposed to the same concentrations of GO (Akhavan & Ghaderi, 2010).

This observation concurred with other reports (Gurunathan et al., 2013; Krishnamoorthy et al., 2012; Liu et al., 2011). The higher concentrations of GO provided increased contact with bacterial cells in which the abundant GO sheets could entrap bacterial cells through the wrapping mechanism. The wrapping mechanism explains that GO separates the bacterial cells from the nutrients that are present in the growth medium, thus inhibiting cell proliferation resulting in cell death (Perreault et al., 2015; Zhao, Wang, White, & Xing, 2014).

As GO concentration of 10 µg/mL was able to inactivate more than 60% of live cells, this concentration was selected for subsequent experiments. Gao *et al.* (2017) too reported that 10 µg/mL of GO suspension was able to exert toxic effects towards bacteria as higher concentrations would possibly cause indirect toxic effects through cell entrapment mechanism which separates bacterial cells from the reaction medium (Gao et al., 2017).

### 5.2.2 Membrane integrity analysis through LDH cytotoxicity assay

Since the increasing concentrations of GO reduced the viability of bacterial cells in suspension, it was necessary to validate these results with a molecular approach. Furthermore, as GO is known to induce physical damage to the bacterial membrane, it was important to determine if this characteristic of GO was also affirmed in this study.

Therefore, membrane integrity analysis of bacterial cells in suspension was analyzed using the LDH cytotoxicity assay. This enzyme is stable and it is also exclusive to the cell cytoplasm only. Hence, the presence of this enzyme in the reaction medium would indicate a loss of membrane integrity (Zhang et al., 2016).

It was found that increasing concentrations of GO caused enhanced levels of LDH detected in the reaction medium as seen in Figure 4.8. This result was concordant with the bacterial viability assay which indicated the same results as well. It is commonly known that GO is the oxidized variety of graphene nanosheets, where there is an abundance of oxygen molecules on its edges and basal plane in the form of carbonyl, epoxy, carboxylic and hydroxyl functional groups (Kumar, Huo, Zhang, & Liu, 2019). These oxygen-rich functional groups enable interactions between GO sheet and biomolecules on the bacterial cell membrane (Sengupta et al., 2019).

Besides this, GO is also able to induce physical damage to the bacterial cells through its sharp edges (Lu et al., 2017b). These types of interactions had caused continual bacterial cell death among the tested Gram-positive and Gram-negative bacteria. Moreover, increase in the concentrations of GO also promoted contact between GO sheets and bacteria which then resulted in leakage of cell content and eventual bacterial cell death (Olivi et al., 2016). Therefore, this caused in the increasing trend of GO cytotoxicity noticed among the tested bacteria.

Furthermore, GO was more selective towards Gram-positive *S. aureus* and *E. faecalis* compared to Gram-negative *E. coli* and *P. aeruginosa* when treated with lower concentrations of GO (<40 µg/mL) as shown in Figure 4.8. One of the main differences between these two types of bacteria is in the structure of bacterial cell membrane structure.

The existence of additional layers of lipopolysaccharide and phospholipid on the outer membrane as an exclusive part of its cell membrane structure proves to be a barrier against physical interactions between GO and Gram-negative bacteria (Eaton, Fernandes, Pereira, Pintado, & Xavier Malcata, 2008).

Comparatively, peptidoglycan layers of Gram-positive bacteria act as an adhesive towards the GO nanosheets prompting bacterial wrapping and subsequent restrictions in the entry of nutrients (Kell et al., 2008). However, this selective characteristic of GO was not observed when the concentration of GO was increased during the LDH cytotoxicity assay. This is possibly due to the oversaturated presence of GO in the reaction medium which has prompted almost complete bactericidal effect among the Gram-positive and Gram-negative bacteria.

### 5.2.3 Time dependent activity through time-kill assay

Time dependent activity of GO (10 µg/mL) against Gram-positive and Gram-negative bacteria was also tested for 8 h with a 2-hour interval time. More than 60% of viability loss were seen at the 4$^{th}$ hour, which indicated better contact between the bacteria and GO as shown in Figure 4.9. Therefore, increased contact mediated enhanced antibacterial activity and this resulted in major cell loss especially at the 8$^{th}$ hour of incubation. Similarly, Gurunathan *et al.* (Gurunathan et al., 2013) and Liu *et al.* (Liu et al., 2011) also described that a major proportion of cell death occurred in the early phase of incubation time which is consistent with this study. This phenomenon suggests that increasing incubation time contributed to longer interaction time and improved contact of GO sheets towards bacterial cells. Additionally, with increasing time of contact, the overall proliferation of bacteria may be hindered because a large proportion of bacteria were rendered non-viable at early hours of incubation time. Therefore, the results indicated that the antibacterial activity of GO is concentration and time dependent.

### 5.2.4 Visualization of the bacterial cell upon exposure to graphene oxide through electron microscopy techniques

Visualization of GO treated bacterial cells indicated certain differences in the mechanistic actions of GO towards the Gram-positive and Gram-negative bacteria as shown in Figure 4.10. Surface morphology of GO treated *S. aureus* and *E. faecalis* were observed to be surrounded by GO sheets. The wrapping mechanism of bacterial cells *via* GO sheets is a documented antibacterial mechanism of action where the cells are actively isolated from the nutrient medium and undergo cell death (Perreault et al., 2015). In this study, this mechanism was observed clearly for the Gram-positive cells only. As Gram-positive bacteria (*S. aureus* and *E. faecalis*) are usually present in clusters, this increased the surface area of exposure to GO sheets and these cells get trapped leading to the higher death rate. The total surface area of the Gram-positive cells exposed to GO sheets is higher as these bacterial cells (*S. aureus* and *E. faecalis*) usually occur in clusters. Hence more cells are trapped, leading to higher cell death.

In contrast, the Gram-negative *E. coli* and *P. aeruginosa* were observed to display minor levels of membrane damage that did not entirely affect their viability rate. The membrane damage are the effects of physical disruption due to the sharp edges of GO and destructive extraction of lipid molecules. For instance, *E. coli* has been observed to display a slight loss in cytoplasmic content where gaps existed between the cytoplasm and cell wall in the TEM images (Figure 4.11(G)). The membrane damage observed for the Gram-negative bacteria may be contributory to the sharp edge effect of GO. When the Gram-negative bacteria were exposed to GO, close contact between the bacterial cells and GO sheets may have caused the sharp edges of GO to induce disruptions on the bacterial cell membrane. Similar observations were made by Hu *et al.* (Hu et al., 2010) and Li *et al.* (Li et al., 2016b) where bacterial cells treated with GO appear to have suffered a loss in cellular integrity along with leakage of cytoplasmic content.

Additionally, the GO treated *P. aeruginosa* cells were noted to display a reduction in the intracellular density compared to the cytoplasm leakage observed among the *E. coli* cells. This may be due to the destructive extraction of lipid molecules in the phospholipid bilayer. A similar observation reported by Tu *et al.* (2013) showed that GO treated bacterial cells suffered lower surface phospholipid density due to partial membrane damage. Molecular simulations have suggested that the lipid bilayer may be extracted out of the membrane formation through high hydrophobic interactions between the lipid bilayer and $sp^2$ carbons on the GO sheets (Tu et al., 2013). Therefore, close contact between bacterial cells and GO sheets induces membrane disruptions on the cell membrane. Liu *et al.* (2011) indicated that the membrane damage happens only after direct contact with graphene-based materials and the damage appears to be irreversible.

The difference in the loss of viability between Gram-positive and Gram-negative bacteria may be explained by the tendency of the Gram-positive bacteria to form cell clusters besides the apparent difference in the cell wall structure. In contrast, Gram-negative bacteria are usually present in single or paired cells, thus a lesser number of bacterial cells will be exposed to GO at any given time, hence lower viability loss for the Gram-negative bacteria was found in this study (Barenfanger & Drake, 2001). Therefore, the antibacterial potential of GO is influenced by the degree of contact between bacterial cells and GO sheets. Similarly, a study conducted by Perreault *et. al.* (Perreault et al., 2015) also reported that the close contact between the GO sheets and bacteria cells could compromise the integrity of bacterial membranes.

### 5.2.5 Interactions between bacterial cell membrane and graphene oxide at molecular level

ATR-FTIR spectra of bacterial cells are usually conducted to analyze the surface chemistry and functional groups that are present on the cell walls of the bacteria (Davis & Mauer, 2010). This technique is commonly used for the identification, detection and classification of bacteria (Kuhm, Suter, Felleisen, & Rau, 2009; Rebuffo, Schmitt, Wenning, von Stetten, & Scherer, 2006). It is also used to detect changes at the molecular level in bacterial cell wall structure. The ATR-FTIR spectra of untreated and GO treated bacterial cells were analyzed to deduce the different actions of GO on Gram-positive and Gram-negative bacteria. In this study, the ATR-FTIR for Gram-positive (*S. aureus*) treated with GO spectrum indicates that the carboxylic acid, primary and secondary amides and the amino acid functional groups altered after the treatment process (Garip et al., 2007; Kannan, 2014). In the case of *E. faecalis* treated with GO, the C-H asymmetric of $CH_2$ in fatty acids, O-H groups in carboxylic acid and monoalkyl acetylene have been diminished (Thirunavukkarasu et al., 2013). These data are in good agreement with the visualization of GO treated bacterial cells via FESEM and TEM analyses. It is strongly confirmed that the thick peptidoglycan layer together with the teichoic acids, lipoids and amino acids on the surface of these bacteria tend to interact with GO sheets through molecular interactions and have contributed to mechanical wrapping.

In the case of Gram-negative (*E. coli*) treated with GO, the ATR-FTIR spectra showed that the band which corresponded to C-H stretching was strengthened and the intensity of N-H bend, C-N stretching, COO- symmetric and $PO^{2-}$ symmetric stretching were reduced in strength as compared to the ATR-FTIR spectrum of *E. coli* alone (Suzuki et al., 2013). The ATR-FTIR spectrum of GO-P. *aeruginosa* showed that $PO^{2-}$ symmetric stretching band decreased and the peak which corresponded to C-H stretching has become stronger.

It can be concluded that, all the changes in the vibration bands indicated that Gram-negative bacteria interacted with GO through direct physical contact, thus causing damage to the bacterial membrane. These results were concordant and supported the FESEM and TEM analyses.

## 5.3 Mechanism of action of graphene oxide towards Gram-positive and Gram-negative bacteria in suspension

This study showed that the antibacterial effects of GO on Gram-positive bacteria were greater compared to Gram-negative bacteria. Additionally, ATR-FTIR characterizations of untreated and treated bacterial isolates confirmed molecular interactions that occurred between the bacterial cell and GO sheets. Briefly, the exposed part of the bacteria that is available for the GO to immediately act on is the outer membrane layer for Gram-negative bacteria and the peptidoglycan layer for Gram-positive bacteria (Brown, Wolf, Prados-Rosales, & Casadevall, 2015). This dissimilarity plays a role in determining the type of interactions that occur between the two classes of bacteria with GO. Similar observations were made by Deokar *et al.* (Deokar et al., 2013) who reported that Gram-positive *S. aureus* was more susceptible towards the antibacterial activity of carbon nanotube compared to Gram-negative *E. coli*. The authors suggested that Gram-positive bacteria interacted with these nanomaterials through electrostatic or hydrogen bonding besides physical piercing of cell membrane while Gram-negative bacteria interacted with the nanomaterial through direct physical contact only (Deokar et al., 2013).

The thick peptidoglycan layer in Gram-positive bacteria and additional presence of teichoic acids, lipoids and amino acids on the surface of these bacteria may have contributed to the added interaction between the Gram-positive bacteria and GO (Deokar et al., 2013; Liang et al., 2017).

The peptidoglycan layers have an adherence characteristic which may have caused this layer to behave as a chelating agent (Kell et al., 2008) and this can be attributed to the presence of surface proteins such as teichoic acids and adhesins (Silhavy et al., 2010).

In general, Gram-positive bacteria such as *S. aureus* and *E. faecalis* are commensal bacteria on humans where the former resides on the skin and the latter resides in the gastrointestinal tract (Chiller, Selkin, & Murakawa, 2001; Kommineni et al., 2015). However, these bacteria are also opportunistic pathogens which could cause invasive infections when there is a breach in the epithelial lining by adhering to the host tissues to initiate bacterial colonization (Silhavy et al., 2010). Therefore, it is proposed here that similar adhering mechanism has prompted interactions with the GO sheets, whereby the surface proteins on the peptidoglycan layer have interacted with GO.

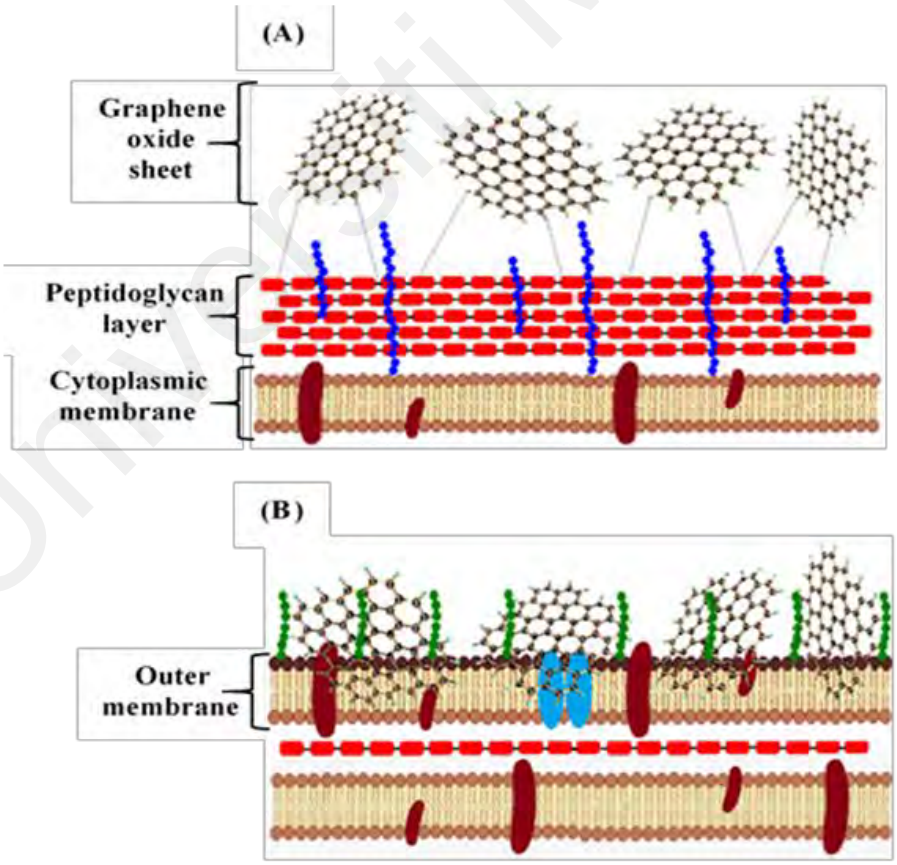


**Figure 5.1:** Schematic diagram of the possible mechanism of action of GO towards Gram-positive and Gram-negative bacteria. (A) mechanical wrapping in Gram-positive bacteria and (B) membrane damage in Gram-negative bacteria.

The interactions of GO with Gram-positive bacteria may have contributed to the mechanical wrapping of GO sheets onto *S. aureus* and *E. faecalis* as indicated in Figure 5.1 (A) and (B). Thus, the peptidoglycan layer tends to interact with GO sheets once it is in close proximity and this necessitates adherence of GO onto the bacterial membrane.

Membrane corrugations observed on the Gram-negative bacteria are contributory to the physical interactions which occurred between the Gram-negative *E. coli* and *P. aeruginosa* and the GO nanosheets. Sharp edges of GO may have served as "cutters" that damage and disrupt the bacterial cell membrane upon close contact (Liu et al., 2011). Therefore, this has resulted in the loss of cytoplasm content mainly observed for the *E. coli* cells in the TEM image in Figure 4.11(G). Moreover, GO treated *P. aeruginosa* cells were observed to display a reduction in the intracellular density. This may have been due to the destructive extraction of lipid molecules in the phospholipid bilayer. When GO comes into contact with the bacterial cells, the GO sheets start to extract phospholipid molecules from the cell membrane onto its own surface (Tu et al., 2013). This phenomenon may have led to a less dense lipid bilayer as observed in the TEM image in Figure 4.11(H).

Additionally, the outer membrane layer on Gram-negative bacteria forms an extra protective layer for these bacteria from interacting closely to GO sheets. Although membrane damage to *E. coli* and *P. aeruginosa* had been observed, mechanical wrapping of these cells was not observed in the FESEM or the TEM images. The outer membrane is essential to the survival of Gram-negative bacteria as this layer offers protection to the bacteria in a hostile environment including in the presence of antibiotics and it is one of the key reasons that Gram-negative bacteria are generally resistant towards antibiotics (Delcour, 2009).

The lipopolysaccharide (LPS) that is found on the outer leaflet of the outer membrane plays a role in the effective exclusion of hydrophobic molecules (Kamio & Nikaido, 1976; Silhavy et al., 2010). It was suggested LPS molecules may contribute to the overall repulsive forces on Gram-negative bacteria through steric repulsion (Nikaido, 2003).

It has been noted that interaction between the bacteria and GO are mainly repulsive as reported by Castrill n *et al.* (Romero-Vargas Castrill n, Perreault, De Faria, & Elimelech, 2015) who investigated the effects of GO - functionalized atomic force microscopy (AFM) probe puncture on *E. coli* cell wall. The repulsive force may have arisen from the electrostatic repulsion from the negatively charged bacterial outer membrane and deprotonated carboxylic acid groups existing on GO (Camesano & Logan, 2000; Dreyer, Todd, & Bielawski, 2014). However, sporadic adhesions were measured upon AFM probe pull-off and it was suggested to be due to LPS stretching effects which bridges cell surface and AFM tip upon pull-off (Romero-Vargas Castrill n et al., 2015).

In this study, similar events may have occurred where LPS on the cell surface of Gram-negative bacteria were stretched upon the ensuing repulsive force during interactions between bacteria and GO in the reaction medium. The bridging effects of LPS may have been responsible for the indentations that are observed on the surface of Gram-negative bacteria in the FESEM images in Figure 4.10. Correspondingly, an investigation that was conducted to study the puncturing effects of AFM tip on the Gram-negative *Salmonella* Typhimurium, reported that this bacterium managed to survive after multiple puncturing of their cell wall. Lipid bilayers and peptidoglycan layer of the bacteria are suggested to be self-repairing as it retains the integrity, viability and reproductive ability even after repeated puncturing of the cell membrane (Suo, Avci, Deliorman, Yang, & Pascual, 2009).

## 5.4 Antibiofilm activity of graphene oxide against Gram-positive and Gram-negative bacteria

### 5.4.1 Concentration dependent activity through viability assay

GO was found to enhance the biofilm formation of Gram-positive S. *aureus* and *E. faecalis* and Gram-negative *E. coli* and *P. aeruginosa* despite increase in the concentration of GO that was used for their treatment. This contrasts with the strong antibacterial activity displayed by GO towards the same set of bacteria in suspension. Several factors can be attributed to the increase in the biofilm viability although GO has been shown to have antibacterial activity. Mainly, bactericidal effects of GO were attenuated in the biofilm matrix due to the secretion of extracellular polymeric substances (EPS) by the biofilm cells that has interacted with the functional groups of GO whereby inactivating them (He et al., 2017).

Mature biofilm cells have been noted to secrete EPS to improve attachment of biofilm cells to a surface and maintain the structure of the biofilm scaffold (Flemming & Wingender, 2010). Additionally, the EPS layer is highly viscous and this too can reduce the penetration and transport of nanomaterial effectively inhibiting direct contact with biofilm cells (Harper et al., 2019; He et al., 2017). Similarly, Wirth *et al.* reported that silver nanoparticles that were previously exposed to natural organic matter were shown to increase the viability of *P. fluosrescens* biofilm compared to silver nanoparticles alone (Wirth, Lowry, & Tilton, 2012).

Polysaccharides, lipids, proteins and nucleic acids are among the actively secreted components of the EPS layer (Decho & Gutierrez, 2017). Therefore, non-covalent interactions among GO's surface functional groups and these secreted components of the EPS layer may have rendered GO's antibacterial potential in biofilm (Hui et al., 2014).

A study that was conducted to investigate the availability of basal planes on GO found that, adsorption of protein-based compounds onto GO's basal plane reduced its bactericidal capacity (Hui et al., 2014). Therefore, it is proposed that similar adsorption mechanism may have occurred in this study, where adsorption of EPS components onto the basal planes of GO has mitigated its antibacterial property. Moreover, as GO normally exists in a sheet-like formation, this characteristic of GO may have provided additional surface area for bacterial attachment and this explains the increase in biofilm viability despite exposure to high concentrations of GO (Zou et al., 2016).

### 5.4.2 Membrane integrity analysis through LDH cytotoxicity assay

Membrane integrity analysis that was conducted against the GO treated biofilm cells of Gram-positive *S. aureus*, *E. faecalis* and Gram-negative *E. coli* and *P. aeruginosa* found that levels of LDH cytotoxicity were reduced overall for all the biofilm cells. In contrast to bacterial cells in suspension, exposure of GO towards biofilm cells at various time points increased the viability of the biofilm cells just as observed with the biofilm viability assay in Figure 4.13. As observed with the viability assay, biofilm cells are protected by the EPS layer and also biofilm cells are notably tolerant of the harsh environment (Donlan & Costerton, 2002). Therefore, this explains the low cytotoxicity value of the LDH assay which indicates that GO was unable to cause membrane damage or entrap the bacterial cells as observed with the bacterial cells in suspension.

Additionally, the LDH enzyme detected for the biofilm cells considerably varied according to the maturity of the biofilm. As detection of LDH enzyme is a measure of cell's cytotoxicity, the 72 h-biofilm released the least amount of LDH into the growth medium compared to 48 h- and 24 h-biofilm. This can be attributed to the maturity and cell density of the biofilm cells where aging of the biofilm cells causes physical and physiological changes in the biofilm (Stewart, 2015).

Therefore, mature biofilm cells are able to withstand exposure to GO due to the changes in their physiology where they are able to endure harsh environment compared to less mature biofilm (Flemming et al., 2016).

### 5.4.3 Time dependent activity through time-kill assay

All biofilm cells of *S. aureus, E. faecalis, E. coli* and *P. aeruginosa* were treated with a fixed concentration of GO (100 µg/mL). These time dependent assays were performed with an interval period of 3 h, 6 h, 12 h and 24 h for all biofilm of 24 h, 48 h and 72 h maturity period. A ten-fold higher concentration of GO was used for this investigation compared to 10 µg/mL of GO that was previously used for the bacterial cells in suspension. A higher concentration of GO was used here in biofilm study as biofilm viability assay that was carried out in the previous section increased biofilm's viability although treated with higher concentrations of GO as shown in Figure 4.13.

In contrast to the bacterial cells in suspension, exposure of GO towards biofilm cells at various time points increased the viability of the biofilm cells just as observed with the biofilm viability assay in Figure 4.13. Although the biofilm cells were exposed to GO for longer exposure time, the mass of biofilm increased with time of exposure. A similar study conducted by He *et al.* (2017) to investigate the effects of GO on *Streptococcus mutans* biofilm found that GO has no effect on mature biofilm. The authors accredited this to the secretion of polysaccharide biomolecules from the EPS layer which made it viscous and therefore reduced the transport of nanomaterials and their interactions with the bacterial cells within the biofilm matrix (He et al., 2017).

Additionally, it was noted that increase in biofilm viability can be observed for almost all bacteria when there is an increase in GO exposure period regardless of biofilm maturity. Longer exposure period has allowed for better attachment of biofilm onto the surface of GO sheets which has been described in the time dependent biofilm assay in Figure 4.15 (Zou et al., 2016). Therefore, GO enhanced the viability of biofilm cells regardless of exposure period as GO provides additional surface area for the growth and adhesion of biofilm cells (Ruiz et al., 2011).

## 5.5 Interactions between graphene oxide and antibiotics at molecular level

ATR-FTIR analysis was conducted to verify the interactions between GO and selected antibiotics (ampicillin, chloramphenicol, tetracycline). The comparison between ATR-FTIR spectra of GO, antibiotics and GO loaded antibiotics has confirmed the physical adsorption of antibiotics onto GO through molecular interactions such as hydrophobic interactions, electrostatic interactions, π-π interactions, H-bonding interactions or a combination of these interaction mechanisms (Peng et al., 2016).

The UV-Vis spectrum showed that the absorbance and the $\lambda_{max}$ of GO-antibiotic combinations differ slightly from that of GO and antibiotic alone. This is suggesting that the antibiotics were effectively adsorbed on the surface of GO and this adsorption made GO lose the π–π* transition of the aromatic C=C bonds (Gao et al., 2017). It can be concluded that three GO-antibiotics combinations were different from each other suggesting that the mechanisms of adsorption between GO and the antibiotics may be unique based on both ATR-FTIR and UV-Vis spectra techniques.

## 5.6 Synergistic behaviour of GO with selected antibiotics against Gram-positive and Gram-negative bacteria in suspension

Interest in the antibacterial activity of graphene-based nanomaterial has stimulated more antimicrobial studies with these nanomaterials. Combinatorial activity of nanoparticles and antibiotics has been mostly studied for silver, titanium dioxide, zinc and gold nanoparticles (Allahverdiyev et al., 2011). Therefore, the synergistic actions of GO with antibiotics such as ampicillin, chloramphenicol and tetracycline have been investigated against *S. aureus*, *E. faecalis*, *E. coli* and *P. aeruginosa*. These antibiotics were mainly chosen due to their regular use in human medicine worldwide and their broad-spectrum activities for treating bacterial infections caused by both Gram-positive and Gram-negative bacteria (Lewis, 2013).

The ability of GO to disrupt bacterial membrane integrity would enable better diffusion of antibiotics into the cell membrane and may potentiate improved antibacterial activity. Thus, *S. aureus*, *E. faecalis*, *E. coli* and *P. aeruginosa* have been treated with ampicillin, chloramphenicol and tetracycline in combination with GO. Generally, ampicillin is a member of β-lactam antibiotics and this antibiotic acts through inhibition of cell wall synthesis. The major binding target of this drug is penicillin-binding protein (PBP) found in the cytoplasmic membrane of bacteria (Lewis, 2013). Tetracycline binds to 30S ribosomal Unit and they effectively prevent protein translation by inhibiting the binding of tRNA to the ribosomes (Wilson, 2014). Similarly, chloramphenicol also inhibits protein synthesis but this drug binds to the 50S ribosomal Unit and prevents the elongation step in protein synthesis (Wilson, 2014). The difference in the mode of action has prompted the need to investigate the effects of GO in enhancing the antibacterial activity of these antibiotics.

Increasing concentrations of antibiotics (1 - 10 µg/mL) in combination with GO (10 µg/mL) were tested for ampicillin, chloramphenicol and tetracycline against both the Gram-positive and Gram-negative bacteria. The inactivation of bacteria after treatment with antibiotic and GO was calculated using the formula $[\log_{10}(T_0/T)]$ where $T_0$ is the number of bacteria in the control reaction and T is residual bacterial cells in the reaction medium at a certain antibiotic concentration or combination of antibiotic + GO concentration. Figures 4.18, 4.19 and 4.20 illustrated the increase in the antibacterial action of antibiotic + GO compared to antibiotic alone or GO only.

Combinations of GO and chloramphenicol showed better antibacterial action towards all bacteria except *P. aeruginosa*. Similar observations were made for the remaining antibiotics as well. *P. aeruginosa* is intrinsically resistant to chloramphenicol, tetracycline and most β-lactam antibiotics due to the multidrug efflux systems that is inducible through sub-inhibitory antibiotic concentrations (Morita, Kimura, Mima, Mizushima, & Tsuchiya, 2001; Morita, Tomida, & Kawamura, 2014). Therefore, this explains the lower log-reduction values of *P. aeruginosa* compared to other bacteria in this study.

Nevertheless, a significant log-reduction values were observed for almost all combinations of GO and antibiotics ($p < 0.05$) which indicates synergistic antibacterial effects of GO and antibiotics among the four bacterial species. This can be attributed to the "facilitated transport" mechanism where the high adsorption rates of GO may have mediated buildup of antibiotics in high concentrations in the cell cytoplasm (Schwab et al., 2013; Xuezhi Zhang et al., 2007). Thus, this contributed to the release of the antibiotic molecules in high quantities upon contact with the bacterial membrane (Serag et al., 2011).

In addition, the damaged bacterial cell membrane upon accumulation of GO sheets on its' membrane may have enhanced diffusion of the antibiotics into the cytoplasm (Delcour, 2009). As per the findings on the successful adsorption of antibiotics onto GO using ATR-FTIR methods, it is speculated that GO has acted as a delivery agent for transporting the antibiotics to the bacteria. As GO disrupted the bacterial membrane, the antibiotics then gained entry into the bacterial cytoplasm to initiate their mechanism of action respectively.

The antibacterial action of GO + antibiotics worked better in Gram-positive bacteria (*S. aureus* and *E. faecalis*) as compared to the Gram-negative bacteria (*E. coli* and *P. aeruginosa*) as indicated in Figures 4.18, 4.19 and 4.20. This may be attributed to the absence of an outer membrane that is only exclusive in the Gram-negative bacteria (Reith & Mayer, 2011). GO is more selective towards Gram-positive bacteria due to the chelating effects of peptidoglycan layer that may have interacted with GO through contact mechanism (Deokar et al., 2013). Therefore, diffusion of antibiotics into the cytoplasm of Gram-positive bacteria may be higher along with the added effects of antimicrobial actions of GO that seem to be more preferential among these bacterial types (Yadav et al., 2017). Thus, the combinatorial actions of GO + antibiotics produce better antibacterial activity than treatment with antibiotics alone in *S. aureus* and *E. faecalis*.

On the other hand, the existence of a robust outer membrane in Gram-negative bacteria may have limited the diffusion of antibiotics into the cytoplasm although its cell membrane is debilitated through contact with GO sheets (Krishnamoorthy et al., 2017). Consequently, the selective permeability barrier (outer membrane) plays a role in contributing towards lower log-reduction values in Gram-negative bacteria especially *P. aeruginosa* compared to the Gram-positive *S. aureus* and *E. faecalis*.

Gao *et al.* (2017) reported that GO acted as an antibiotic carrier when used in combination with lincomycin hydrochloride, chloramphenicol and gentamycin sulfate on *S. aureus* and *E. coli*. The authors postulated that this activity is dependent on the interaction between GO and antibiotic, interaction between GO and bacteria and the susceptibility of bacteria to the respective antibiotic (Gao et al., 2017).

## 5.7 Synergistic behaviour of GO with selected antibiotics against the biofilm cells of Gram-positive and Gram-negative bacteria

Combinations of GO and selected antibiotics (ampicillin, chloramphenicol and tetracycline) against bacteria in suspension were found to inhibit the growth of all tested bacteria and it was also observed that these GO and antibiotic combinations worked even better in exhibiting its antibacterial property compared to GO alone. Therefore, it was repeated for the biofilm cells of all bacteria despite negative antibacterial activity of GO alone for biofilm viability assays. Hence, increasing concentrations of ampicillin, chloramphenicol and tetracycline (2 - 10 µg/mL) in combination with GO (100 µg/mL) was tested against both the biofilm cells of Gram-positive and Gram-negative bacteria respectively.

It was observed that the activity of GO + antibiotic combinations seemed to be hindered when in contact with 24 h-, 48 h- and 72 h-biofilm cells as shown in Figures 4.21, 4.22 and 4.23. As GO was found to be an antibiotic adjuvant when tested against the bacteria in suspension, however, the use of GO with antibiotic against the biofilm cells was found to be obstructing the antibacterial activity of the antibiotics tested. As shown in Figures 4.21, 4.22 and 4.23, the activity of GO in combination with antibiotic was lower compared to antibiotics alone. The activity of the GO + antibiotic was found to be similar to the activity of GO with respect to the maturity of the biofilm and bacterial strain.

Although the antibacterial activity of antibiotic alone was observed for all biofilm cells, however, the combinations of GO and antibiotics do not inhibit the biofilm growth and in fact enhances its viability. In previous sections, characterizations of GO and antibiotic interactions were categorized as molecular interactions and these combinations proved to enhance the antibacterial activity of the GO + antibiotic towards bacterial cells in suspension. However, antibacterial activity of GO + antibiotic towards biofilm cells were even lower than the antibacterial activity of the antibiotic.

Bacterial cells within the biofilm matrix have been shown to have increased tolerance to antibiotics due to the diverse range of metabolic state of the bacterial colonies within the particular biofilm (Hall & Mah, 2017). As antibiotics often target metabolically-active bacteria, majority of the bacterial cells in a biofilm are in the dormant state and exposure to antibiotics such as ciprofloxacin, tobramycin, tetracycline and β-lactams has been observed to have no effect on the bacterial cells in the biofilm (Høiby, Bjarnsholt, Givskov, Molin, & Ciofu, 2010; Pamp, Gjermansen, Johansen, & Tolker-Nielsen, 2008).

However, when the biofilm in this study were treated with antibiotics alone, antibacterial activity was noted for most of the biofilm despite articles reporting weakened activity of the antibiotic among biofilm cells. This may be contributory to the use of single species biofilm that was investigated in this study compared to polymicrobial biofilm that consist of several species (Algburi, Comito, Kashtanov, Dicks, & Chikindas, 2017). Antibiotic-resistant bacterial populations in a biofilm have been reported to protect the whole biofilm community and also at the same time preserves the susceptible bacterial population within the biofilm from the effects of antibiotic (Rojo-Molinero, Macià, & Oliver, 2019).

It was discussed in the previous sections that antibiotics were loaded unto GO through molecular interactions such as hydrophobic, electrostatic, H-bonding interactions or combinations of these interaction mechanisms. Therefore, it is proposed here that the combined structure of GO + antibiotic did not induce any antibacterial activity among the biofilm cells as opposed to the bacterial cells in suspension due to the inactivation of the GO-antibiotic structure. GO was previously observed to not induce bactericidal activity against the biofilm in this study, therefore, similar mechanism of GO inactivation may have hindered the GO-antibiotic structure from exhibiting its antibacterial properties.

Briefly, GO-antibiotic structure was hindered by the presence of the EPS layer of the biofilm cells as observed for the tested biofilm cells in this study (Elias & Banin, 2012). Additionally, the transport of GO-antibiotic structure was inhibited from penetrating the highly viscous EPS layer and this inhibited direct contact of GO-antibiotic structure with the biofilm cells (Harper et al., 2019). Moreover, GO-antibiotic structure may have been trapped by the biofilm and incorporated into the biofilm matrix. Electrically conductive inorganic particles such as graphite, charcoal and granular activated carbon have been shown to support interspecies electron transfer in biofilm (Flemming et al., 2016). Therefore, GO which is also an electrically conductive inorganic material, may be trapped onto the biofilm matrix for interspecies electron transfer, a process of syntrophic interaction between microbes to facilitate biological conductive networks such as ethanol metabolism (Kouzuma, Kato, & Watanabe, 2015).

## 5.8 Toxicological effects of graphene oxide against human epidermal keratinocytes

### 5.8.1 MTT viability assay

Since GO enhanced the antibacterial activity of antibiotics, it is interesting to explore the compatibility of GO for biomedical applications. Since one potential use of GO + antibiotic is in topical applications, the cytotoxicity effects of GO when it comes into contact with the normal/healthy skin layer was investigated against the HaCaT cells. MTT cytotoxicity assay that was conducted against the HaCaT cells with exposure to increasing concentrations of GO was found to cause no effects on the viability of the HaCaT cells at lower GO concentrations (<100 µg/mL) as shown in Figure 4.24. Higher concentrations of GO may have a toxic effect on cell viability after 24 h, suggesting cytotoxic potential at increased concentrations (Pelin et al., 2018).

Similarly, Pelin *et al.* (2017) described reduced mitochondrial activity and plasma-membrane damages in HaCaT cells after treatment with GO. The authors postulated that GO is harmful when used at high concentrations and prolonged periods of exposure. If used at lower GO concentrations, the cytotoxic effects at the skin level could be minimal (Pelin et al., 2017). Minimal toxic effect of GO was further proven when low concentrations of GO (20 µg/mL) were investigated against a human lung carcinoma cell line, A549, where only a slight decrease (~20%) in cytotoxicity was noted after 24 h (Hu et al., 2010). Hence, minimal cytotoxic effects that was observed for GO concentrations lower than <100 µg/mL concurred with others (Hu et al., 2010; Pelin et al., 2017).

Besides that, the adherence characteristic of the HaCaT cells may have played a role in the low cytotoxicity effects observed when the cells were treated with GO. Geis *et al.* (2018) noted that GO is the least toxic when exposed to adherent cells compared to semi-adherent or suspension cells (Gies & Zou, 2018).

The authors also explained that only a small percentage of adhering cells come into contact with the sharp edges of GO compared to cells in the suspension form. Therefore, this explains the low cytotoxicity rate observed among the adhering HaCaT cells in this study.

### 5.8.2 Generation of reactive oxygen species

The ability of GO in inducing the generation of reactive oxygen species among the HaCaT cells was explored in this study as well. It was found that GO significantly increased generation of ROS from concentration of 100 µg/mL and above after 2 h of the exposure period. As observed with the MTT assay, concentrations of GO from 5 - 50 µg/mL did not exert significant ROS production compared to the untreated HaCaT cells.

As generation of ROS has been linked to the inflammation process, negligible production of ROS upon exposure to GO at lower concentrations is highly beneficial for its suggested antibacterial use. Furthermore, measurements of ROS among the HaCaT cells were found to be dose dependent as increase in the concentrations of GO stimulated higher production of ROS. It was well-known that oxidative stress due to the escalating generation of ROS is one of the main toxicological mechanism associated to nanomaterials (Manke, Wang, & Rojanasakul, 2013).

This study's findings concurred with the study by Pelin *et al.* (2018) in which the production of ROS was mediated by time and concentration dependent exposure of GO towards HaCaT cells. Additionally, Pelin *et al.* (2018) also observed an increase in mitochondrial membrane polarization by GO which had been induced by cellular ROS production upon exposure to GO (Pelin et al., 2018). It was also noted that the abundance of functional groups that contained oxygen such as –COOH and –OH on the surface of GO may have contributed to the increased production of ROS (Zou et al., 2016).

A different study by Chang *et al.* (2011) which investigated the toxic effects GO on A549 cells indicated that GO might be considered to be a safe material at the cellular level as they observed relatively low cytotoxic effects besides reporting optimal A549 cell growth on the GO film (Chang et al., 2011).

### 5.8.3 Membrane integrity analysis

The integrity of the HaCaT cell membrane was investigated by measuring the concentration of LDH enzyme in the cell medium after GO exposure as graphene has been observed to impair cell membrane integrity through direct and indirect mechanisms in several types of mammalian cells (Li et al., 2014; Xu et al., 2016). As this enzyme is often found in the intact cell membrane, thus the leakage of this enzyme into the cell medium indicates cytotoxicity and membrane damage. It was found that the concentration of LDH detected in the cell culture medium increased with the rise in the concentration of GO that was exposed to the HaCaT cells.

Similar to the MTT cytotoxicity assay, it was found that significant cytotoxic effect was only observed for GO concentrations higher than 100 µg/mL as shown in Figure 4.26. Similarly, Chang *et al.* (2011) too noted low cytotoxic effects of GO towards lung epithelial cells (A549) when investigated using LDH leakage assay (Chang et al., 2011). Concentrations of GO from 5 to 50 µg/mL did not induce significant leakage of LDH enzyme into the HaCaT cell culture medium. It was also observed that the LDH leakage into the reaction medium was found to increase when the HaCaT cells were exposed to increasing concentrations of GO. Higher concentrations of GO impaired the stability of the HaCaT cells by inducing membrane damage (Gurunathan, Arsalan Iqbal, et al., 2019). This membrane damage was due to the physical interactions between the HaCaT cells and GO nanosheets.

Therefore, cytotoxicity of GO towards HaCaT cells is dose dependent as was observed with MTT viability and ROS generation assays in the previous sections. Similar to the results in this study, Cho *et al.* (2016) too reported dose-dependent cytotoxicity behaviour of single and multi-layered GO on human monocytic (THP-1) cells (Cho, Pak, Joo, Lee, & Chung, 2016). Moreover, Gurunathan *et al.* (2019) too reported that GO induced dose-dependent leakage of LDH enzyme in germ cell lines of male reproductive organ, Leydig (TM3) and Sertoli (TM4) cells (Gurunathan, Kang, Jeyaraj, & Kim, 2019).

### 5.8.4 Cell surface morphology analysis

The cell surface of the GO treated HaCaT cells was noted to display changes in the appearance as shown in Figure 4.27. As observed with the MTT-based viability assay, LDH leakage and DCFH-DA assay for the generation of ROS in this study, no significant decrease in the cell viability and production of ROS have been noted at GO concentrations below 100 µg/mL. The cell surface morphology analysis of HaCaT cells treated with 100 µg/mL of GO did not show visible damage on the cell membrane besides reduction in the number of microvilli structures and minor trapping of cells by the GO sheets.

Similarly, Gao *et al.* (2016) also reported the reduction in the microvilli structure of the HaCaT cell upon exposure to zinc oxide (ZnO) nanoparticles. They reported the presence of small membrane-bound apoptotic bodies that were present on the HaCaT cells for exposure of ZnO at 20 and 50 µg/mL of ZnO nanoparticles (Gao et al., 2016). However, no membrane-bound apoptotic bodies were noticed which indicated the low toxic effects exerted by GO sheets upon exposure to HaCaT cells. Lingaraju *et al.* (2019) described that graphene-based nanomaterials may tend to interact with the cells' plasma membrane or the extracellular matrix when in contact. The graphene-based nanomaterials may enter the cell membrane through endocytosis, diffusion or through receptor bindings (Lingaraju, Raja Naika, Nagaraju, & Nagabhushana, 2019).

Therefore, interaction with GO nanosheets may have caused membrane damage to the HaCaT cells as observed in the FESEM images in Figure 4.27.

## 5.9 Challenges encountered in this study

As one of the objectives of this study was to determine the mechanistic actions of GO against Gram-positive and Gram-negative bacteria, however, detailed information from previous studies focusing on a similar objective was lacking in the literature. Therefore, interactions of GO against bacteria at molecular levels using physicochemical techniques such as ATR-FTIR and UV-Vis spectroscopy were included in this study to grasp a better understanding of the interaction mechanism of GO when encountering bacterial cells. Despite using these techniques to further elucidate the mechanism of action of GO, limitations in the available source of information in the literature proved to be a challenge in deciphering the collected data. However, existing information on basic surface functional groups on bacteria and GO functioned as a guideline in discussing the nature of their interaction mechanism.

Moreover, conflicting results in the literature regarding the antibacterial efficacy of GO was also a challenge in this study. A thorough literature searches and understanding of the experimental concepts used in the published articles in the similar field demonstrated to be a valuable source of information that guided the protocols that were conducted in this study. Therefore, this current study was able to determine and elucidate the antibacterial and antibiofilm efficacy of GO against Gram-positive and Gram-negative bacteria through the use of molecular techniques described in this study.

## 5.10 Limitations of this study

This current research has highlighted the efficacy of GO in inhibiting the growth of bacterial cells. However, the bacterial species that was included in the current study were limited to model bacteria from Gram-positive and Gram-negative categories only.

As antibiotic resistance is rapidly increasing all over the world, the use of multidrug resistant bacterial strains should have been included in this type of study. However, the access to multidrug resistant bacteria was limited and ethical approvals were also needed to address this issue. Therefore, model bacterial organisms such as *S. aureus*, *E. faecalis*, *E. coli* and *P. aeruginosa* were included in this research to elucidate the antibacterial efficacy of GO on Gram-positive and Gram-negative bacteria.

The investigations on the synergistic effects of GO with selected antibiotics in this study may have been improved with the use of current antibiotics in practice for bacterial infection treatments such as meropenem, amoxicillin/clavulanic acid and cefuroxime. However, use of ampicillin, chloramphenicol and tetracycline was opted for this research. This is mainly to determine the ability of GO in acting as a transport mechanism to deliver antibiotics to the bacterial cell initially prior to the investigations that can be conducted with the current antibiotics in use. Besides that, less frequent use of effective antibiotics may become an advantage for these drugs when in clinical use as lower usage of antibiotics has been linked to reduction in microbial resistance.

## 5.11 Contribution of the study to the body of science

This study was able to contribute further to the existing information that is available on the antimicrobial activity of GO towards bacteria. Here, it is shown definitely with evidence that there is a difference between the mechanism of action of GO towards Gram-positive and Gram-negative bacteria. Previous literatures on this topic were only able to speculate the dissimilarity in the antibacterial actions of GO, however, through this research, confirmations backed by molecular-based experiments and electron microscopic images were used to arrive at conclusion discussed here.

Moreover, synergistic actions of GO with conventional antibiotics investigated in this study were able to contribute to the limiting literature existing on this topic as well.

Here, it was shown that GO may have played the role as a facilitated transport for antibiotics to successfully enter the bacterial cell. The results of this investigation would be able to renew interest on the antibiotics that have been shown to be ineffective previously.

Besides that, the inability of GO to act against biofilm cells is among the new information that this study can contribute to the body of science. Literature in this field is lacking although biofilm have an importance in the clinical sector especially for wound management. Finally, this study has also shown that the concentration of GO that was proposed for antibacterial activity did not affect the viability of the HaCaT cells investigated in this study. Therefore, this research was able to contribute significantly to the body of science especially in the field of nanomaterial-based antibacterial works.

# CHAPTER 6: CONCLUSION

## 6.1 Conclusion

Advances in the nanotechnology field have made possible for invention of nanomaterials with antibacterial properties. One such nanomaterial is the carbon-based nanomaterial, graphene oxide (GO) which is well-known for its antibacterial activity. In this study, GO nanomaterial that was provided was characterized through UV-Vis, Raman and ATR-FTIR spectroscopy techniques, FESEM and TEM analysis for morphological characterizations and finally through XRD analysis for compound identification. GO was investigated for its bactericidal properties against Gram-positive *S. aureus* and *E. faecalis* and Gram-negative *E. coli* and *P. aeruginosa* cells in suspension and in biofilm. Additionally, combinatorial activity of GO and selected antibiotic against these bacterial cells in suspension and biofilm was determined. Moreover, the cytotoxicity of this nanomaterial was also explored for human use in *in vitro* HaCaT cell line as GO has been proposed for antibacterial use in the clinical sector.

In this study, the physicochemical properties of GO were confirmed through several characterization methods that the as-received GO had the physicochemical properties of GO. Most importantly, the antibacterial activity of GO was found to be concentration and time dependent towards *S. aureus*, *E. faecalis*, *E. coli* and *P. aeruginosa* in suspension form. Higher concentrations of GO and prolonged exposure time affected bacterial viability through bacterial inactivation at early phase of the incubation period and bacterial death increased with higher GO concentrations. In contrast, GO enhanced the viability of biofilm cells when exposed to higher concentrations of GO and similarly, longer exposure time too increased the viability of biofilm cells.

The inactivity of GO towards biofilm cells is mainly due to the secretion of polysaccharides, proteins and lipids by the EPS layer which may have reacted with the surface functional groups of GO. Surface morphology of bacterial cells in suspension after exposure of GO showed evidence of membrane disruptions and bacterial entrapment under GO sheets that have contributed to cell death. ATR-FTIR analysis proved that the interaction of GO with bacterial membrane occurs upon contact, resulting in changes in the IR spectra of untreated and treated bacterial culture. As the antibacterial effects of GO have enormous potential for antimicrobial applications, the mechanism of action of GO towards bacteria must be clearly elucidated to ensure complete bacterial inactivation.

In addition, GO enhanced antibacterial activity of empirical antibiotics such as ampicillin, chloramphenicol and tetracycline by assisting in better adsorption of antibiotic compound as GO severely disrupted bacterial membrane albeit more selective towards Gram-positive bacteria for the bacterial cells in suspension only. Therefore, combinatorial therapy of GO + antibiotics may improve the use of empirical antibiotics for the treatment of bacterial infections. On the other hand, combinatorial activity of GO + antibiotic did not affect the biofilm cells regardless of the biofilm maturity. Contact between the GO-antibiotic structure and the biofilm cells is inhibited contributory to the existence of viscous EPS layer which limits the transport of nanomaterial across the EPS layer.

Finally, the cytotoxic effects of GO towards HaCaT cells investigated through MTT-based viability assay, LDH leakage and DCFH-DA assay for the generation of ROS in this study were found to be dose-dependent and no significant decrease in the cell viability and production of ROS have been noted at GO concentrations below 100 µg/mL. Hence, the minimal GO concentration (10 µg/mL) that is proposed as an antibiotic adjuvant in this study may be considered to be safe for use.

Therefore, it is suggested here that the route of possible application for combinatorial therapy of GO + antibiotic is through dispersion on an open wound and retained on the site to reduce and eliminate infection for fast wound recovery. Additionally, as topical forms of ampicillin, chloramphenicol and tetracycline are available for use in the consumer market, combining these antibiotics with GO for better antibacterial activity has been proposed in this work. This might be beneficial for first aids treatment as it permits prolonged exposure of the wound to GO and the antibiotic for effective recovery, without affecting the integrity of the unaffected skin and also to prevent the infection from becoming systemic. This knowledge would improve the understanding of the application of GO sheets for optimal antibacterial action and concurrent reduction in antibiotic resistance in preserving the use of the newer generation of antibiotics. Detailed studies should also be carried out to determine the nanosafety aspects of GO for future clinical use.

## 6.2 Recommendations for future work

It is recommended here that further investigations into the differences between mechanistic actions of GO towards Gram-positive and Gram-negative bacteria should be carried out further through additional physicochemical or analytical techniques. This would enable a clearer understanding of the whole concept of bactericidal mechanisms of GO towards bacteria. Additionally, the non-efficacy of GO towards biofilm cells also grants further investigations to map out the reasons for the inability of GO in inhibiting the progress of biofilm growth. This may be researched by exploring the secretion of molecules and surface proteins on biofilm of various maturity levels and by determining the factors that inactivate GO from exhibiting its antibacterial activity.

Moreover, antibacterial effects of GO on multidrug resistant bacteria should be carried out in the future to determine if the bactericidal ability of GO still remains optimal as observed among the bacteria in suspension in this study. This would substantiate the recommended use of GO in the clinical sector mainly as a topical antibacterial agent. On the same note, additional toxicological experiments should be carried out to understand the toxic effects of GO among various types of cell cultures besides the HaCaT cells that were used in this study. A comparison of GO's activity among these different human cell cultures would pave way for subsequent animal studies to investigate the nanosafety of GO for human use.

Additionally, synergistic effects of antibiotics with GO should be investigated for antibiotics from different classes. This is needed to determine if the enhancing effects of GO towards antibiotics from this study can be observed among other antibiotics as well. Therefore, the results of this future work would be able to give more recognition to antibiotics that are currently used less frequently due to the increase in antibiotic resistance. In that way, newer antibiotics may be preserved for critical cases and also to prevent the rise in antibiotic resistance.

## REFERENCES


Acik, M., & Chabal, Y. J. (2011). Nature of graphene edges: a review. Japanese Journal of Applied Physics, 50(7R), 070101.

Admassie, M. (2018). Current review on molecular and phenotypic mechanism of bacterial resistance to antibiotic. Science, 7(2), 13-19.

Ahmad, N., Kausar, A., & Muhammad, B. (2016). An investigation on 4-aminobenzoic acid modified polyvinyl chloride/graphene oxide and PVC/graphene oxide based nanocomposite membranes. Journal of Plastic Film & Sheeting, 32(4), 419-448.

Akhavan, O., & Ghaderi, E. (2010). Toxicity of graphene and graphene oxide nanowalls against bacteria. ACS Nano, 4(10), 5731-5736. doi: 10.1021/nn101390x

Akhavan, O., & Ghaderi, E. (2012). *Escherichia coli* bacteria reduce graphene oxide to bactericidal graphene in a self-limiting manner. Carbon, 50(5), 1853-1860.

Algburi, A., Comito, N., Kashtanov, D., Dicks, L. M., & Chikindas, M. L. (2017). Control of biofilm formation: antibiotics and beyond. Applied and Environmental Microbiology, 83(3), e02508-02516.

Ali-Boucetta, H., Bitounis, D., Raveendran-Nair, R., Servant, A., Van den Bossche, J., & Kostarelos, K. (2013). Purified graphene oxide dispersions lack *in vitro* cytotoxicity and *in vivo* pathogenicity. Advanced Healthcare Materials, 2(3), 433-441.

Allahverdiyev, A. M., Kon, K. V., Abamor, E. S., Bagirova, M., & Rafailovich, M. (2011). Coping with antibiotic resistance: combining nanoparticles with antibiotics and other antimicrobial agents. Expert Review of Anti-infective Therapy, 9(11), 1035-1052.

Amato, S. M., Fazen, C. H., Henry, T. C., Mok, W. W., Orman, M. A., Sandvik, E. L., . . . Brynildsen, M. P. (2014). The role of metabolism in bacterial persistence. Frontiers in Microbiology, 5, 70.

Ameen, S., Akhtar, M. S., Seo, H.-K., & Shin, H. S. (2013). Advanced ZnO–graphene oxide nanohybrid and its photocatalytic applications. Materials Letters, 100, 261-265.

Amenta, V., & Aschberger, K. (2015). Carbon nanotubes: potential medical applications and safety concerns. Wiley Interdisciplinary Reviews: Nanomedicine and Nanobiotechnology, 7(3), 371-386.

Aminov, R. I. (2010). A brief history of the antibiotic era: lessons learned and challenges for the future. Frontiers in Microbiology, 1, 134.

Ansari, M. A., Khan, H. M., Khan, A. A., Sultan, A., & Azam, A. (2012). Characterization of clinical strains of MSSA, MRSA and MRSE isolated from skin and soft tissue infections and the antibacterial activity of ZnO nanoparticles. World Journal of Microbiology and Biotechnology, 28(4), 1605-1613.

Badhulika, S., Terse-Thakoor, T., Chaves Villarreal, C. M., & Mulchandani, A. (2015). Graphene hybrids: synthesis strategies and applications in sensors and sensitized solar cells. Frontiers in Chemistry, 3, 38.

Banin, E., Hughes, D., & Kuipers, O. P. (2017). Editorial: Bacterial pathogens, antibiotics and antibiotic resistance. FEMS Microbiology Reviews, 41(3), 450-452.

Barenfanger, J., & Drake, C. A. (2001). Interpretation of Gram stains for the nonmicrobiologist. Laboratory medicine, 32(7), 368-375.

Bellio, P., Luzi, C., Mancini, A., Cracchiolo, S., Passacantando, M., Di Pietro, L., . . . Celenza, G. (2018). Cerium oxide nanoparticles as potential antibiotic adjuvant. Effects of CeO2 nanoparticles on bacterial outer membrane permeability. Biochimica et Biophysica Acta (BBA) - Biomembranes, 1860(11), 2428-2435.

Beyth, N., Houri-Haddad, Y., Domb, A., Khan, W., & Hazan, R. (2015). Alternative antimicrobial approach: Nano-antimicrobial materials. Evidence-Based Complementary and Alternative Medicine, 2015, 16.

Bhat, R. (2013). Potential use of Fourier transform infrared spectroscopy for identification of molds capable of producing mycotoxins. International journal of Food Properties, 16(8), 1819-1829.

Bitounis, D., Ali-Boucetta, H., Hong, B. H., Min, D. H., & Kostarelos, K. (2013). Prospects and challenges of graphene in biomedical applications. Advanced Materials, 25(16), 2258-2268.

Blair, J. M., Webber, M. A., Baylay, A. J., Ogbolu, D. O., & Piddock, L. J. (2015). Molecular mechanisms of antibiotic resistance. Nature Reviews Microbiology, 13(1), 42.

Blecher, K., Nasir, A., & Friedman, A. (2011). The growing role of nanotechnology in combating infectious disease. Virulence, 2(5), 395-401.

Boehm, H.-P., Clauss, A., Fischer, G., & Hofmann, U. (1962). Das adsorptionsverhalten sehr dünner kohlenstoff-folien. Zeitschrift für anorganische und allgemeine Chemie, 316(3-4), 119-127.

Boehm, H. P., Setton, R., & Stumpp, E. (1994). Nomenclature and terminology of graphite intercalation compounds (IUPAC Recommendations 1994). Pure and Applied Chemistry, 66(9), 1893-1901.

Bondarenko, O., Sihtmäe, M. M., Kuzmičiova, J., Ragelienė, L., Kahru, A., & Daugelavičius, R. (2018). Bacterial plasma membrane is the main cellular target of silver nanoparticles in *Escherichia coli* and *Pseudomonas aeruginosa*. bioRxiv, 322727.

Bravo, A., & Anacona, J. R. (1998). Synthesis and characterization of metal complexes with ampicillin. Journal of Coordination Chemistry, 44(1-2), 173-182.

Brown-Jaque, M., Calero-Cáceres, W., & Muniesa, M. (2015). Transfer of antibiotic-resistance genes via phage-related mobile elements. Plasmid, 79, 1-7.

Brown, E. D., & Wright, G. D. (2016). Antibacterial drug discovery in the resistance era. Nature, 529(7586), 336.

Brown, L., Wolf, J. M., Prados-Rosales, R., & Casadevall, A. (2015). Through the wall: extracellular vesicles in Gram-positive bacteria, mycobacteria and fungi. Nature Reviews Microbiology, 13(10), 620.

Brown, M. R. W., Allison, D. G., & Gilbert, P. (1988). Resistance of bacterial biofilms to antibiotics a growth-rate related effect? Journal of Antimicrobial Chemotherapy, 22(6), 777-780.

Camesano, T. A., & Logan, B. E. (2000). Probing bacterial electrosteric interactions using atomic force microscopy. Environmental Science & Technology, 34(16), 3354-3362.

Chaiyakun, S., Witit-Anun, N., Nuntawong, N., Chindaudom, P., Oaew, S., Kedkeaw, C., & Limsuwan, P. (2012). Preparation and characterization of graphene oxide nanosheets. Procedia Engineering, 32, 759-764.

Chang, Y., Yang, S.-T., Liu, J.-H., Dong, E., Wang, Y., Cao, A., . . . Wang, H. (2011). *In vitro* toxicity evaluation of graphene oxide on A549 cells. Toxicology letters, 200(3), 201-210.

Chatterjee, N., Eom, H.-J., & Choi, J. (2014). A systems toxicology approach to the surface functionality control of graphene–cell interactions. Biomaterials, 35(4), 1109-1127.

Chatterjee, N., Yang, J., & Choi, J. (2016). Differential genotoxic and epigenotoxic effects of graphene family nanomaterials (GFNs) in human bronchial epithelial cells. Mutation Research/Genetic Toxicology and Environmental Mutagenesis, 798, 1-10.

Chen, G.-Y., Meng, C.-L., Lin, K.-C., Tuan, H.-Y., Yang, H.-J., Chen, C.-L., . . . Hu, Y.-C. (2015). Graphene oxide as a chemosensitizer: diverted autophagic flux, enhanced nuclear import, elevated necrosis and improved antitumor effects. Biomaterials, 40, 12-22.

Chen, G.-Y., Yang, H.-J., Lu, C.-H., Chao, Y.-C., Hwang, S.-M., Chen, C.-L., . . . Tuan, H.-Y. (2012). Simultaneous induction of autophagy and toll-like receptor signaling pathways by graphene oxide. Biomaterials, 33(27), 6559-6569.

Chen, G. Y., Chen, C. L., Tuan, H. Y., Yuan, P. X., Li, K. C., Yang, H. J., & Hu, Y. C. (2014). Graphene oxide triggers toll-like receptors/autophagy responses *in vitro* and inhibits tumor growth *in vivo*. Advanced Healthcare Materials, 3(9), 1486-1495.

Chiller, K., Selkin, B. A., & Murakawa, G. J. (2001). Skin microflora and bacterial infections of the skin. Journal of Investigative Dermatology Symposium Proceedings, 6(3), 170-174.

Cho, Y. C., Pak, P. J., Joo, Y. H., Lee, H.-S., & Chung, N. (2016). *In vitro* and *in vivo* comparison of the immunotoxicity of single- and multi-layered graphene oxides with or without pluronic F-127. Scientific Reports, 6, 38884. doi: 10.1038/srep38884

Choucair, M., Thordarson, P., & Stride, J. A. (2009). Gram-scale production of graphene based on solvothermal synthesis and sonication. Nature Nanotechnology, 4(1), 30-33.

Ciccia, A., & Elledge, S. J. (2010). The DNA damage response: making it safe to play with knives. Molecular Cell, 40(2), 179-204.

Ciofu, O., Rojo-Molinero, E., Macià, M. D., & Oliver, A. (2017). Antibiotic treatment of biofilm infections. Apmis, 125(4), 304-319.

Clardy, J., Fischbach, M. A., & Currie, C. R. (2009). The natural history of antibiotics. Current Biology, 19(11), R437-R441.

Cogan, N., Brown, J., Darres, K., & Petty, K. (2012). Optimal control strategies for disinfection of bacterial populations with persister and susceptible dynamics. Antimicrobial Agents and Chemotherapy, 56(9), 4816-4826.

Crabbé, A., Jensen, P. Ø., Bjarnsholt, T., & Coenye, T. (2019). Antimicrobial tolerance and metabolic adaptations in microbial biofilms. Trends in Microbiology, 27(10):850-863.

Crosera, M., Prodi, A., Mauro, M., Pelin, M., Florio, C., Bellomo, F., . . . Bovenzi, M. (2015). Titanium dioxide nanoparticle penetration into the skin and effects on HaCaT cells. International Journal of Environmental Research and Public Health, 12(8), 9282-9297.

Czaplewski, L., Bax, R., Clokie, M., Dawson, M., Fairhead, H., Fischetti, V. A., . . . Harper, D. (2016). Alternatives to antibiotics—a pipeline portfolio review. The Lancet Infectious Diseases, 16(2), 239-251.

Davies, J. (2006). Where have all the antibiotics gone? Canadian Journal of Infectious Diseases and Medical Microbiology, 17(5), 287-290.

Davies, J., & Davies, D. (2010). Origins and evolution of antibiotic resistance. Microbiology and Molecular Biology Reviews, 74(3), 417-433.

Davis, R., & Mauer, L. (2010). Fourier transform infrared (FT-IR) spectroscopy: a rapid tool for detection and analysis of foodborne pathogenic bacteria. Current Research, Technology and Education Topics in Applied Microbiology and Microbial Biotechnology, 2, 1582-1594.

de la Fuente-Núñez, C., Reffuveille, F., Fernández, L., & Hancock, R. E. W. (2013). Bacterial biofilm development as a multicellular adaptation: antibiotic resistance and new therapeutic strategies. Current Opinion in Microbiology, 16(5), 580-589.

Decho, A. W., & Gutierrez, T. (2017). Microbial extracellular polymeric substances (EPSs) in ocean systems. Frontiers in Microbiology, 8, 922.

Delcour, A. H. (2009). Outer membrane permeability and antibiotic resistance. Biochimica et Biophysica Acta (BBA)-Proteins and Proteomics, 1794(5), 808-816.

Deng, H., McShan, D., Zhang, Y., Sinha, S. S., Arslan, Z., Ray, P. C., & Yu, H. (2016). Mechanistic study of the synergistic antibacterial activity of combined silver nanoparticles and common antibiotics. Environmental Science & Technology, 50(16), 8840-8848.

Deokar, A. R., Lin, L.-Y., Chang, C.-C., & Ling, Y.-C. (2013). Single-walled carbon nanotube coated antibacterial paper: preparation and mechanistic study. Journal of Materials Chemistry B, 1(20), 2639-2646.

Desai, M., Bühler, T., Weller, P., & Brown, M. (1998). Increasing resistance of planktonic and biofilm cultures of *Burkholderia cepacia* to ciprofloxacin and ceftazidime during exponential growth. The Journal of Antimicrobial Chemotherapy, 42(2), 153-160.

Ding, Z., Zhang, Z., Ma, H., & Chen, Y. (2014). *In vitro* hemocompatibility and toxic mechanism of graphene oxide on human peripheral blood T lymphocytes and serum albumin. ACS Applied Materials & Interfaces, 6(22), 19797-19807.

Dong, S., Hirani, A. A., Colacino, K. R., Lee, Y. W., & Roman, M. (2012). Cytotoxicity and cellular uptake of cellulose nanocrystals. Nano Life, 2(03), 1241006.

Donlan, R. M., & Costerton, J. W. (2002). Biofilms: survival mechanisms of clinically relevant microorganisms. Clinical Microbiology Reviews, 15(2), 167-193.

Drawz, S. M., & Bonomo, R. A. (2010). Three decades of β-lactamase inhibitors. Clinical Microbiology Reviews, 23(1), 160-201.

Dreyer, D. R., Todd, A. D., & Bielawski, C. W. (2014). Harnessing the chemistry of graphene oxide. Chemical Society Reviews, 43(15), 5288-5301.

Duan, G., Zhang, Y., Luan, B., Weber, J. K., Zhou, R. W., Yang, Z., . . . Zhou, R. (2017). Graphene-induced pore formation on cell membranes. Scientific Reports, 7, 42767.

Duch, M. C., Budinger, G. R., Liang, Y. T., Soberanes, S., Urich, D., Chiarella, S. E., . . . Mutlu, G. M. (2011). Minimizing oxidation and stable nanoscale dispersion improves the biocompatibility of graphene in the lung. Nano Letters, 11(12), 5201-5207.

Eaton, P., Fernandes, J. C., Pereira, E., Pintado, M. E., & Xavier Malcata, F. (2008). Atomic force microscopy study of the antibacterial effects of chitosans on *Escherichia coli* and *Staphylococcus aureus*. Ultramicroscopy, 108(10), 1128-1134.

Elias, S., & Banin, E. (2012). Multi-species biofilms: living with friendly neighbors. FEMS Microbiology Reviews, 36(5), 990-1004.

Emmerson, A., & Jones, A. (2003). The quinolones: decades of development and use. Journal of Antimicrobial Chemotherapy, 51(suppl_1), 13-20.

Endes, C., Schmid, O., Kinnear, C., Mueller, S., Camarero-Espinosa, S., Vanhecke, D., . . . Weder, C. (2014). An *in vitro* testing strategy towards mimicking the inhalation of high aspect ratio nanoparticles. Particle and Fibre Toxicology, 11(1), 40.

Fair, R. J., & Tor, Y. (2014). Antibiotics and bacterial resistance in the 21st century. Perspectives in Medicinal Chemistry, 6, PMC. S14459.

Fallatah, H., Elhaneid, M., Ali-Boucetta, H., Overton, T. W., El Kadri, H., & Gkatzionis, K. (2019). Antibacterial effect of graphene oxide (GO) nano-particles against *Pseudomonas putida* biofilm of variable age. Environmental Science and Pollution Research, 26(24), 25057-25070.

Fleming, A. (1929). On the antibacterial action of cultures of a penicillium, with special reference to their use in the isolation of *B. influenzae*. British journal of Experimental Pathology, 10(3), 226.

Flemming, H.-C., & Wingender, J. (2010). The biofilm matrix. Nature Reviews Microbiology, 8(9), 623.

Flemming, H.-C., Wingender, J., Szewzyk, U., Steinberg, P., Rice, S. A., & Kjelleberg, S. (2016). Biofilms: an emergent form of bacterial life. Nature Reviews Microbiology, 14(9), 563.

Fujita, K., Take, S., Tani, R., Maru, J., Obara, S., & Endoh, S. (2018). Assessment of cytotoxicity and mutagenicity of exfoliated graphene. Toxicology in Vitro, 52, 195-202.

Gabriel, S., Rasheed, A. K., Siddiqui, R., Appaturi, J. N., Fen, L. B., & Khan, N. A. (2018). Development of nanoparticle-assisted PCR assay in the rapid detection of brain-eating amoebae. Parasitology Research, 117(6), 1801-1811.

Galpaya, D., Wang, M., George, G., Motta, N., Waclawik, E., & Yan, C. (2014). Preparation of graphene oxide/epoxy nanocomposites with significantly improved mechanical properties. Journal of Applied Physics, 116(5), 053518.

Gao, F., Ma, N., Zhou, H., Wang, Q., Zhang, H., Wang, P., . . . Li, L. (2016). Zinc oxide nanoparticles-induced epigenetic change and G2/M arrest are associated with apoptosis in human epidermal keratinocytes. International Journal of Nanomedicine, 11, 3859.

Gao, W., Alemany, L. B., Ci, L., & Ajayan, P. M. (2009). New insights into the structure and reduction of graphite oxide. Nature Chemistry, 1(5), 403.

Gao, Y., Wu, J., Ren, X., Tan, X., Hayat, T., Alsaedi, A., . . . Chen, C. (2017). Impact of graphene oxide on the antibacterial activity of antibiotics against bacteria. Environmental Science: Nano, 4(5), 1016-1024.

Garip, S., Bozoglu, F., & Severcan, F. (2007). Differentiation of mesophilic and thermophilic bacteria with Fourier transform infrared spectroscopy. Applied Spectroscopy, 61(2), 186-192.

Garneau-Tsodikova, S., & Labby, K. J. (2016). Mechanisms of resistance to aminoglycoside antibiotics: overview and perspectives. MedChemComm, 7(1), 11-27.

Geng, J., Kong, B.-S., Yang, S. B., & Jung, H.-T. (2010). Preparation of graphene relying on porphyrin exfoliation of graphite. Chemical Communications, 46(28), 5091-5093.

Gies, V., & Zou, S. (2018). Systematic toxicity investigation of graphene oxide: evaluation of assay selection, cell type, exposure period and flake size. Toxicology Research, 7(1), 93-101.

Gill, E. E., Franco, O. L., & Hancock, R. E. (2015). Antibiotic adjuvants: diverse strategies for controlling drug-resistant pathogens. Chemical Biology & Drug Design, 85(1), 56-78.

Gould, F. K. (2011). Linezolid: safety and efficacy in special populations. Journal of Antimicrobial Chemotherapy, 66(suppl_4), iv3-iv6.

Gould, K. (2016). Antibiotics: from prehistory to the present day. Journal of Antimicrobial Chemotherapy, 71(3), 572-575.

Greenwood, D. (1988). Microbiological properties of teicoplanin. Journal of Antimicrobial Chemotherapy, 21(suppl_A), 1-13.

Guillemot, D., Varon, E., Bernède, C., Weber, P., Henriet, L., Simon, S., . . . Carbon, C. (2005). Reduction of antibiotic use in the community reduces the rate of colonization with Penicillin G—nonsusceptible *Streptococcus pneumoniae*. Clinical Infectious Diseases, 41(7), 930-938.

Guo, Y., & Guo, W. (2012). Electronic and field emission properties of wrinkled graphene. The Journal of Physical Chemistry C, 117(1), 692-696.

Guo, Z., Xie, C., Zhang, P., Zhang, J., Wang, G., He, X., . . . Zhang, Z. (2017). Toxicity and transformation of graphene oxide and reduced graphene oxide in bacteria biofilm. Science of The Total Environment, 580, 1300-1308.

Gupta, V., Sharma, N., Singh, U., Arif, M., & Singh, A. (2017). Higher oxidation level in graphene oxide. Optik - International Journal for Light and Electron Optics, 143(Supplement C), 115-124.

Gurunathan, S., Arsalan Iqbal, M., Qasim, M., Park, C. H., Yoo, H., Hwang, J. H., . . . Do, J. T. (2019). Evaluation of graphene oxide induced cellular toxicity and transcriptome analysis in human embryonic kidney cells. Nanomaterials, 9(7), 969.

Gurunathan, S., Han, J. W., Dayem, A. A., Eppakayala, V., Park, M.-R., Kwon, D.-N., & Kim, J.-H. (2013). Antibacterial activity of dithiothreitol reduced graphene oxide. Journal of Industrial and Engineering Chemistry, 19(4), 1280-1288.

Gurunathan, S., Kang, M.-H., Jeyaraj, M., & Kim, J.-H. (2019). Differential cytotoxicity of different sizes of graphene oxide nanoparticles in Leydig (TM3) and Sertoli (TM4) cells. Nanomaterials, 9(2), 139.

Hall, C. W., & Mah, T.-F. (2017). Molecular mechanisms of biofilm-based antibiotic resistance and tolerance in pathogenic bacteria. FEMS Microbiology Reviews, 41(3), 276-301.

Händel, N., Schuurmans, J. M., Brul, S., & ter Kuile, B. H. (2013). Compensation of the metabolic costs of antibiotic resistance by physiological adaptation in *Escherichia coli*. Antimicrobial Agents and Chemotherapy, 57(8), 3752-3762.

Hanif, Z., Ahmed, F. R., Shin, S. W., Kim, Y.-K., & Um, S. H. (2014). Size-and dose-dependent toxicity of cellulose nanocrystals (CNC) on human fibroblasts and colon adenocarcinoma. Colloids and Surfaces B: Biointerfaces, 119, 162-165.

Hanke, M. L., & Kielian, T. (2012). Deciphering mechanisms of staphylococcal biofilm evasion of host immunity. Frontiers in Cellular and Infection Microbiology, 2, 62.

Hannukainen, K.-S., Suhonen, S., Savolainen, K., & Norppa, H. (2012). Genotoxicity of nanofibrillated cellulose in vitro as measured by enzyme comet assay. Toxicology Letters (211), S71.

Harper, R. A., Carpenter, G. H., Proctor, G. B., Harvey, R. D., Gambogi, R. J., Geonnotti, A. R., . . . Jones, S. A. (2019). Diminishing biofilm resistance to antimicrobial nanomaterials

through electrolyte screening of electrostatic interactions. Colloids and Surfaces B: Biointerfaces, 173, 392-399.

He, H., Pham-Huy, L. A., Dramou, P., Xiao, D., Zuo, P., & Pham-Huy, C. (2013). Carbon nanotubes: applications in pharmacy and medicine. Biomed Research International, 2013, 578290.

He, J., Zhu, X., Qi, Z., Wang, C., Mao, X., Zhu, C., . . . Tang, Z. (2015). Killing dental pathogens using antibacterial graphene oxide. ACS Applied Materials & Interfaces, 7(9), 5605-5611.

He, J., Zhu, X., Qi, Z., Wang, L., Aldalbahi, A., Shi, J., . . . Tang, Z. (2017). The inhibition effect of graphene oxide nanosheets on the development of *Streptococcus mutans* biofilms. Particle & Particle Systems Characterization, 34(5), 1700001.

Hemeg, H. A. (2017). Nanomaterials for alternative antibacterial therapy. International Journal of Nanomedicine, 12, 8211.

Hernández-Jiménez, E., del Campo, R., Toledano, V., Vallejo-Cremades, M. T., Muñoz, A., Largo, C., . . . López-Collazo, E. (2013). Biofilm vs. planktonic bacterial mode of growth: which do human macrophages prefer? Biochemical and Biophysical Research Communications, 441(4), 947-952.

Høiby, N., Bjarnsholt, T., Givskov, M., Molin, S., & Ciofu, O. (2010). Antibiotic resistance of bacterial biofilms. International Journal of Antimicrobial Agents, 35(4), 322-332.

Horvath, L., Magrez, A., Burghard, M., Kern, K., Forro, L., & Schwaller, B. (2013). Evaluation of the toxicity of graphene derivatives on cells of the lung luminal surface. Carbon, 64, 45-60.

Hou, W.-C., Lee, P.-L., Chou, Y.-C., & Wang, Y.-S. (2017). Antibacterial property of graphene oxide: The role of phototransformation. Environmental Science: Nano, 4(3), 647-657.

Hu, C., Lu, T., Chen, F., & Zhang, R. (2013). A brief review of graphene–metal oxide composites synthesis and applications in photocatalysis. Journal of the Chinese Advanced Materials Society, 1(1), 21-39.

Hu, W., Peng, C., Luo, W., Lv, M., Li, X., Li, D., . . . Fan, C. (2010). Graphene-based antibacterial paper. ACS Nano, 4(7), 4317-4323.

Hu, W., Peng, C., Lv, M., Li, X., Zhang, Y., Chen, N., . . . Huang, Q. (2011). Protein corona-mediated mitigation of cytotoxicity of graphene oxide. ACS Nano, 5(5), 3693-3700.

Hui, L., Piao, J. G., Auletta, J., Hu, K., Zhu, Y., Meyer, T., . . . Yang, L. (2014). Availability of the basal planes of graphene oxide determines whether it is antibacterial. ACS Applied Materials & Interfaces, 6(15), 13183-13190.

Hummers Jr, W. S., & Offeman, R. E. (1958). Preparation of graphitic oxide. Journal of the American Chemical Society, 80(6), 1339-1339.

Hwang, I.-s., Hwang, J. H., Choi, H., Kim, K.-J., & Lee, D. G. (2012). Synergistic effects between silver nanoparticles and antibiotics and the mechanisms involved. Journal of Medical Microbiology, 61(12), 1719-1726.

Jain, K. (2012). Advances in use of functionalized carbon nanotubes for drug design and discovery. Expert Opinion on Drug Discovery, 7(11), 1029-1037.

Jennifer, M., & Maciej, W. (2013). Nanoparticle technology as a double-edged sword: cytotoxic, genotoxic and epigenetic effects on living cells. Journal of Biomaterials and Nanobiotechnology, 4(01), 53.

Jorio, A., Ferreira, E. H. M., Moutinho, M. V., Stavale, F., Achete, C. A., & Capaz, R. B. (2010). Measuring disorder in graphene with the G and D bands. physica status solidi (b), 247(11-12), 2980-2982.

Kalita, S., Kandimalla, R., Sharma, K. K., Kataki, A. C., Deka, M., & Kotoky, J. (2016). Amoxicillin functionalized gold nanoparticles reverts MRSA resistance. Materials Science and Engineering: C, 61, 720-727.

Kamio, Y., & Nikaido, H. (1976). Outer membrane of *Salmonella* Typhimurium: accessibility of phospholipid head groups to phospholipase c and cyanogen bromide activated dextran in the external medium. Biochemistry, 15(12), 2561-2570.

Kannan, S. (2014). FT-IR and EDS analysis of the seaweeds *Sargassum wightii* (brown algae) and *Gracilaria corticata* (red algae). International Journal of Current Microbiology and Applied Sciences, 3(4), 341-351.

Karthikeyan, S. (2013). Spectroscopic study of characterisation of commercial drug and its mixture. Paper presented at the Proceedings of the Indian National Science Academy.

Kell, A. J., Stewart, G., Ryan, S., Peytavi, R., Boissinot, M., Huletsky, A., . . . Simard, B. (2008). Vancomycin-modified nanoparticles for efficient targeting and preconcentration of Gram-positive and Gram-negative bacteria. ACS Nano, 2(9), 1777-1788.

Kim, K. S., Zhao, Y., Jang, H., Lee, S. Y., Kim, J. M., Kim, K. S., . . . Hong, B. H. (2009). Large-scale pattern growth of graphene films for stretchable transparent electrodes. Nature, 457(7230), 706-710.

Koch, G., Yepes, A., Forstner, K. U., Wermser, C., Stengel, S. T., Modamio, J., . . . Lopez, D. (2014). Evolution of resistance to a last-resort antibiotic in *Staphylococcus aureus* via bacterial competition. Cell, 158(5), 1060-1071. doi: 10.1016/j.cell.2014.06.046

Kommineni, S., Bretl, D. J., Lam, V., Chakraborty, R., Hayward, M., Simpson, P., . . . Salzman, N. H. (2015). Bacteriocin production augments niche competition by enterococci in the mammalian gastrointestinal tract. Nature, 526(7575), 719.

Königs, A. M., Flemming, H.-C., & Wingender, J. (2015). Nanosilver induces a non-culturable but metabolically active state in *Pseudomonas aeruginosa*. Frontiers in Microbiology, 6, 395.

Koo, H., Allan, R. N., Howlin, R. P., Stoodley, P., & Hall-Stoodley, L. (2017). Targeting microbial biofilms: current and prospective therapeutic strategies. Nature Reviews Microbiology, 15(12), 740.

Kosynkin, D. V., Higginbotham, A. L., Sinitskii, A., Lomeda, J. R., Dimiev, A., Price, B. K., & Tour, J. M. (2009). Longitudinal unzipping of carbon nanotubes to form graphene nanoribbons. Nature, 458(7240), 872-876.

Kouzuma, A., Kato, S., & Watanabe, K. (2015). Microbial interspecies interactions: recent findings in syntrophic consortia. Frontiers in Microbiology, 6, 477.

Kowalski, T. J., Berbari, E. F., & Osmon, D. R. (2005). Epidemiology, treatment, and prevention of community-acquired methicillin-resistant *Staphylococcus aureus* infections. Paper presented at the Mayo Clinic Proceedings.

Krishnamoorthy, G., Leus, I. V., Weeks, J. W., Wolloscheck, D., Rybenkov, V. V., & Zgurskaya, H. I. (2017). Synergy between active efflux and outer membrane diffusion defines rules of antibiotic permeation into Gram-negative bacteria. MBio, 8(5), e01172-01117.

Krishnamoorthy, K., Veerapandian, M., Zhang, L.-H., Yun, K., & Kim, S. J. (2012). Antibacterial efficiency of graphene nanosheets against pathogenic bacteria via lipid peroxidation. The Journal of Physical Chemistry C, 116(32), 17280-17287.

Król, J. E., Wojtowicz, A. J., Rogers, L. M., Heuer, H., Smalla, K., Krone, S. M., & Top, E. M. (2013). Invasion of E. coli biofilms by antibiotic resistance plasmids. Plasmid, 70(1), 110-119.

Kuhm, A. E., Suter, D., Felleisen, R., & Rau, J. (2009). Application of Fourier transform infrared spectroscopy (FT-IR) for the identification of *Yersinia enterocolitica* on species and subspecies level. Applied and Environmental Microbiology, 75(18), 5809-5813

Kumar, P., Huo, P., Zhang, R., & Liu, B. (2019). Antibacterial properties of graphene-based nanomaterials. Nanomaterials, 9(5), 737.

Lam, S. J., O'Brien-Simpson, N. M., Pantarat, N., Sulistio, A., Wong, E. H., Chen, Y.-Y., . . . Reynolds, E. C. (2016). Combating multidrug-resistant Gram-negative bacteria with structurally nanoengineered antimicrobial peptide polymers. Nature Microbiology, 1(11), 16162.

Lammel, T., Boisseaux, P., Fernández-Cruz, M.-L., & Navas, J. M. (2013). Internalization and cytotoxicity of graphene oxide and carboxyl graphene nanoplatelets in the human hepatocellular carcinoma cell line Hep G2. Particle and Fibre Toxicology, 10(1), 27.

Langdon, A., Crook, N., & Dantas, G. (2016). The effects of antibiotics on the microbiome throughout development and alternative approaches for therapeutic modulation. Genome Medicine, 8(1), 39.

Lebedeva, O., Chesnokova, A., Badlueva, T., Sipkina, E., Rzhechitskii, A., & Pozhidaev, Y. N. (2015). Hybrid ion-exchange membranes based on heteroaromatic sulfonic acid derivatives. Petroleum Chemistry, 55(5), 333-338.

Lee, C.-R., Cho, I., Jeong, B., & Lee, S. (2013). Strategies to minimize antibiotic resistance. International Journal of Environmental Research and Public Health, 10(9), 4274-4305.

Lerner, A., Matthias, T., & Aminov, R. (2017). Potential effects of horizontal gene exchange in the human gut. Frontiers in Immunology, 8, 1630.

Levine, D. P. (2006). Vancomycin: A history. Clinical Infectious Diseases, 42(Supplement_1), S5-S12.

Levy, S. B. (1992). Active efflux mechanisms for antimicrobial resistance. Antimicrobial Agents and Chemotherapy, 36(4), 695.

Levy, S. B., & Marshall, B. (2004). Antibacterial resistance worldwide: causes, challenges and responses. Nature Medicine, 10(12s), S122.

Lewis, K. (2012). Antibiotics: Recover the lost art of drug discovery. Nature, 485(7399), 439.

Lewis, K. (2013). Platforms for antibiotic discovery. Nature Reviews Drug discovery, 12(5), 371-387.

Li, B., & Webster, T. J. (2018). Bacteria antibiotic resistance: New challenges and opportunities for implant-associated orthopedic infections. Journal of Orthopaedic Research®, 36(1), 22-32.

Li, H., Toh, P. Z., Tan, J. Y., Zin, M. T., Lee, C.-Y., Li, B., . . . Kang, L. (2016). Selected biomarkers revealed potential skin toxicity caused by certain copper compounds. Scientific Reports, 6, 37664.

Li, J., Wang, G., Zhu, H., Zhang, M., Zheng, X., Di, Z., . . . Wang, X. (2014). Antibacterial activity of large-area monolayer graphene film manipulated by charge transfer. Scientific Reports, 4, 4359.

Li, M., Yang, X., Ren, J., Qu, K., & Qu, X. (2012). Using graphene oxide high near-infrared absorbance for photothermal treatment of Alzheimer's disease. Advanced Materials, 24(13), 1722-1728.

Li, R., Mansukhani, N. D., Guiney, L. M., Ji, Z., Zhao, Y., Chang, C. H., . . . Xia, T. (2016b). Identification and optimization of carbon radicals on hydrated graphene oxide for ubiquitous antibacterial coatings. ACS Nano, 10(12), 10966-10980.

Li, Y., Wu, Q., Zhao, Y., Bai, Y., Chen, P., Xia, T., & Wang, D. (2014b). Response of microRNAs to *in vitro* treatment with graphene oxide. ACS Nano, 8(3), 2100-2110.

Li, Y., Yuan, H., Von Dem Bussche, A., Creighton, M., Hurt, R. H., Kane, A. B., & Gao, H. (2013). Graphene microsheets enter cells through spontaneous membrane penetration at edge asperities and corner sites. Proceedings of the National Academy of Sciences, 110(30), 12295-12300.

Liang, H., DeMeester, K. E., Hou, C.-W., Parent, M. A., Caplan, J. L., & Grimes, C. L. (2017). Metabolic labelling of the carbohydrate core in bacterial peptidoglycan and its applications. Nature Communications, 8, 15015.

Liang, X., Wang, H., Liu, X., Grice, J., Xu, Z. P., & Roberts, M. S. (2017b). Related topic: Safety evaluation of nanomaterials skin permeation and disposition of therapeutic and cosmeceutical compounds (pp. 313-322): Springer.

Liao, K. H., Lin, Y. S., Macosko, C. W., & Haynes, C. L. (2011). Cytotoxicity of graphene oxide and graphene in human erythrocytes and skin fibroblasts. ACS Applied Materials & Interfaces, 3(7), 2607-2615.

Lingaraju, K., Raja Naika, H., Nagaraju, G., & Nagabhushana, H. (2019). Biocompatible synthesis of reduced graphene oxide from *Euphorbia heterophylla (L.)* and their *in-vitro* cytotoxicity against human cancer cell lines. Biotechnology Reports, 24, e00376.

Liu, S., Hu, M., Zeng, T. H., Wu, R., Jiang, R., Wei, J., . . . Chen, Y. (2012). Lateral dimension-dependent antibacterial activity of graphene oxide sheets. Langmuir, 28(33), 12364-12372.

Liu, S., Tian, J., Wang, L., Li, H., Zhang, Y., & Sun, X. (2010). Stable aqueous dispersion of graphene nanosheets: noncovalent functionalization by a polymeric reducing agent and their subsequent decoration with Ag nanoparticles for enzymeless hydrogen peroxide detection. Macromolecules, 43(23), 10078-10083.

Liu, S., Zeng, T. H., Hofmann, M., Burcombe, E., Wei, J., Jiang, R., . . . Chen, Y. (2011). Antibacterial activity of graphite, graphite oxide, graphene oxide, and reduced graphene oxide: membrane and oxidative stress. ACS Nano, 5(9), 6971-6980.

Liu, Y., Wen, J., Gao, Y., Li, T., Wang, H., Yan, H., . . . Guo, R. (2018). Antibacterial graphene oxide coatings on polymer substrate. Applied Surface Science, 436, 624-630.

Liu, Z., Robinson, J. T., Sun, X., & Dai, H. (2008). PEGylated nanographene oxide for delivery of water-insoluble cancer drugs. Journal of the American Chemical Society, 130(33), 10876-10877.

Lu, C.-J., Jiang, X.-F., Junaid, M., Ma, Y.-B., Jia, P.-P., Wang, H.-B., & Pei, D.-S. (2017). Graphene oxide nanosheets induce DNA damage and activate the base excision repair (BER) signaling pathway both *in vitro* and *in vivo*. Chemosphere, 184, 795-805.

Lu, X., Feng, X., Werber, J. R., Chu, C., Zucker, I., Kim, J.-H., . . . Elimelech, M. (2017b). Enhanced antibacterial activity through the controlled alignment of graphene oxide nanosheets. Proceedings of the National Academy of Sciences, 114(46), E9793-E9801.

Luo, Z., Lu, Y., Somers, L. A., & Johnson, A. T. C. (2009). High yield preparation of macroscopic graphene oxide membranes. Journal of the American Chemical Society, 131(3), 898-899.

Lv, M., Zhang, Y., Liang, L., Wei, M., Hu, W., Li, X., & Huang, Q. (2012). Effect of graphene oxide on undifferentiated and retinoic acid-differentiated SH-SY5Y cells line. Nanoscale, 4(13), 3861-3866.

Ma, J., Liu, R., Wang, X., Liu, Q., Chen, Y., Valle, R. P., . . . Liu, S. (2015). Crucial role of lateral size for graphene oxide in activating macrophages and stimulating pro-inflammatory responses in cells and animals. ACS Nano, 9(10), 10498-10515.

Madsen, J. S., Burmølle, M., Hansen, L. H., & Sørensen, S. J. (2012). The interconnection between biofilm formation and horizontal gene transfer. FEMS Immunology & Medical Microbiology, 65(2), 183-195.

Magdolenova, Z., Collins, A., Kumar, A., Dhawan, A., Stone, V., & Dusinska, M. (2014). Mechanisms of genotoxicity. A review of *in vitro* and *in vivo* studies with engineered nanoparticles. Nanotoxicology, 8(3), 233-278.

Maisonneuve, E., & Gerdes, K. (2014). Molecular mechanisms underlying bacterial persisters. Cell, 157(3), 539-548.

Male, K. B., Leung, A. C., Montes, J., Kamen, A., & Luong, J. H. (2012). Probing inhibitory effects of nanocrystalline cellulose: inhibition versus surface charge. Nanoscale, 4(4), 1373-1379.

Mangadlao, J. D., Santos, C. M., Felipe, M. J., de Leon, A. C., Rodrigues, D. F., & Advincula, R. C. (2015). On the antibacterial mechanism of graphene oxide (GO) Langmuir-Blodgett films. Chemical Communications (Camb), 51(14), 2886-2889.

Mani, V., Chen, S.-M., & Lou, B.-S. (2013). Three dimensional graphene oxide-carbon nanotubes and graphene-carbon nanotubes hybrids. International Journal of Electrochemical Science, 8(11641), e60.

Manke, A., Wang, L., & Rojanasakul, Y. (2013). Mechanisms of nanoparticle-induced oxidative stress and toxicity. BioMed Research International, 2013.

McKenna, M. (2013). Antibiotic resistance: The last resort. Nature, 499(7459), 394-396.

Medina Cruz, D., Mi, G., & Webster, T. J. (2018). Synthesis and characterization of biogenic selenium nanoparticles with antimicrobial properties made by *Staphylococcus aureus*, methicillin-resistant *Staphylococcus aureus* (MRSA), *Escherichia coli*, and *Pseudomonas aeruginosa*. Journal of Biomedical Materials Research Part A, 106(5), 1400-1412.

Melnyk, A. H., Wong, A., & Kassen, R. (2015). The fitness costs of antibiotic resistance mutations. Evolutionary Applications, 8(3), 273-283.

Mokkapati, V., Pandit, S., Kim, J., Martensson, A., Lovmar, M., Westerlund, F., & Mijakovic, I. (2018). Bacterial response to graphene oxide and reduced graphene oxide integrated in agar plates. Royal Society Open Science, 5(11), 181083.

Molnar, A. (2019). Antimicrobial resistance awareness and games. Trends in Microbiology, 27(1), 1-3.

Monzón, M., Oteiza, C., Leiva, J., Lamata, M., & Amorena, B. (2002). Biofilm testing of *Staphylococcus epidermidis* clinical isolates: low performance of vancomycin in relation to other antibiotics. Diagnostic Microbiology and Infectious Disease, 44(4), 319-324.

Morita, Y., Kimura, N., Mima, T., Mizushima, T., & Tsuchiya, T. (2001). Roles of MexXY-and MexAB-multidrug efflux pumps in intrinsic multidrug resistance of *Pseudomonas aeruginosa* PAO1. The Journal of General and Applied Microbiology, 47(1), 27-32.

Morita, Y., Tomida, J., & Kawamura, Y. (2014). Responses of *Pseudomonas aeruginosa* to antimicrobials. Frontiers in Microbiology, 4, 422.

Munita, J. M., & Arias, C. A. (2016). Mechanisms of antibiotic resistance. Microbiology Spectrum, 4(2).

Nairi, V., Medda, L., Monduzzi, M., & Salis, A. (2017). Adsorption and release of ampicillin antibiotic from ordered mesoporous silica. Journal of Colloid and Interface Science, 497, 217-225.

Nanda, S. S., Yi, D. K., & Kim, K. (2016). Study of antibacterial mechanism of graphene oxide using Raman spectroscopy. Sci Rep, 6, 28443.

Nathan, C., & Cunningham-Bussel, A. (2013). Beyond oxidative stress: An immunologist's guide to reactive oxygen species. Nature Reviews Immunology, 13(5), 349.

Nikaido, H. (1996). Multidrug efflux pumps of Gram-negative bacteria. Journal of Bacteriology, 178(20), 5853.

Nikaido, H. (2003). Molecular basis of bacterial outer membrane permeability revisited. Microbiology and Molecular Biology Reviews, 67(4), 593-656.

Novoselov, K. S., Geim, A. K., Morozov, S. V., Jiang, D., Zhang, Y., Dubonos, S. V., . . . Firsov, A. A. (2004). Electric field effect in atomically thin carbon films. Science, 306(5696), 666-669.

Novoselov, K. S., Jiang, Z., Zhang, Y., Morozov, S. V., Stormer, H. L., Zeitler, U., . . . Geim, A. K. (2007). Room-temperature quantum Hall effect in graphene. Science, 315(5817), 1379.

Nyquist, R. A., & Kagel, R. O. (2012). Handbook of infrared and Raman spectra of inorganic compounds and organic salts: Infrared spectra of inorganic compounds (Vol. 4): Academic Press.

O'Connor, R., O'Doherty, J., O'Regan, A., & Dunne, C. (2018). Antibiotic use for acute respiratory tract infections (ARTI) in primary care; what factors affect prescribing and why is it important? A narrative review. Irish Journal of Medical Science (1971-), 187(4), 969-986.

O'neill, J. (2014). Antimicrobial resistance: tackling a crisis for the health and wealth of nations. Review on Antimicrobial Resistance, 20, 1-16.

Olivi, M., Alfè, M., Gargiulo, V., Valle, F., Mura, F., Di Giosia, M., . . . Fiorito, S. (2016). Antimicrobial properties of graphene-like nanoparticles: coating effect on *Staphylococcus aureus*. Journal of Nanoparticle Research, 18(12), 358.

Olsen, I. (2015). Biofilm-specific antibiotic tolerance and resistance. European Journal of Clinical Microbiology & Infectious Diseases, 34(5), 877-886.

Organization, W. H. (2017). WHO model list of essential medicines, 20th list (March 2017, amended August 2017)

Ostrikov, K., Neyts, E., & Meyyappan, M. (2013). Plasma nanoscience: from nano-solids in plasmas to nano-plasmas in solids. Advances in Physics, 62(2), 113-224.

Ou, L., Song, B., Liang, H., Liu, J., Feng, X., Deng, B., . . . Shao, L. (2016). Toxicity of graphene-family nanoparticles: a general review of the origins and mechanisms. Particle and Fibre Toxicology, 13(1), 57.

Ouwehand, A. C., Forssten, S., Hibberd, A. A., Lyra, A., & Stahl, B. (2016). Probiotic approach to prevent antibiotic resistance. Annals of Medicine, 48(4), 246-255.

Palmieri, V., Bugli, F., Lauriola, M. C., Cacaci, M., Torelli, R., Ciasca, G., ... & De Spirito, M. (2017). Bacteria meet graphene: modulation of graphene oxide nanosheet interaction with human pathogens for effective antimicrobial therapy. ACS Biomaterials Science & Engineering, 3(4), 619-627.

Pamp, S. J., Gjermansen, M., Johansen, H. K., & Tolker-Nielsen, T. (2008). Tolerance to the antimicrobial peptide colistin in *Pseudomonas aeruginosa* biofilms is linked to metabolically active cells, and depends on the pmr and mexAB-oprM genes. Molecular Microbiology, 68(1), 223-240.

Panáček, A., Smékalová, M., Kilianová, M., Prucek, R., Bogdanová, K., Večeřová, R., . . . Chojniak, J. (2016). Strong and nonspecific synergistic antibacterial efficiency of antibiotics combined with silver nanoparticles at very low concentrations showing no cytotoxic effect. Molecules, 21(1), 26.

Pandey, V. K., Srivastava, K. R., Ajmal, G., Thakur, V. K., Gupta, V. K., Upadhyay, S. N., & Mishra, P. K. (2019). Differential susceptibility of catheter biomaterials to biofilm-associated infections and their remedy by drug-encapsulated Eudragit RL100 nanoparticles. International Journal of Molecular Sciences, 20(20), 5110.

Pang, L., Dai, C., Bi, L., Guo, Z., & Fan, J. (2017). Biosafety and antibacterial ability of graphene and graphene oxide *in vitro* and *in vivo*. Nanoscale research letters, 12(1), 564.

Papi, M., Palmieri, V., Bugli, F., De Spirito, M., Sanguinetti, M., Ciancico, C., . . . Conti, C. (2016). Biomimetic antimicrobial cloak by graphene-oxide agar hydrogel. Scientific Reports, 6(1), 12.

Papp-Wallace, K. M., Endimiani, A., Taracila, M. A., & Bonomo, R. A. (2011). Carbapenems: Past, present, and future. Antimicrobial Agents and Chemotherapy, 55(11), 4943.

Pareek, V., Gupta, R., & Panwar, J. (2018). Do physico-chemical properties of silver nanoparticles decide their interaction with biological media and bactericidal action? A review. Materials Science and Engineering: C, 90, 739-749.

Park, S., & Ruoff, R. S. (2009). Chemical methods for the production of graphenes. Nature Nanotechnology, 4(4), 217-224.

Partridge, S. R., Kwong, S. M., Firth, N., & Jensen, S. O. (2018). Mobile genetic elements associated with antimicrobial resistance. Clinical Microbiology Reviews, 31(4), e00088-00017.

Pelgrift, R. Y., & Friedman, A. J. (2013). Nanotechnology as a therapeutic tool to combat microbial resistance. Advanced Drug Delivery Reviews, 65(13-14), 1803-1815.

Pelin, M., Fusco, L., León, V., Martín, C., Criado, A., Sosa, S., . . . Prato, M. (2017). Differential cytotoxic effects of graphene and graphene oxide on skin keratinocytes. Scientific Reports, 7, 40572.

Pelin, M., Fusco, L., Martín, C., Sosa, S., Frontiñán-Rubio, J., González-Domínguez, J. M., . . . Tubaro, A. (2018). Graphene and graphene oxide induce ROS production in human HaCaT skin keratinocytes: The role of xanthine oxidase and NADH dehydrogenase. Nanoscale, 10(25), 11820-11830.

Peng, B., Chen, L., Que, C., Yang, K., Deng, F., Deng, X., . . . Wu, M. (2016). Adsorption of antibiotics on graphene and biochar in aqueous solutions induced by π-π interactions. Scientific Reports, 6, 31920.

Perreault, F., de Faria, A. F., Nejati, S., & Elimelech, M. (2015). Antimicrobial properties of graphene oxide nanosheets: Why size matters. ACS Nano, 9(7), 7226-7236.

Pham, T. N., Loupias, P., Dassonville-Klimpt, A., & Sonnet, P. (2019). Drug delivery systems designed to overcome antimicrobial resistance. Medicinal Research Reviews.

Pham, V. T., Truong, V. K., Quinn, M. D., Notley, S. M., Guo, Y., Baulin, V. A., . . . Ivanova, E. P. (2015). Graphene induces formation of pores that kill spherical and rod-shaped bacteria. ACS Nano, 9(8), 8458-8467.

Pumera, M. (2010). Graphene-based nanomaterials and their electrochemistry. Chemical Society Reviews, 39(11), 4146-4157.

Qu, G., Liu, S., Zhang, S., Wang, L., Wang, X., Sun, B., . . . Chen, J.-J. (2013). Graphene oxide induces toll-like receptor 4 (TLR4)-dependent necrosis in macrophages. ACS Nano, 7(7), 5732-5745.

Ranghar, S., Sirohi, P., Verma, P., & Agarwal, V. (2014). Nanoparticle-based drug delivery systems: promising approaches against infections. Brazilian Archives of Biology and Technology, 57(2), 209-222.

Rebuffo, C. A., Schmitt, J., Wenning, M., von Stetten, F., & Scherer, S. (2006). Reliable and rapid identification of *Listeria monocytogenes* and *Listeria* species by artificial neural network-based Fourier transform infrared spectroscopy. Applied and Environmental Microbiology, 72(2), 994-1000.

Reina, A., Jia, X., Ho, J., Nezich, D., Son, H., Bulovic, V., . . . Kong, J. (2008). Large area, few-layer graphene films on arbitrary substrates by chemical vapor deposition. Nano letters, 9(1), 30-35.

Reith, J., & Mayer, C. (2011). Peptidoglycan turnover and recycling in Gram-positive bacteria. Applied Microbiology and Biotechnology, 92(1), 1.

Ren, H., Wang, C., Zhang, J., Zhou, X., Xu, D., Zheng, J., . . . Zhang, J. (2010). DNA cleavage system of nanosized graphene oxide sheets and copper ions. ACS Nano, 4(12), 7169-7174.

Resistance, R. o. A. (2016). Tackling drug-resistant infections globally: Final report and recommendations: Review on Antimicrobial Resistance.

Robinson, J. T., Tabakman, S. M., Liang, Y., Wang, H., Sanchez Casalongue, H., Vinh, D., & Dai, H. (2011). Ultrasmall reduced graphene oxide with high near-infrared absorbance for photothermal therapy. Journal of the American Chemical Society, 133(17), 6825-6831.

Rojo-Molinero, E., Macià, M. D., & Oliver, A. (2019). Social behavior of antibiotic resistant mutants within *Pseudomonas aeruginosa* biofilm communities. Frontiers in Microbiology, 10, 570.

Roman, M. (2015). Toxicity of cellulose nanocrystals: a review. Industrial Biotechnology, 11(1), 25-33.

Romero, M. P., Marangoni, V. S., de Faria, C. G., Leite, I. S., Maroneze, C. M., Pereira-da-Silva, M. A., ... & Inada, N. M. (2020). Graphene oxide mediated broad-spectrum antibacterial based on bimodal action of photodynamic and photothermal effects. Frontiers in Microbiology, 10, 2995.

Romero-Vargas Castrill n, S., Perreault, F. o., De Faria, A. F., & Elimelech, M. (2015). Interaction of graphene oxide with bacterial cell membranes: insights from force spectroscopy. Environmental Science & Technology Letters, 2(4), 112-117.

Ruiz, O. N., Fernando, K. S., Wang, B., Brown, N. A., Luo, P. G., McNamara, N. D., . . . Bunker, C. E. (2011). Graphene oxide: A nonspecific enhancer of cellular growth. ACS Nano, 5(10), 8100-8107.

Russell, A. D. (1975). The antibacterial activity of a new cephalosporin, cefamandole. Journal of Antimicrobial Chemotherapy, 1(1), 97-101.

Saga, T., & Yamaguchi, K. (2009). History of antimicrobial agents and resistant bacteria. JMAJ, 52(2), 103-108.

Saha, S., Ahmed, K., Islam, S., Islam, M., Khan, M., & Saha, C. (2018). Antibiotic resistance: A crisis needs to be encountered. Mediscope, 5(1), 33-37.

Salas, E. C., Sun, Z., L ttge, A., & Tour, J. M. (2010). Reduction of graphene oxide via bacterial respiration. ACS Nano, 4(8), 4852-4856.

Saleem, H., Haneef, M., & Abbasi, H. Y. (2018). Synthesis route of reduced graphene oxide via thermal reduction of chemically exfoliated graphene oxide. Materials Chemistry and Physics, 204(Supplement C), 1-7.

Sanchez, V. C., Jachak, A., Hurt, R. H., & Kane, A. B. (2012). Biological interactions of graphene-family nanomaterials–an interdisciplinary review. Chemical Research in Toxicology, 25(1), 15.

Sandoval-Motta, S., & Aldana, M. (2016). Adaptive resistance to antibiotics in bacteria: a systems biology perspective. Wiley Interdisciplinary Reviews: Systems Biology and Medicine, 8(3), 253-267.

Schütz, C. A., Juillerat-Jeanneret, L., Mueller, H., Lynch, I., & Riediker, M. (2013). Therapeutic nanoparticles in clinics and under clinical evaluation. Nanomedicine, 8(3), 449-467.

Schwab, F., Bucheli, T. D., Camenzuli, L., Magrez, A., Knauer, K., Sigg, L., & Nowack, B. (2013). Diuron sorbed to carbon nanotubes exhibits enhanced toxicity to *Chlorella vulgaris*. Environmental Science & Technology, 47(13), 7012-7019.

Sengupta, I., Bhattacharya, P., Talukdar, M., Neogi, S., Pal, S. K., & Chakraborty, S. (2019). Bactericidal effect of graphene oxide and reduced graphene oxide: Influence of shape of bacteria. Colloid and Interface Science Communications, 28, 60-68.

Serag, M. F., Kaji, N., Venturelli, E., Okamoto, Y., Terasaka, K., Tokeshi, M., . . . Baba, Y. (2011). Functional platform for controlled subcellular distribution of carbon nanotubes. ACS Nano, 5(11), 9264-9270.

Sharar, N. S., Chai, L. C., & Thong, K. L. (2018). Catabolic activity and biofilm formation of foodborne *Listeria monocytogenes* strains. Journal of Consumer Protection and Food Safety, 13(3), 289-298.

Sharma, D., Misba, L., & Khan, A. U. (2019). Antibiotics versus biofilm: an emerging battleground in microbial communities. Antimicrobial Resistance & Infection Control, 8(1), 1-10.

Shi, P., Su, R., Zhu, S., Zhu, M., Li, D., & Xu, S. (2012). Supported cobalt oxide on graphene oxide: Highly efficient catalysts for the removal of Orange II from water. Journal of Hazardous Materials, 229-230(Supplement C), 331-339.

Si, C., Sun, Z., & Liu, F. (2016). Strain engineering of graphene: a review. Nanoscale, 8(6), 3207-3217.

Silhavy, T. J., Kahne, D., & Walker, S. (2010). The Bacterial Cell Envelope. Cold Spring Harbor Perspectives in Biology, 2(5), a000414.

Slavin, Y. N., Asnis, J., Häfeli, U. O., & Bach, H. (2017). Metal nanoparticles: Understanding the mechanisms behind antibacterial activity. Journal of Nanobiotechnology, 15(1), 65.

Sodhi, N. (2016). New mechanism of resistance in a last-resort antibiotic. Australian Veterinary Journal, 94(1-2), N8-9.

Soltani, T., & Lee, B.-K. (2017). Low intensity-ultrasonic irradiation for highly efficient, eco-friendly and fast synthesis of graphene oxide. Ultrasonics Sonochemistry, 38, 693-703.

Sondi, I., & Salopek-Sondi, B. (2004). Silver nanoparticles as antimicrobial agent: A case study on *E. coli* as a model for Gram-negative bacteria. Journal of Colloid and Interface Science, 275(1), 177-182.

Song, T., Duperthuy, M., & Wai, S. N. (2016). Sub-Optimal Treatment of Bacterial Biofilms. Antibiotics (Basel, Switzerland), 5(2), 23.

Stalder, T., & Top, E. (2016). Plasmid transfer in biofilms: A perspective on limitations and opportunities. NPJ Biofilms and Microbiomes, 2, 16022.

Stewart, P. S. (2015). Antimicrobial tolerance in biofilms. Microbiology spectrum, 3(3), 10.1128/microbiolspec. MB-0010-2014.

Su, H., Wang, Y., Gu, Y., Bowman, L., Zhao, J., & Ding, M. (2018). Potential applications and human biosafety of nanomaterials used in nanomedicine. Journal of Applied Toxicology, 38(1), 3-24.

Sun, X., Liu, Z., Welsher, K., Robinson, J. T., Goodwin, A., Zaric, S., & Dai, H. (2008). Nano-graphene oxide for cellular imaging and drug delivery. Nano Research, 1(3), 203-212.

Suo, Z., Avci, R., Deliorman, M., Yang, X., & Pascual, D. W. (2009). Bacteria survive multiple puncturings of their cell walls. Langmuir, 25(8), 4588-4594.

Suzuki, H., Yu, J., Kobayashi, T., Nakanishi, H., Nixon, P. J., & Noguchi, T. (2013). Functional roles of D2-Lys317 and the interacting chloride ion in the water oxidation reaction of photosystem II as revealed by Fourier transform infrared analysis. Biochemistry, 52(28), 4748-4757.

Syed, A. (2019). Antibiotic use and resistance. International Journal Current Research in Medical Sciences, 5(4), 17-23.

Szunerits, S., & Boukherroub, R. (2016). Antibacterial activity of graphene-based materials. Journal of Materials Chemistry B, 4(43), 6892-6912.

Tang, Z., Wu, H., Cort, J. R., Buchko, G. W., Zhang, Y., Shao, Y., . . . Lin, Y. (2010). Constraint of DNA on functionalized graphene improves its biostability and specificity. Small, 6(11), 1205-1209.

Thirunavukkarasu, R., Pandiyan, P., Balaraman, D., Subaramaniyan, K., Edward Gnana Jothi, G., Manikkam, S., & Sadaiyappan, B. (2013). Isolation of bioactive compound from marine seaweeds against fish pathogenic bacteria *Vibrio alginolyticus* (VA09) and characterisation by FTIR. Journal of Coastal Life Medicine, 1(1), 26-33.

Trastoy, R., Manso, T., Fernandez-Garcia, L., Blasco, L., Ambroa, A., Del Molino, M. P., . . . Tomas, M. (2018). Mechanisms of bacterial tolerance and persistence in the gastrointestinal and respiratory environments. Clinical Microbiology Reviews, 31(4), e00023-00018.

Trivedi, M., Patil, S., Shettigar, H., Bairwa, K., & Jana, S. (2015). Spectroscopic characterization of chloramphenicol and tetracycline: An impact of biofield treatment.

Tu, Y., Lv, M., Xiu, P., Huynh, T., Zhang, M., Castelli, M., . . . Zhou, R. (2013). Destructive extraction of phospholipids from *Escherichia coli* membranes by graphene nanosheets. Nature Nanotechnology, 8(8), 594-601.

Valentini, L., Bon, S. B., Monticelli, O., & Kenny, J. M. (2012). Deposition of amino-functionalized polyhedral oligomeric silsesquioxanes on graphene oxide sheets immobilized onto an amino-silane modified silicon surface. Journal of Materials Chemistry, 22(13), 6213-6217.

Venkatasubbu, G. D., Baskar, R., Anusuya, T., Seshan, C. A., & Chelliah, R. (2016). Toxicity mechanism of titanium dioxide and zinc oxide nanoparticles against food pathogens. Colloids and Surfaces B: Biointerfaces, 148, 600-606.

von Wintersdorff, C. J., Penders, J., van Niekerk, J. M., Mills, N. D., Majumder, S., van Alphen, L. B., . . . Wolffs, P. F. (2016). Dissemination of antimicrobial resistance in microbial ecosystems through horizontal gene transfer. Frontiers in Microbiology, 7, 173.

Waldetoft, K. W., & Brown, S. P. (2017). Alternative therapeutics for self-limiting infections—An indirect approach to the antibiotic resistance challenge. PLoS biology, 15(12), e2003533.

Wan, B., Wang, Z.-X., Lv, Q.-Y., Dong, P.-X., Zhao, L.-X., Yang, Y., & Guo, L.-H. (2013). Single-walled carbon nanotubes and graphene oxides induce autophagosome accumulation and lysosome impairment in primarily cultured murine peritoneal macrophages. Toxicology Letters, 221(2), 118-127.

Wang, A., Pu, K., Dong, B., Liu, Y., Zhang, L., Zhang, Z., . . . Zhu, Y. (2013). Role of surface charge and oxidative stress in cytotoxicity and genotoxicity of graphene oxide towards human lung fibroblast cells. Journal of Applied Toxicology, 33(10), 1156-1164.

Wang, L., Hu, C., & Shao, L. (2017). The antimicrobial activity of nanoparticles: present situation and prospects for the future. International Journal of Nanomedicine, 12, 1227.

Wang, T. Z., Kodiyanplakkal, R. P. L., & Calfee, D. P. (2019). Antimicrobial resistance in nephrology. Nature Reviews Nephrology, 1.

Wang, X., Bai, H., & Shi, G. (2011). Size fractionation of graphene oxide sheets by pH-assisted selective sedimentation. Journal of the American Chemical Society, 133(16), 6338-6342.

Wang, Z., Yu, J., Gui, R., Jin, H., & Xia, Y. (2016). Carbon nanomaterials-based electrochemical aptasensors. Biosensors and Bioelectronics, 79, 136-149.

Wilson, D. N. (2014). Ribosome-targeting antibiotics and mechanisms of bacterial resistance. Nature Reviews Microbiology, 12(1), 35-48.

Wirth, S. M., Lowry, G. V., & Tilton, R. D. (2012). Natural organic matter alters biofilm tolerance to silver nanoparticles and dissolved silver. Environmental Science & Technology, 46(22), 12687-12696.

Wong, P., Wong, R. K., Caputo, T. A., Godwin, T. A., & Rigas, B. (1991). Infrared spectroscopy of exfoliated human cervical cells: Evidence of extensive structural changes during carcinogenesis. Proceedings of the National Academy of Sciences, 88(24), 10988-10992.

World Health Organization, W. (2014). Antimicrobial resistance: Global report on surveillance: World Health Organization.

Wright, G. D. (2010). Q&A: Antibiotic resistance: Where does it come from and what can we do about it? BMC biology, 8(1), 123.

Wu, L., Liu, L., Gao, B., Mu oz-Carpena, R., Zhang, M., Chen, H., . . . Wang, H. (2013). Aggregation kinetics of graphene oxides in aqueous solutions: Experiments, mechanisms, and modeling. Langmuir, 29(49), 15174-15181.

Wu, S.-Y., An, S. S. A., & Hulme, J. (2015). Current applications of graphene oxide in nanomedicine. International Journal of Nanomedicine, 10(Spec Iss), 9.

Wu, X., Tan, S., Xing, Y., Pu, Q., Wu, M., & Zhao, J. X. (2017). Graphene oxide as an efficient antimicrobial nanomaterial for eradicating multi-drug resistant bacteria *in vitro* and *in vivo*. Colloids and Surfaces B: Biointerfaces, 157, 1-9.

Xiong, Z., Zhang, X., Zhang, S., Lei, L., Ma, W., Li, D., ... & Xing, B. (2018). Bacterial toxicity of exfoliated black phosphorus nanosheets. Ecotoxicology and Environmental Safety, 161, 507-514.

Xu, L., Wang, H., & Xiao, Y. (2004). Spectrophotometric determination of ampicillin sodium in pharmaceutical products using sodium 1,2-naphthoquinone-4-sulfonic as the chromogentic reagent. Spectrochimica Acta Part A: Molecular and Biomolecular Spectroscopy, 60(13), 3007-3012.

Xu, M., Zhu, J., Wang, F., Xiong, Y., Wu, Y., Wang, Q., . . . Liu, S. (2016). Improved *in vitro* and *in vivo* biocompatibility of graphene oxide through surface modification: poly (acrylic acid)-functionalization is superior to PEGylation. ACS Nano, 10(3), 3267-3281.

Yadav, N., Dubey, A., Shukla, S., Saini, C. P., Gupta, G., Priyadarshini, R., & Lochab, B. (2017). Graphene oxide-coated surface: Inhibition of bacterial biofilm formation due to specific surface–interface interactions. ACS Omega, 2(7), 3070-3082.

Yang, J. H., Bening, S. C., & Collins, J. J. (2017). Antibiotic efficacy—context matters. Current Opinion in Microbiology, 39, 73-80.

Yang, K., Feng, L., Shi, X., & Liu, Z. (2013). Nano-graphene in biomedicine: theranostic applications. Chemical Society Reviews, 42(2), 530-547.

Yang, P., Pageni, P., Rahman, M. A., Bam, M., Zhu, T., Chen, Y. P., . . . Tang, C. (2019). Gold nanoparticles with antibiotic-metallopolymers toward broad-spectrum antibacterial effects. Advanced Healthcare Materials, 8(6), 1800854.

Yang, Y., Asiri, A. M., Tang, Z., Du, D., & Lin, Y. (2013b). Graphene based materials for biomedical applications. Materials Today, 16(10), 365-373.

Yilbas, B. S., Ibrahim, A., Ali, H., Khaled, M., & Laoui, T. (2018). Hydrophobic and optical characteristics of graphene and graphene oxide films transferred onto functionalized silica particles deposited glass surface. Applied Surface Science, 442, 213-223.

Zhang, H., Peng, C., Yang, J., Lv, M., Liu, R., He, D., . . . Huang, Q. (2013). Uniform ultrasmall graphene oxide nanosheets with low cytotoxicity and high cellular uptake. ACS Applied Materials & Interfaces, 5(5), 1761-1767.

Zhang, L., Liang, J., Huang, Y., Ma, Y., Wang, Y., & Chen, Y. (2009). Size-controlled synthesis of graphene oxide sheets on a large scale using chemical exfoliation. Carbon, 47(14), 3365-3368.

Zhang, L., Pornpattananangkul, D., Hu, C.-M., & Huang, C.-M. (2010). Development of nanoparticles for antimicrobial drug delivery. Current Medicinal Chemistry, 17(6), 585-594.

Zhang, M., Yan, Z., Li, Y., Jing, J., & Xie, J. (2015). Preparation of cobalt silicide on graphene as Pt electrocatalyst supports for highly efficient and stable methanol oxidation in acidic media. Electrochimica Acta, 161(Supplement C), 48-54.

Zhang, W., Wang, C., Li, Z., Lu, Z., Li, Y., Yin, J. J., . . . Nie, G. (2012). Unraveling stress-induced toxicity properties of graphene oxide and the underlying mechanism. Advanced Materials, 24(39), 5391-5397.

Zhang, W., Zou, X., & Zhao, J. (2015b). Preparation and performance of a novel graphene oxide sheets modified rare-earth luminescence material. Journal of Materials Chemistry C, 3(6), 1294-1300.

Zhang, X., Hu, W., Li, J., Tao, L., & Wei, Y. (2012b). A comparative study of cellular uptake and cytotoxicity of multi-walled carbon nanotubes, graphene oxide, and nanodiamond. Toxicology Research, 1(1), 62-68.

Zhang, X., Li, Y., Li, B., Mao, Y., Wu, X., Zou, X., . . . Chen, H. (2016). Three supplementary methods for analyzing cytotoxicity of *Escherichia coli* O157:H7. Journal of Microbiological Methods, 120, 34-40.

Zhang, X., Sun, H., Zhang, Z., Niu, Q., Chen, Y., & Crittenden, J. C. (2007). Enhanced bioaccumulation of cadmium in carp in the presence of titanium dioxide nanoparticles. Chemosphere, 67(1), 160-166.

Zhao, J., Wang, Z., White, J. C., & Xing, B. (2014). Graphene in the aquatic environment: adsorption, dispersion, toxicity and transformation. Environmental Science & Technology, 48(17), 9995-10009.

Zhou, K., Gui, Z., Hu, Y., Jiang, S., & Tang, G. (2016). The influence of cobalt oxide–graphene hybrids on thermal degradation, fire hazards and mechanical properties of thermoplastic polyurethane composites. Composites Part A: Applied Science and Manufacturing, 88(Supplement C), 10-18.

Zhou, S., & Bongiorno, A. (2013). Origin of the chemical and kinetic stability of graphene oxide. Scientific Reports, 3, 2484.

Zou, F., Zhou, H., Jeong, D. Y., Kwon, J., Eom, S. U., Park, T. J., . . . Lee, J. (2017). Wrinkled surface-mediated antibacterial activity of graphene oxide nanosheets. ACS Applied Materials & Interfaces, 9(2), 1343-1351.

Zou, X., Zhang, L., Wang, Z., & Luo, Y. (2016). Mechanisms of the antimicrobial activities of graphene materials. Journal of American Chemical Society, 138(7), 2064-2077.

Żur, J., Wojcieszyńska, D., & Guzik, U. (2016). Metabolic responses of bacterial cells to immobilization. Molecules, 21(7), 958.